A Molecular Perspective on Membrane Fission Mechanisms in Vacuolar Protein Sorting

विद्या वाचस्पति की उपाधि की अपेक्षाओं की आंशिक पूर्ति में प्रस्तुत शोध प्रबंध

A thesis submitted in partial fulfillment of the requirements of the degree of
Doctor of Philosophy

द्वारा / By

शिल्पा गोपन / **Shilpa Gopan)**

पंजीकरण सं. / Registration No.

20183587

शोध प्रबंध पर्यवेक्षक / Thesis Supervisor

Prof. Thomas Pucadyil

भारतीय विज्ञान शिक्षा एवं अनुसंधान संस्थान पुणे

INDIAN INSTITUTE OF SCIENCE EDUCATION AND RESEARCH PUNE

2025

Certificate

Certified that the work incorporated in the thesis entitled '**A molecular perspective on membrane fission mechanisms in Vacuolar Protein Sorting'** submitted by Shilpa Gopan was carried out by the candidate, under my supervision. The work presented here or any part of it has not been included in any other thesis submitted previously for the award of any degree or diploma from any other University or institution.

Thomas Pucadyil

(Supervisor)

21.03.2025

Declaration

Name of Student	: Shilpa Gopan
Reg. No.	: 20183587
Thesis Supervisor	: Prof. Thomas Pucadyil
Department	: Biology
Date of joining program	: 01/08/2018
Date of Pre-Synopsis Seminar	: 21/08/2024
Title of Thesis	: A molecular perspective on membrane fission mechanisms in Vacuolar Protein Sorting

I declare that this written submission represents my ideas in my own words and where others' ideas have been included; I have adequately cited and referenced the original sources. I declare that I have acknowledged collaborative work and discussions wherever such work has been included. I also declare that I have adhered to all principles of academic honesty and integrity and have not misrepresented or fabricated or falsified any idea/data/fact/source in my submission. I understand that violation of the above will be cause for disciplinary action by the institute and can also evoke penal action from the sources which have thus not been properly cited or from whom proper permission has not been taken when needed. The work reported in this thesis is the original work done by me under the guidance of Prof. Thomas Pucadyil.

Shilpa Gopan

21.03.2025

To Achan and Amma

Acknowledgements

No achievement stands alone, and I am deeply grateful to those who have been my guiding stars along the way.

I want to express my heartfelt gratitude to Prof. Thomas Pucadyil for his unwavering support, guidance, and encouragement throughout this journey. His vast knowledge and deep understanding of the subject have shaped my scientific thinking and instilled in me the discipline and curiosity essential for meaningful research. I have always admired his meticulous approach to problem-solving using first principles and the ability to articulate complex ideas with clarity. Thomas' passion for research and commitment to excellence have been truly inspiring, and his belief in my abilities has given me the confidence to grow as a researcher. Beyond being a supervisor, he has been a mentor and a source of motivation, teaching me invaluable lessons that extend far beyond the lab. I will always cherish the insightful discussions and constructive feedback that have shaped my academic and personal growth. For all this and more, I am deeply grateful.

I would like to express my sincere thanks to Dr. Aurnab Ghose and Dr. Nagaraj Balasubramaniam for their insightful discussions and valuable inputs throughout my PhD journey. Special thanks to Dr. Mridula Nambiar for the enriching discussions that contributed to my research. I am also grateful to Dr. Saravanan Palani from IISc for his help in setting up the yeast model system in our lab. I extend my appreciation to Dr. Mara Duncan from the University of Michigan for generously sharing yeast strains from her library, which were integral to the work presented in Chapter 8.

My journey would not have been the same without the wonderful members of the Pucadyil lab. I am thankful to all past and present lab members with whom I had the privilege to collaborate. I cherish the brief yet impactful overlap with Rounaq Deo, Sukrut Kamerkar, and Devika Andhare, who provided guiding stones during the early stages of my PhD. I am especially grateful to my seniors, Himani Khurana, Krishnendu Roy, and Soumya Bhattacharya, who supported me and pushed my limits, helping me grow as a researcher. I deeply admire Gregor Jose for his unwavering support and valuable scientific inputs. My sincere thanks to Gurmail Singh for his contributions to the experiments in Chapters 3–7 and for the enlightening scientific discussions we shared. I am also grateful to Uma Swaminathan, Raksha Bhansali, and Prasanna Iyer for their collaboration on the experiments in Chapter 8. Their contributions

have been invaluable to this thesis. Keerti Singh has been a friend in need and I will always cherish her support. I am also grateful to Meghadeepa Sarkar, Sannidhya De, Aman Sharma, Sejal Shivarkar, Shivansh Singh, Parul Sood, Rakhee Lohia and Swayam Prakash Singh for creating a lively and cheerful lab environment, offering much-needed moments of joy and stress relief.

I thank the IISER Pune biology department, microscopy facility, proteomics facility, Bio-office, and all the facility staff for their invaluable support throughout this journey. Their dedication and assistance have played a crucial role in making my PhD journey smoother. Additionally, I am grateful to the Council of Scientific and Industrial Research (CSIR) for providing me with a graduate student fellowship during my PhD tenure.

Beyond the lab, my friends have been my pillars of strength. I am especially thankful to My batchmates; Mamatha, Ardhra, Akshay, Dhruv, Soumya, Nikita, Netra, and Anirudh; who have been a constant source of support, and I cherish the camaraderie we shared. I would also like to thank Sajina, Atreyee, Sreya and Aruna for being the incredible friends whom I can rely on no matter what.

My deepest gratitude goes to my family. My parents have always stood by me, supporting my dreams and decisions unconditionally. Their love and encouragement have been my greatest strength. My sisters especially, have been an incredible source of support, listening to my joys, grievances, and frustrations throughout this journey, I am truly blessed to have them by my side. Lastly, I extend my heartfelt thanks to Unni, who has been my constant through every phase of this journey. He inspired me at times, reminded me of my potential during moments of doubt and always encouraged me to aim higher. His belief in me has been a source of strength, for which I am truly grateful.

Above all, I thank Almighty for giving me strength and resilience, especially in moments of hopelessness. This journey has been challenging yet fulfilling, and I am forever thankful to everyone who has played a part in it.

Contents

Synopsis

Membranes are dynamic and resilient structures formed by the self-assembly of lipid molecules in an aqueous environment and make the fundamental unit of the cell. This organization provides a physical barrier and establishes the basis for cellular compartmentalization. The inherent asymmetry and fluidity of the membrane facilitate the formation of different organelles characterized by unique biomolecular pools and physiological conditions, such as pH gradient and ionic concentration, critical for orchestrating a myriad of cellular processes. The exchange of resources between different cellular compartments occurs primarily through vesicular transport pathways that involve the formation of vesicular and tubular intermediates. Vesicular transport is essential for the targeted transport of a diverse range of cargo, including proteins and lipids, between various cellular compartments. The bending or remodelling of membrane from planar to curved surfaces that finally pinch off to vesicles is crucial for the initiation of vesicular trafficking.

Membrane remodelling is an energetically demanding process that requires the involvement of specialized proteins to overcome the inherent energy barriers associated with altering membrane curvature. Briefly, the curvature-generating proteins bend the membrane, and the fission proteins facilitate the pinching of budding membrane. Among the fission proteins, the Dynamin family of proteins has been extensively studied due to their ability to constrict and sever membrane through GTP hydrolysis, thereby orchestrating the precise formation of vesicular transport carriers.

The vacuolar protein sorting (VPS) pathway is one of the vesicular transport pathways required for maintaining cellular homeostasis. Lysosomes, which function as signalling hub, storage unit, and degradation centre, rely on the VPS pathway to accurately deliver specific vacuolar proteins. In higher order eukaryotes, this pathway ensures that proteins destined for degradation or recycling are trafficked to lysosomes, while in yeast, analogous proteins are directed to the vacuole. Despite the vast studies on the VPS pathway, our understanding of proteins responsible for the fission of tubular-vesicular carriers at various stages of the VPS pathway remains limited.

Vps1, a member of the Dynamin family in yeast, has been implicated in mediating membrane fission in the VPS pathway. Although Vps1 was identified as a component of the VPS pathway

over three decades ago, its precise biochemical properties and cellular functions have yet to be fully elucidated. Recent studies suggest that Vps1 may participate in the fission of budding vesicles, thereby contributing to the efficient sorting and trafficking of vacuolar proteins. In this thesis, we attempt to systematically characterize Vps1 to unravel its role in the vacuolar protein sorting pathway with the aim of enhancing our understanding of the underlying mechanisms of membrane dynamics and organelle biogenesis.

This thesis is divided into 9 sections:

Chapter 1 broadly introduces the importance of vesicular transport in cellular processes and the different stages involved in it. Next, we look at the various screens that shed light on the players involved in vesicular transport, focus on one of the vesicular transport pathways, vacuolar protein sorting and one of the proteins involved in it, Vps1. By comparing Vps1 with its well-studied mammalian counterpart, dynamins, this chapter frames the current understanding and highlights critical questions regarding Vps1 function.

Chapter 2 elaborately discusses the methods used in the study. It also talks about the chemical resources used and the yeast strains and plasmids generated to understand Vps1 functions.

Chapter 3 describes the characterization of the membrane remodelling abilities of Vps1 using different biochemical assays under physiologically relevant membrane conditions. From these assays for the first time, we establish that Vps1 is sufficient to cause membrane fission.

Vps1 is a Dynamin family protein. Dynamin-mediated fission is governed by its GTP binding and hydrolysis. **Chapter 4** tries to further mechanistically elaborate Vps1-mediated membrane fission by carefully varying the factors involved. We analyzed how Vps1's preference for membrane curvature, nucleotide state and oligomerization fine-tune Vps1-mediated fission. Further, we dissect the stage-specific effects of Vps1 binding, oligomerization, and hydrolysis on the underlying membrane to undergo fission. We see that Vps1-mediated fission is extremely tuned to act on curvatures similar to endosomal sizes and is also controlled by the different nucleotide states it is bound to.

Moving into a cellular context, **Chapter 5** dives into the preparation and validation of knock-in strains used to understand the effect of Vps1 in vacuolar protein sorting.

With the assays standardized to understand Vps1 functions in isolation and inside cells, in **Chapter 6** we uncover the role of InsertB region of Vps1 in mechanical and cellular functions

of Vps1. We see that InsertB region is important for Vps1 membrane binding. Our assays suggest that the InsertB region might be involved in the oligomerization of Vps1 and its binding to adaptor proteins, other than membrane binding.

In **Chapter 7**, we tries to understand the global effect of Vps1 deletion on vacuolar proteome by implementing quantitative mass-spectrometry methods. We further validate the results in mass-spectrometry by imaging certain protein hits for their vacuole localization.

The occurrence of different trafficking pathways unhindered upon Vps1 deletion indicates the presence of alternate fission proteins in yeast. In **Chapter 8**, we employed a screen to fish out novel fission proteins in yeast. Our initial results suggest the involvement of proteins with unannotated membrane binding domains to carry out membrane fission in a nucleotide-independent manner.

Finally, **Chapter 9** summarizes our findings on Vps1's role in vesicular trafficking and discusses these results in the context of existing literature. It also outlines future directions to elucidate further the mechanisms of membrane fission and its broader implications in cellular physiology.

List of Figures

List of Tables

Chapter 1
Introduction

1.1 Vesicular transport

Cell membranes delineate the cell boundary and compartmentalize its interior into distinct organelles, each with unique properties and create specialized microenvironment that allow organelles to perform distinct functions. Inter-organelle communication and resource exchange is important for maintaining the cellular homeostasis. As small molecules get transferred through diffusion or by binding to specific transport proteins that are embedded in the membrane, transport of proteins and lipids across organelles occur through a much complex, membrane-bound and membrane-less transport mechanisms[1–3].

For instance, proteins synthesized in the cytoplasm or endoplasmic reticulum (ER) are transported to the Golgi apparatus, which has a distinct lipid composition[4,5]. These proteins undergo post-translational modifications in the Golgi before being packaged into vesicles for transport[6,7]. Vesicle-mediated transport is essential for directing proteins to other organelles, plasma membrane or for secretion outside the cell[2]. Similarly, materials from outside the cell can be internalized through endocytic processes, where remodelling of the plasma membrane forms the vesicular compartments, necessary for uptake[8]. Bulk of the lipids also get transported through the formation of vesicles. Although there are lipid transfer proteins that bind specific lipids at their hydrophobic cavities and transport between organelles[9], the above means of lipid transfer occurs majorly near membrane contact sites, where two organelle membrane are in close proximity. Otherwise, bulk of the protein and lipid transport in cells is mediated by formation of vesicular transport intermediates.

As membrane are stabilized by hydrophobic interactions, bending or remodelling them requires a significant energy input, making spontaneous curvature thermodynamically unfavourable. Hence, specific set of curvature generating proteins facilitates this process by binding to the membrane and inducing curvature thus remodelling the flat surfaces into buds or tubules[10,11]. These curved regions are eventually pinched-off from the parent membrane with the help of fission proteins[12,13]. The newly formed vesicles are transported along microtubule tracks to their target compartments, where the fusion proteins mediate their fusion with the acceptor membrane[14].

The sequence, from vesicle budding at the donor compartment to fusion at the acceptor compartment, defines vesicular trafficking. This process is critical for maintaining cellular organization and function and is carried out by a vast set of proteins.

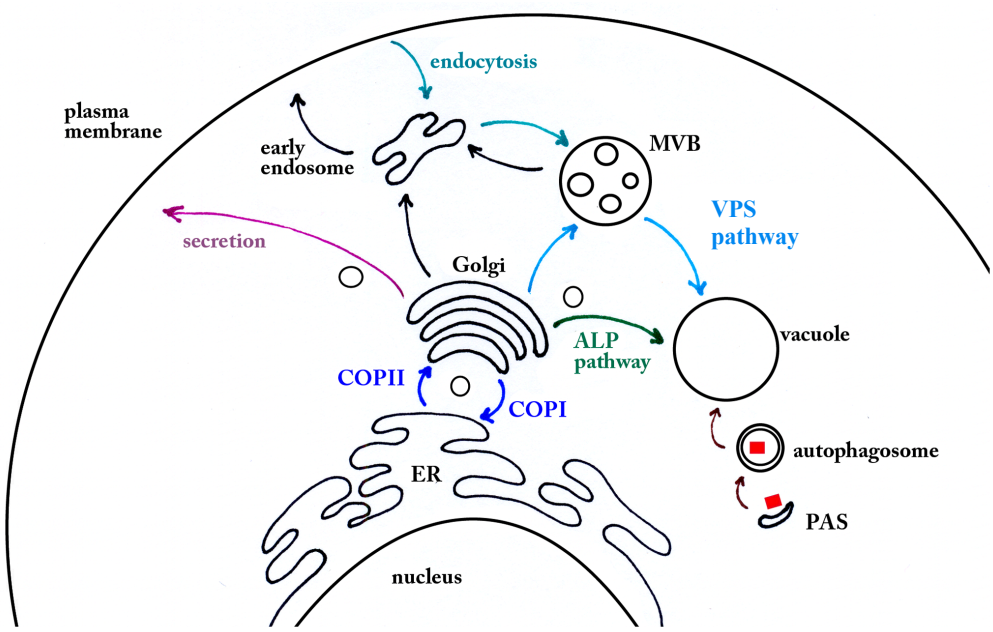

Figure 1.1 Schematic depiction of various vesicular transport pathways in yeast. The endoplasmic reticulum (ER) is the site for protein synthesis and initial processing before transport to the Golgi via COPII-coated vesicles. COPI-coated vesicles mediate retrograde transport between the Golgi and ER. Secretory vesicles facilitate protein export to the plasma membrane. Endocytosis allows the uptake of extracellular materials through the formation of the early endosomes, and proteins destined for degradation follow the endosome maturation and multivesicular bodies (MVBs) to reach the vacuole. Some vacuolar resident proteins take the VPS pathway to reach the vacuole, while the ALP pathway directs membrane proteins to the vacuole. In the autophagy pathway, pre-autophagosomal structure (PAS) becomes autophagosomes and eventually fuses with the vacuole to release cellular components for degradation. These pathways show the complexity and coordination required for maintaining cellular homeostasis through vesicle-mediated transport. Figure reproduced from Hecht et al., 2014[15].

1.2 Screens for understanding players in vesicular transport

Early insights into vesicle-mediated transport came from negative electron micrographs of pancreatic cells by George Palade, which revealed the distinct morphologies of organelles and the presence of vesicular intermediates[16]. Later, various genetic, biochemical and cellular based studies widened our understanding on the players involved in vesicular transport pathways across organelles. However, studying vesicular trafficking in higher order eukaryotes posed challenges due to the redundancy of protein orthologs and splice variants. Some of the initial understanding came about from the random mutagenesis screens conducted in yeast strain *S. cerevisiae* using simple phenotypes as readouts. Having single copies of genes and a highly conserved proteome compared to mammalian cells, along with robust genetic manipulation

techniques made yeast a good model for dissecting the molecular mechanisms of vesicular transport. Some of the major screens in this regard are the SEC screen, the Autophagy screen and the VPS screen.

1.2.1 SEC screen for proteins involved in secretory pathway

The initial screen that shed light on vesicular transport is the SEC screen that identified the players involved in the secretory pathway. In these studies, Randy Schekman and Peter Novick observed that mutations in specific genes led to the accumulation of vesicles within the cell at non-permissive temperature of 37 °C [17]. This led to conducting a random mutagenesis screen on yeast and isolated strains exhibiting this vesicle accumulation phenotype. Backtracking the mutations responsible for these defects led to identifying 23 complementation groups, now known as SEC genes[18], critical for the secretory process. The SEC screen provided key insights into the secretory pathway, starting from endoplasmic reticulum to plasma membrane via the Golgi. Mutation in any of the SEC gene blocks the secretory transport pathway, causing intracellular enrichment of secretory proteins, and vesicle accumulation at various stages of the pathway[19].

1.2.2 Autophagy screen

Another pivotal genetic screen that has deepened our understanding of intracellular trafficking is the autophagy screen. Autophagy is a conserved cellular process through which cells degrade and recycle their cytoplasmic components, including damaged organelles, to maintain homeostasis and ensure survival under nutrient-deprived conditions[20]. Although the initial understanding about autophagy process was in the field from 1960's, there was few understanding about the exact process or the players involved in it[21]. The initial understanding of the proteins involved in autophagy arose from the autophagy screen in protease-deficient yeast strains. Under nitrogen starvation, protease-deficient stains were observed to accumulate numerous small vesicular structures, termed autophagic bodies, within the vacuole. Such structures were transient in wild-type cells, as vacuolar proteases rapidly degrade them[22]. The accumulation of autophagic bodies inside the vacuole, provided a clear and quantifiable phenotype to understand autophagy related proteins.

A random mutagenesis screen using the absence of autophagic bodies during nitrogen starvation as the primary readout led to the identification of autophagy-related (ATG) genes critical for the autophagic process[22,23]. Each ATG gene encodes a protein that contributes to

distinct steps in autophagy, from the initiation of autophagosome formation to the eventual fusion of autophagosomes with the vacuole[24–26].

The autophagy screen not only elucidated the molecular machinery underlying autophagy but also provided critical insights into how cells regulate intracellular trafficking during stress. The discovery of ATG genes have far-reaching implications, linking autophagy to essential cellular functions such as nutrient recycling and quality control[9]. Moreover, given the evolutionary conservation of many ATG proteins, these findings in yeast have laid the groundwork for understanding autophagy in higher order eukaryotes and its relevance to human health, including its roles in neurodegeneration, cancer, and infectious diseases[9,27].

1.2.3 Vacuolar protein sorting and the VPS screen

Endosomal protein sorting is a highly orchestrated process essential for maintaining lysosome integrity by ensuring the selective trafficking of proteins and lipids within the endomembrane system. It relies on continuous membrane remodelling, which includes precise cargo selection, membrane deformation, and a series of fission–fusion events that generate vesicular and tubular carriers[28].

Soluble lysosomal proteins in higher order eukaryotes and vacuolar resident proteins in yeast are delivered to their destinations via the vacuolar protein sorting (VPS) pathway. The current model of the VPS pathway in yeast indicates that the pathway begins at the Golgi, where specific receptors recognize proteins destined for the vacuole. These protein–receptor complexes are then packaged into vesicles through budding and fission events, which transport them from the Golgi to early endosomes. Endosomes fuses with the pre-vacuolar compartment (PVC), releasing the soluble cargo. Finally, the PVC merges with the vacuole, delivering the proteins to their functional destination. Further, the receptors are retrieved back from the PVC to the Golgi, thereby allowing for repeated rounds of protein sorting[29–32].

This cycle of vesicle formation, transport, and fusion from the Golgi to the endosome and back is crucial for maintaining the proper composition and function of the vacuole. Mutation in any component of the VPS pathway disrupts and lead to the mislocalization of vacuolar hydrolases via secretory pathway to outside the cell rather than its delivery to the vacuole[32]. The foundational understanding of the VPS pathway emerged from pioneering genetic screens conducted in the 1980s independently by Tom Stevens and Scott Emr. These researchers employed random mutagenesis in yeast and selected mutants that mis-localized CPY to the

secretory pathway as a clear and quantifiable phenotype[33,34]. The VPS screen identified approximately 40 distinct VPS proteins, originally named Vps1 through Vps40, in the order of their discovery[32,35]. Later more proteins involved in the VPS pathway were identified[36]. These studies mapped out the components required for proper vacuolar protein sorting and highlighted the intricate network of interactions necessary for vesicular trafficking within the cell.

1.3 Vacuolar protein sorting1 (VPS1)

Vacuolar protein Sorting 1 (Vps1) was the first protein identified in the vacuolar protein sorting (VPS) screen[32,33] and has since emerged as a pivotal regulator of multiple intracellular trafficking pathways. Deleting the VPS1 gene results in various phenotypes, including pronounced growth defects at non-permissive temperatures (37 °C)[37], highlighting its essential role in cellular function. One of the critical functions of Vps1 is in the retrieval of the CPY receptor, Vps10, from the vacuole back to the Golgi. Vps10 is a transmembrane protein that acts as receptor for CPY and other soluble hydrolases, and essential for the effective transport of these hydrolases from Golgi to the vacuole[38]. In the wild-type (WT) cells, Vps10 exhibits a punctate localization at the Golgi and endosomes. Whereas, in *vps1Δ* strains, Vps10 accumulates in the vacuole, indicating a failure in receptor recycling to the Golgi[31,39]. Imaging Vps1 inside cells shows Vps1 colocalization with retromer-coated tubules at the endosome, and in the absence of Vps1, retromer/SNX4/Mvp1-coated tubules become unusually long-lived, suggesting a defect in the membrane fission required for the release of the tubules[30,39,40].

Vps1 functions extend beyond vacuolar protein sorting, encompassing roles in the maintenance of vacuolar morphology[41,42]. Vps1 deletion shows vacuolar fragmentation under steady-state conditions. During osmotic stress, where the wild-type vacuoles typically fragment, Vps1 deletions inhibit vacuole fragmentation[41]. Vps1 also interacts with SNARE complexes, which are crucial for vacuolar fusion, and are required for SNARE complex interaction with the vesicle tethering complex at the site of fusion[41,43,44]. Further studies suggest that these effects likely result from disrupted vacuolar membrane organization and protein recycling rather than a direct fusion function of Vps1[31]. Both Vps1 and retromer deletions cause similar vacuolar defects, including SNARE mislocalization and fusion impairments, which can be rescued by external addition of SNAREs. This indicates that Vps1 deletion leads to vacuole fragmentation and fusion defects as secondary consequences of altered membrane homeostasis and SNARE recycling.

Vps1 deletion also affects peroxisome fission. EM studies show the accumulation of giant peroxisomes upon Vps1 deletion[45]. Vps1 is thought to act on the peroxisome by interacting with Pex19, a shuttling receptor for peroxisomal membrane proteins and Peroxisomal membrane protein Pex27[46,47]. Furthermore, deletion of Vps1 and Dnm1 completely blocks peroxisomal fission, highlighting its essential role in this process[48].

Some reports suggest the involvement of Vps1 in secretory pathway, as disruptions in VPS1 or Clathrin heavy chain (CHC1) genes prevent the formation of a subset of secretory vesicles in yeast and cause mislocalization of invertase proteins[49,50]. Additionally, Vps1 is thought to facilitate membrane invagination and fission during endocytosis. Vps1-deficient cells show impaired endocytic degradation and delayed endosomal cargo trafficking[51–54]. Vps1 also shows direct interaction with the BAR-domain-containing protein Rvs167, crucial for endocytosis.

Moreover, Vps1 is critical for autophagy[55]. *vps1Δ* strains exhibit a complete block in autophagy and show an altered distribution of lipid scramblase Atg9 protein essential for the growth of the pre-autophagosomal structure (PAS)[56]. Split-GFP experiments further confirm a direct interaction between Vps1 and Atg9, underlining its fundamental role in the regulation of autophagy.

1.4 Mechanism of Dynamin-mediated membrane fission

Vps1 belongs to the dynamin superfamily of proteins, which share a GTP-binding G-domain[37,57]. Classical Dynamins are well-studied in higher order eukaryotes. They utilize GTP hydrolysis to constrict membrane, leading to fission and are a key player in receptor-mediated endocytosis[58,59]. The domain architecture of classical dynamins includes a globular G-domain, stalk domain, bundle signalling element (BSE), Pleckstrin Homology (PH) domain, and proline-rich domain (PRD) (Figure 1.3.A).

In vitro studies with purified dynamin reveal that its stalk domain has an intrinsic tendency to self-associate. In solution, this leads to tetramer formation, whereas on membrane surfaces, it promotes the assembly of extensive helical polymers[63,64] (Figure 1.3.C). The resulting helical scaffold exhibits several-fold higher GTPase activity, called stimulated GTPase activity, arising from cooperative interactions between adjacent G-domains[65,66]. This conformational change in the G-domain induces bending in the BSE, aligning the G-domain and BSE more closely and transmitting mechanical force to the membrane. This force causes the PH-domain

at the foot region to embed deeper, promoting progressive constriction and destabilization until a twisting force ultimately severs the membrane[12,65,67] (Figure 1.3.B).

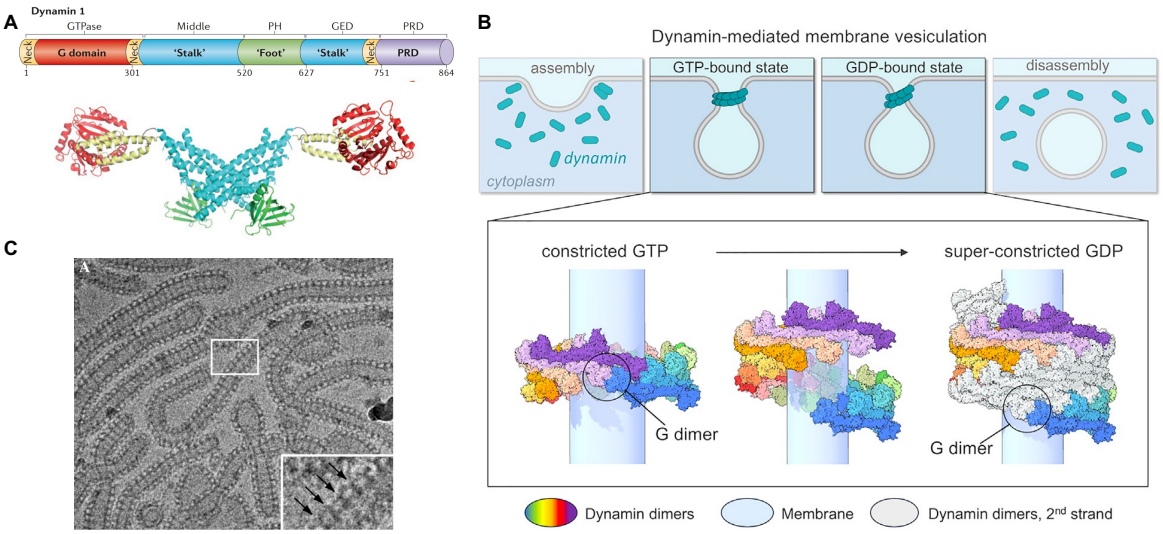

Figure 1.2 Dynamin1 domain organization and membrane fission mechanism A) Domain architecture of Dynamin1 highlighting the GTPase (G) domain, stalk, PH domain, GED, and PRD and the ribbon diagram of the dynamin dimer, colour-coded by domain. Image reproduced from Ferguson and Camilli, 2012[60] B) Cartoon depicting the GTP-driven cycle of dynamin assembly, membrane constriction, and eventual fission. Image reproduced from Jimah et al., 2024[61] C) Electron micrograph showing the Dynamin helices around membrane tubules. Image reproduced from Danino et al., 2004[62].

Cryo-EM structures of Dynamin super-constricted state on membrane show that increased bending of BSE forces the stalk to push the foot further into the membrane, and slight rotations at stalk interfaces allow the scaffold to adapt to varying curvatures by modulating helical pitch and width[61,68]. Moreover, mutations that lock the BSE in a bent conformation arrest fission at a hemi-fission intermediate, while mutations preventing bending impede endocytosis, showing the importance of BSE in Dynamin's mechanical force generation[61,68,69]. Thus, elaborate studies in the past lay a framework for understanding how dynamin-generated mechanical stresses lead to membrane constriction and scission.

1.5 Vps1 structure

Vps1 shares several architectural principles with the classical dynamins, including the G-domain, BSE, and the stalk region. However, in contrast to the classical dynamins, the membrane-binding PH domain is replaced in Vps1 by an unstructured loop region known as InsertB[70,71](Figure 1.4.A). Similarly, the PRD, which interacts with SH3-containing partner

proteins in other dynamins, is absent in Vps1. Despite these structural differences, Vps1 binds to GTP and forms oligomers in solution[70] (Figure 1.4.B).

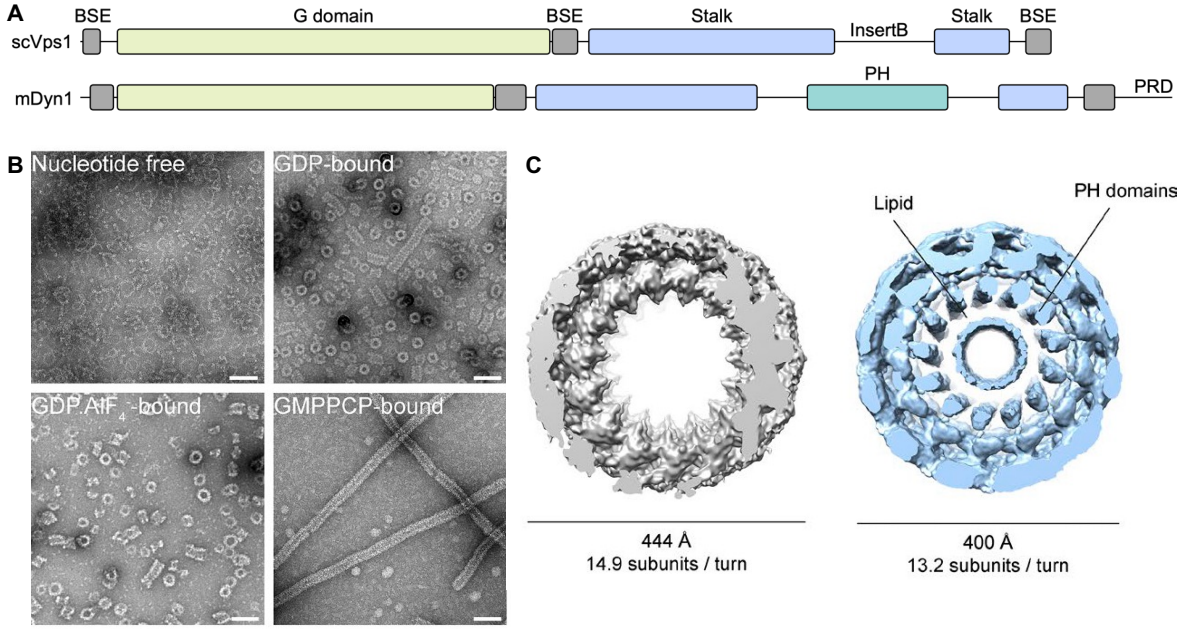

Figure 1.3 Structural organization of Vps1. A) Schematic comparison of domain architectures in classical dynamins versus Vps1. While classical dynamins possess a G-domain (green), bundle signalling element (BSE, beige), stalk region (blue), pleckstrin homology (PH) domain (grey), and proline-rich domain (PRD, black), Vps1 replaces the PH domain with an unstructured loop called InsertB and lacks the PRD. B) Representative electron micrographs (EM) of a minimal *C. thermophilum* Vps1 construct in nucleotide-free, GDP-bound, GDP·AlF_4^--bound, and GMPPCP-bound states. C) CryoEM reconstruction of Vps1 helices in solution highlights the open architecture and larger pitch compared to classical dynamin helices formed on PS membrane. Vps1 helices exhibit outer diameters of ~44.4 nm in GMPPCP bound state compared to 40 nm outer diameter of dynamin. Image reproduced from Varlakhanova et al., 2018[70].

Structural studies on a minimal *C. thermophilum* construct show that the Vps1 GG domain forms dimers via its GTPase regions, and nucleotide binding triggers conformational changes that are further transmitted to the BSE. In the GMPPCP and GDP·AlF_4^- states, the BSE adopts an open conformation, while it becomes disordered in the GDP-bound form. Furthermore, Vps1's BSE is rotated further from the core compared to dynamin, resulting in a more open architecture. CryoEM analysis of full-length Vps1 in solution reveals that the protein forms heterogeneous, curved filaments in the absence of nucleotides. With GDP or GDP·AlF_4^-, it assembles into rings and short stacks with outer diameters of 41–44 nm and lumenal diameters of 17–21 nm. In contrast, incubation with GMPPCP produces extended helices with a lumenal

diameter of 19.1 nm and an outer diameter of 42.4 nm. These helices have more subunits per turn and larger pitch compared to Dynamin1 bound to PS-containing membrane[70] (Figure 1.4.C). Concisely, Vps1 helices display an increased pitch, greater tilt of the BSEs and stalks, and a more open architecture with a larger outer diameter compared to dynamin.

1.6 Rationale

Despite the fact that cellular studies have demonstrated Vps1's involvement in various trafficking processes, the precise mechanistic effect of Vps1 in membrane dynamics and protein sorting remains unclear. In the upcoming sections of the thesis, I try to understand the effect of Vps1 on membrane topologies and correlate these findings with its cellular functions. By bridging the gap between structural and functional analyses, this study aims to elucidate deeper insights into the molecular mechanisms of Vps1 and its contributions to vacuolar protein sorting.

Chapter 2
Materials and Methods

2.1 Bacterial constructs, cloning, and plasmids

For bacterial expression, all constructs used in the study were cloned separately into a pET15b vector with an amino-terminal (N-terminal) hexa-Histidine (6xHis) and a carboxy-terminal (C-terminal) StrepII tag downstream of a T7 promoter, containing an ampicillin selection marker. The clones were generated using restriction free cloning and involves homologous recombination.

2.2 Protein expression, purification, and Fluorescent labelling

All constructs were expressed in *E. coli* T7 Express (BL21 DE3) (NEB, Cat No. C2566I) using IPTG induction. Briefly, plasmids were transformed into *E. coli* T7 Express (BL21 DE3) and grown in LB medium (HiMedia, Cat No. M1245) as primary cultures until saturation. These cultures were used to inoculate 1 L secondary cultures. Cells were grown to mid-log phase (OD 0.6–0.8) at 37 °C, induced with 0.1 mM IPTG (Sigma, Cat No. I6758), and incubated overnight at 22 °C. After 12–16 hours, cultures were pelleted and stored at -40 °C.

For protein purification, frozen pellets were thawed and resuspended in 500 mM HBS (20 mM HEPES, pH 7.4; 500 mM NaCl) containing 1% (w/v) Triton X-100 and 1% PMSF. Cells were lysed by sonication (60% amplitude, 1 s on /3 s off pulses) until reached homogeneity. The lysate was centrifuged at 30,000 × g for 20 min to remove unlysed cells and membrane fractions. Further, the supernatant was loaded onto a 5 mL Strep-Trap HP column (GE Lifesciences, cat No. 28-9075-48) or a Streptactin XT column. After loading the supernatant, the column was washed sequentially with 100 mM EDTA in 500 mM HBS and then with 500 mM HBS. The buffer was exchanged to 150 mM HBS (20 mM HEPES, pH 7.4; 150 mM NaCl). After equilibration, the protein was eluted using either 2.5 mM Desthiobiotin (Sigma, Cat No. D1411-1G) or 5 mM Biotin (HiMedia, Cat No. CMS095-25G) in 150 mM HBS. Protein was purified with relatively good purity and yield as observed on an SDS-PAGE gel.

2.3 Liposome preparation

Lipids 1,2-dioleoyl-sn-glycero-3-phosphocholine (DOPC), 1,2-dioleoyl-sn-glycero-3-phospho-L-serine (sodium salt) (DOPS) and 1,2-dioleoyl-sn-glycero-3-phospho-(1′-myo-inositol-3′-phosphate) (ammonium salt)18:1 (PI(3)P) were purchased from Avanti Polar Lipids. The UV-activable diazirine-containing fluorescent lipid probe conjugated with TMRE (TDPE) was prepared in the lab by using SDA-diazirine (Sigma, 803413) and TopFluor TMR

PE, (Sigma, 810241P) as described before[72,73]. Lipids in desired amounts were aliquoted in chloroform stocks and added to the bottom of a clean glass test tube to a final concentration of 0.5 mM. Required lipids DOPC, DOPS, PI(3)P and TDPE were aliquoted in the proportion of DOPC:DOPS:PI(3)P:TDPE::79:15:5:1 mol% for PI(3)P-containing membrane, DOPC:DOPS:TDPE::84:15:1 mol% for PS-containing membrane and DOPC:TDPE::99:1 for PC membrane. The chloroform mixture was dried to generate a thin film in the bottom of the test tube and kept for drying under vacuum for 3 hours. Required amount of filtered Millipore water was added to the glass test tube and kept for hydrating in a water-bath for 30 min at 50 °C. The mixture was then vortexed vigorously and extruded using an extrusion apparatus through a 100nm polycarbonate filter (Whatman, 800309).

2.4 Proximity-based labelling of membrane associated proteins (PLiMAP)

Membrane binding was performed using Proximity-based labelling of membrane associated proteins (PLiMAP) assay as mentioned in Jose et al. (2020)[72,73]. Proteins were incubated with indicated liposomes at a ratio of 1:100 in 150 mM HBS (20 mM HEPES-NaOH, pH 7.4, 150 mM NaCl) for 30min at RT in the dark. Samples were irradiated with UV (365nm) (UVP crosslinker CL-1000L) at an intensity of 200 mJ cm−2 for 1 minute to crosslink membrane bound protein to TDPE. Samples were run on SDS-PAGE and gels were first imaged using Typhoon Laser-scanner for Tetramethylrhodamine fluorescence. Further the gels were stained with Coomassie brilliant blue and imaged. Data was analysed using graphed prism.

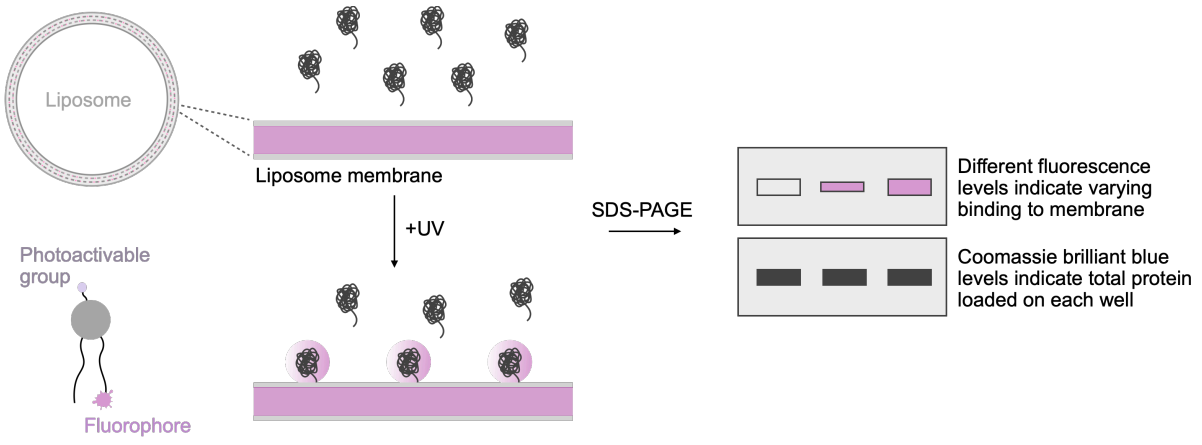

Figure 2.1 Schematic depiction of the workflow of a PLiMAP assay. Proteins are incubated with the indicated liposomes carrying the photoactivatable lipid TDPE at a 1:100 molar ratio for 30 min at room temperature in the dark, UV exposed to crosslink membrane-bound protein. Samples are separated by SDS-PAGE and imaged first for TDPE fluorescence and Coomassie staining to visualize total protein. Image modified from Jose et al., (2020) [72]

2.5 GTPase activity assay

Proteins (1 µM) were mixed with GTP (Jena Biosciences, Cat No. NU-1012) (1 mM) in the absence or presence of liposomes (100 µM) in 20 mM HEPES, pH 7.4, 150 mM NaCl, 1 mM $MgCl_2$ and incubated at 30 °C. 20µl aliquots were taken at regular intervals and the reaction was quenched with 10µl of 0.5 mM EDTA, pH 8.0. The released inorganic phosphate or thiophosphate was assayed with the malachite green reagent using Na_2PO_4 as a standard[74].

2.6 Supported membrane templates (SMrT) preparation and assays

Supported membrane templates (SMrT) were prepared in a flow-cell as described earlier[75,76]. Required lipids DOPC, DOPS, PI(3)P, and Texas-Red DHPE (TxRd-DHPE) (Invitrogen, Cat No. T1395MP) were aliquoted in the proportion of 79:15:5:1 mol% respectively, and diluted to 1 mM total lipid concentration using chloroform in a glass vial and stored at -40 °C. 1.2 µl of this mix was spotted on a passivated coverslip covalently conjugated with PEG400 and dried. The coverslip was assembled in a Bioptech FCS2 chamber. Chamber was hydrated using 150 mM HBS buffer and tubes were formed by shear flow of the buffer. The flow was stopped and the nanotubes were allowed to settle. The source where lipid spotted becomes planar supported bilayer (Figure 2.2).

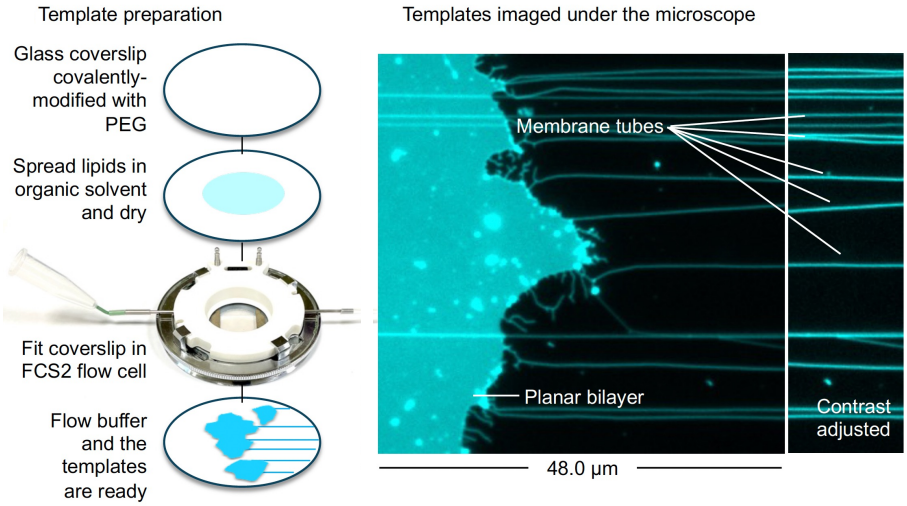

Figure 2.2 Schematic depiction of preparation of supported membrane templates and templates viewed under microscope. Image adapted from Swaminathan and Pucadyil. (2024) [77].

Vps1 was flowed in at a final concentration of 0.5 µM in the presence of 1 mM GTP and 1 mM MgCl2 in 150 mM HBS buffer. Images were acquired 10 min post-incubation unless mentioned. For timelapse imaging, the buffer containing an oxygen scavenger cocktail was

used. Images were acquired on an Olympus IX83 microscope attached to pE-4000 (CoolLED) light source and an Evolve EMCCD camera.

For fluorescent labelling, Alexa488 C5-maleimide or Alexa594 C5-maleimide (Invitrogen, Cat No. A10254 or A10256) stock solutions were prepared by arbitrarily dissolving a minute amount (on a tip) of the dye powder in 10 µl DMSO. The concentration of this stock was estimated in methanol after appropriate serial dilution using the corresponding absorbance maxima peaks obtained on the UV spectrophotometer. For the labelling reaction, purified and freshly spun Vps1 was incubated with fivefold molar excess of the respective dye in 150 mM HBS. This mix is incubated for 5min before adding to SMrT templates with 1mM of appropriate nucleotides (1 mM) and $MgCl_2$ (1mM). The mix was incubated with templates for 15 min, washed extensively to remove excess dye and images were acquired.

2.7 Yeast strains and plasmids

All yeast strains used in the study are listed in Table 1. All plasmids used for yeast genome modification are listed in Table 2. All yeast genome manipulations are done following protocols from Geitz et al. (1993)[78].

2.8 Primer designing for endogenous tagging

For gene deletion and endogenous protein tagging, primers were designed following the protocol by Janke et al. (2004)[79]. Briefly, for VPS1 deletion, two primers (S1 and S2) were generated. The S1 primer consisted of 50 bases upstream of the VPS1 start codon (including the start codon) followed by 5′-CGTACGCTGCAGGTCGAC-3′. The S2 primer was the reverse complement of 50 bases downstream of the VPS1 stop codon (including the stop codon), followed by 5′-ATCGATGAATTCGAGCTCG-3′. A similar strategy was used to introduce tagged VPS1 constructs at the endogenous locus. The desired mutants and selection marker were amplified using S1/S2, and the resulting PCR product was transformed into a *vps1Δ* strain (where VPS1was replaced by a HIS3 cassette). Recombination at the endogenous locus replaced the HIS3 cassette with the tagged VPS1 or mutants and selection marker.

For C-terminal tagging with mNeonGreen or mScarlet, the S3 primer was created by stitching 50 bases downstream of the gene locus (excluding the stop codon) to 5′-CGTACGCTGCAGGTCGAC-3′. The S2 primer remained the same as above.

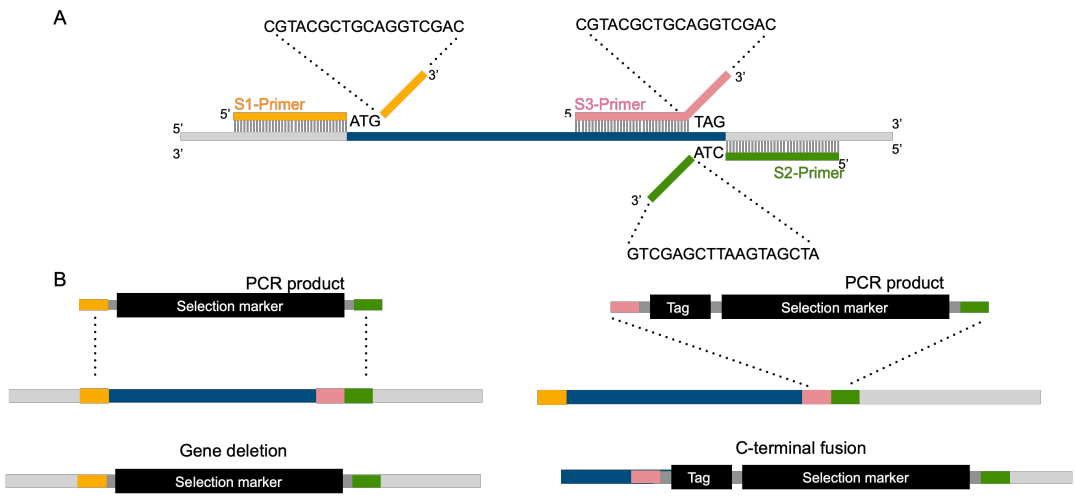

Figure 2.3 Schematic of a yeast gene deletion and genomic tagging strategy using homologous recombination. A) Primer pairs S1/S2 flanks the gene of interest (GOI). Primer pair S3/S2 marks the 3' of the GOI. B) Using homologous recombination, PCR amplicons with S1/S2 flanking regions replace the GOI with the selection marker. Likewise, PCR amplicons with S3/S2 flanking regions add specific tags to the GOI at 3', followed by a selection marker. Image reproduced from Janke et al., (2004)[79].

2.9 Competent cell preparation

Cells were grown on 2-5 ml YPD (1% Yeast extract powder, 2% Peptone, 2% Glucose) media overnight to saturation. Secondary was inoculated from the above primary culture with initial 0.1-0.2 OD and were grown to mid-log phase (0.6-0.8OD) in YPD. Cells were pelleted and washed with half initial volume autoclaved deionized water and further washed with one-fourth initial volume Lithium acetate sorbitol (Li-Sorb) solution. After washing, cells are resuspended in 300 µl of Li-Sorb solution containing 2mg/ml denatured salmon sperm DNA. 50µl of competent cells were aliquoted in autoclaved 1.5ml tubes, frozen and stored at -80°C for use.

Yeast Transformation: Competent cells were thawed at RT for 30 min and mixed with 5-10µl of PCR product or 500 ng of digested plasmid. Cells were incubated for 15 min at RT and 300 µl of Lithium acetate-40% PEG solution (Li-PEG) was added. The solution was vortexed and incubated for 15 min at RT. After incubation 30 µl of DMSO was added, vortexed and incubated at 42 °C for 12-15 min for heat-shock. Furthermore, Cells are pelleted at 3200 x g for 3 min and supernatant was discarded. In case of auxotrophic selection, the pellet was resuspended in 1X DPBS (Thermo, Cat No.14190250) and plated onto agar plates with appropriate selection media. For antibiotic selection, cells were resuspended in 1ml of YPD media and incubated for 12 hours, at 30°C on shaking. Cells are pelleted at 3200 x g for 3 min,

resuspended in 200µl of YPD and plated onto agar plates with appropriate antibiotic selection. After 2-3 days colonies were observed and screened using standard protocols.

2.10 Yeast cell imaging

Cells were grown on 2-5 ml of appropriate media overnight to saturation. Secondary was inoculated from the above culture with initial 0.1-0.2 OD and were grown to mid-log phase (0.6-0.8OD). 1.5 ml of culture was spun and resuspended in 200 µl X DPBS.

Concanavalin A coating: 8-well Lab-Tek chambers (Thermo-Fischer, Cat No. 155409) were etched with 5 N NaOH for 30 min and rigorously washed with deionized water. Lab-Tek chambers were then incubated with 0.5 mg/ml of Concanavalin A (ConA) (lectin from *Canavalia ensiformis*; Sigma, Cat No. L7647) in 1X DPBS solution for 30 min and washed with 1X DPBS solution. Washed cells were incubated with this ConA coated surface for 30 min and washed with 1X DPBS 3-5 times, added 200 µl 1X DPBS and imaged.

Cell imaging: Imaging was carried out on 1.4 NA oil immersion objective on a motorized Olympus IX83 microscope attached to a pE4000 (CoolLED) light source and a Evolve EMCCD (Photometrics) camera or through 100x, 1.4 NA oil immersion objective on a motorized Olympus IX83 microscope attached to a pE300 Ultra (CoolLED) light source and a Clarity laser-free spinning disk module (Aurox) and an Orca Flash 4.0 S-CMOS camera (Hamamatsu). Images were processed using FIJI ImageJ and analyzed using GraphPad prism.

Quantification of protein localization to vacuole: All images were background subtracted and channels split. Vph1 channel (marking the vacuole) was duplicated and set as mask. Mean intensities from cargo protein and Vph1 channels were measured separately with the mask generated. Ratio of Cargo mean fluorescence intensity to Vph1 mean fluorescence intensity was plotted. All values were normalized to WT median.

2.11 Spot assay

Spot assay was performed as per Xu et al (2014)[80] with modifications. Briefly, cells are grown to mid log phase (0.6-0.7 OD) to an equal OD, pelleted and resuspended in MilliQ to a final OD of 0.6. The cultures were diluted sequentially to 10^{-5} times by mixing 10 µl of cultures to 90 µl of MilliQ in a 96-well plate. Further, 5 µl of the culture were spotted on YPD media containing agar plate. The spotting was repeated on a replica plate. The plates were grown at 30 °C and 37 °C for 2 days and imaged.

2.11 Western blotting

Cells were grown to mid log phase (0.6-0.8 OD) to an equal OD. Cells were then spun at 3200 xg for 5 min at 4 °C and pellet was resuspended in 800 µl of cold autoclaved deionized water. Immediately, added 150µl of 1.85N NaOH, vortexed and kept at ice for 5 min. After addition of 150 µl of 55% w/w Trichloro-acetate (TCA), cells were vortexed and kept at ice for 10 min. The precipitated fraction was spun at 18000 xg for 20 min at 4°C and supernatant was discarded. An empty spin was provided at 18,000 xg for 5 min to remove residual TCA. The pellet was further resuspended in HU-DTT buffer (8M urea, 5% SDS, 200mM Tris-HCl (pH 6.8), 0.1mM EDTA, bromophenol blue,10mM DTT) and boiled at 99 °C for 20 min. Equal volume of the sampple was loaded and resolved on a 10% SDS-PAGE gel and transferred to PVDF membrane using standard protocols. Blocking was done using 5% skimmed milk in 1X TBST (1X Tris Buffer Saline, 0.1 Tween-20). The blots were incubated with recommended dilutions of anti-ALFA-HRP for 3 hrs in 5% Skimmed milk. Blots were washed 3 times with 1X TBST and directly processed for imaging using SuperSignal™ West Pico PLUS Chemiluminescent Substrate (Thermo-Fischer, Cat No. 34580) and imaged using iBright-1500 (Invitrogen).

2.13 Vacuole isolation and mass spectrometry

Vacuole isolation: Cells were grown to mid log phase (0.6-0.8 OD), pelleted, resuspended in DTT solution (0.1mM Tris (pH 9.4), 10mM DTT) and incubated at 30°C water bath for 20 min. Cells were then spun at 3200 xg for 5 min and supernatant was discarded. To get spheroplasts, cells were resuspended in Spheroplasting buffer (0.1x YPD, 0.6M Sorbitol, 50Mm Potassium phosphate, pH 7.5) with 1mg/ml Lyticase (L4025-25KU) and incubated for 30 min at 30°C in water bath. Spheroplasts were pelleted at 5300 xg for 5min and resuspended in 15% Ficoll (w/v) in PS buffer (10 mm Pipes/KOH (pH 6.8), 200 mM Sorbitol) with 0.4 mg/ml DEAE dextran (Sigma, Cat No. 93556-1G) and shifted to Beckman Coulter SW 40 tubes. This was incubated in ice for 5 min and then shifted to 30 °C for 1.5 min. A step gradient of 8% Ficoll, 4% Ficoll, 0% Ficoll in PS buffer was layered on top of the mixure. Tubes were placed in SW40 rotor and spun at 1,20,000 xg for 90 min at 4°C. The interface between 0% and 4%, enriched vacuoles was collected and processed for mass spectrometry

Mass spectrometry sample preparation**:** Vacuole fractions were solubilized using 1% Triton X-100 and protein concentration was measured by BCA using BSA as a standard. 50ug of protein was precipitated using Chloroform: Methanol precipitation and pellets from the precipitation

were resuspended in 100 mM TEAB buffer containing 8 M Urea. 5 mM of DTT solution was added to the mix and incubated at 60 °C for 30 min. Samples were cooled down to RT and 15 mM of Iodoacetamide was added and incubated in dark for 15 min. The solution was diluted to a total of 1 M Urea by addition of TEAB. Mixture was incubated with sequencing grade modified Trypsin (Promega, Cat No. V5111) 0.5mg/ml at 37 °C for 16 hr.

Heavy and light labelling: 4% of 0.6M NABHCN with 4% of Formaldehyde-D2 (heavy) or Formaldehyde (light) were added to Trypsin digested solution and incubated at RT for 60 min. After incubation, 4x initial NABHCN volume of 1% of ammonium hydroxide was added along with 1% Trifluoro acetic acid to quench the reaction. The solution was spun at 18000 x g for 20 min at RT to get rid of particulate matter and supernatant was collected. Equal volume of supernatant from heavy and light fraction were mixed and the resultant solution is desalted using C18 column twice, dried and stored in -80 °C.

The stored peptides were resuspended in 0.1% formic acid (FA) and analyzed in a Sciex Triple-TOF6600 mass spectrometer interfaced with an Eksigent nano-LC 425. The trypsin-digested peptides were first flown thorough a Eksigent C18 trap column (to get rid of any common contaminants) and eluted onto an Eksigent C18 analytical column in a linear acetonitrile gradient. All proteomic data acquisition was done in an information-dependent acquisition (IDA) mode over a selected and specified mass range of 300-2000 *m/z*. Each MS survey was followed by a MS/MS scan of 10 peptides with the highest intensity. Peptide identification and quantitation was done using Protein Pilot software.

Mass spectrometry analysis: A Uniprot S. cerevisiae protein database (release date:2021) was used for peptide identification. Data from 6 technical repeats were added and analysed together in protein pilot software. Iodoacetamide was specified as alkylating agent and dimethylation was specified as extra modification. Identification was performed on peptides filtered with <1% FDR. The proteins were sorted first based on the number of peptides. Proteins with >1 peptide number were considered and further scored based on decreasing heavy to light ratio. Further a p-value cut-off of 0.2(-log10 scale) was used. Proteins with scores above 2 were considered enriched in vacuoles, below 0.5 were considered depleted in vacuole, and the ones between 0.5-2 were considered levels unchanged. The list of enriched or depleted proteins were further sorted based on membrane/soluble proteins.

2.14 Yeast lysate preparation and biochemical fractionation

Yeast lysate preparation: Yeast cells were grown using culture conditions described above. After cells in 1 L secondary cultures were grown to mid log phase (0.6-0.8 OD), the cells were pelleted at 5000 rpm and stored at -40 °C. For yeast lysate preparation, the cell pellet was thawed and lysed by sonication in breaking buffer (250mM Tris, 500mM KCl, 5mM EGTA and 5mM EDTA; pH 8.0) with a protease inhibitor cocktail (Roche, Cat No. 5892791001) and 5mM β-mercaptoethanol. The lysate was spun at 1,60,000 g for 45 min at 4 ºC, and the supernatant was desalted using a HiPrep 26/10 desalting column (GE Lifesciences, Cat No. 17-5087-01) in 150 mM HBS. The cytosol prepared were flash-frozen and stored at -80 ºC until further use. The total protein concentration was estimated using the Pierce BCA Protein Assay Kit (Pierce, Cat No. 23227).

Biochemical fractionation: Yeast cytosol was fractionated using a Q-sepharose column (GE Lifesciences, Cat No. 11-0013-03) against a linear NaCl gradient of 150 mM to 1M in 20 mM HEPES (pH 7.4) buffer. These fractions were dialyzed overnight against 20 mM HEPES (pH 7.4) buffer containing 150 mM NaCl. Further, fraction 2 was resolved on a HiPrep 16/60 Sephacryl S-300 HR size exclusion column (GE Lifesciences, Cat No. 17-1167-01) in the same buffer. Fractions were stored at 4 °C.

2.15 Mass spectrometry of SEC fraction

Proteins in the SEC fraction showing peak activity was extracted by chloroform-methanol precipitation. Pellet was dissolved in 6M urea in 100 mM TEAB buffer, sonicated and spun down at 20,000g for 5 mins. Collected supernatant was reduced in 10 mM dithiothreitol (DTT) at 60 °C for 30 minutes, followed by addition of 20mM iodoacetamide (IAA) in dark at room temperature for 15mins for alkylation. The urea was diluted to 1M by addition of 100mM riethyl ammonium bicarbonate buffer (TEAB) (Sigma, cay no. T7408) and the proteins were further subjected to trypsin digestion (Sequencing grade modified trypsin, Promega, Cat No. V5111) at 37 °C for 16 hrs. Once digested, the sample was acidified using 1% trifluoroacetic acid and spun down at 20,000 xg for 20 min to separate the supernatant containing peptides. Sample was further processed by desalting in a column containing C18 resin (Empore C18), eluted in 60% acetonitrile, dried in a centrivap and stored in -80 °C.

The stored peptides were resuspended in 0.1% formic acid (FA) and analyzed in a Sciex Triple-TOF6600 mass spectrometer interfaced with an Eksigent nano-LC 425. The trypsin-digested

peptides (~5µg) were first flown thorough a Eksigent C18 trap column to get rid of any common contaminants and eluted onto an Eksigent C18 analytical column in a linear acetonitrile gradient. A typical LC run was of 240min at a flow rate of 200 nL/min in the presence of a gradient of acetonitrile (0%-60%) in 0.1% formic acid. All proteomic data acquisition was done in an information-dependent acquisition (IDA) mode over a selected and specified mass range of 300-2000 *m/z*. Each MS survey was followed by a MS/MS scan of 10 peptides with the highest intensity.

Peptide identification and quantitation was done using Protein Pilot software. A Uniprot S. cerevisiae protein database (release date:2021) was used for peptide identification. In Protein Pilot, iodoacetamide was specified as the alkylating agent and identification was performed on peptides filtered with <1% FDR. For identification of the protein of interest, first, proteins were sorted based on the number of peptides (>1 peptides were taken for further analysis). The list of proteins from all three independent runs were added to UNIPROT ID mapping to look for proteins that had membrane binding domains based on MBPPred software.

Table 2.1 Yeast strains used in the study

Strain	Genotype in detail	Source
ESM356	*MATa ura3-52 leu2Δ1 trp1Δ63 his3Δ200*	Gift from Dr. Saravanan Palani, IISc
PL1	*ESM356; vps1Δ::His3MX6*	This study
PL21	*ESM356; VPS10-mNG::KanMX6; VPH1-mScarlet::natNT2*	This study
PL22	*ESM356; vps1Δ::His3MX6; VPS10-mNG::KanMX6; VPH1-mScarlet::natNT2*	This study
PL32	*ESM356; VPS10-mNG::KanMX6; VPH1-mScarlet::natNT2; vps1Δ::6xHis-TEV-Vps1-StrepII-ALFA-hphNT1*	This study
PL33	*ESM356; VPS10-mNG::KanMX6; VPH1-mScarlet::natNT2; vps1Δ::6xHis-TEV-Vps1(G436D)-StrepII-ALFA-hphNT1*	This study
PL43	*ESM356; VPS10-mNG::KanMX6; VPH1-mScarlet::natNT2; vps1Δ::6xHis-TEV-Vps1(K42A)-StrepII-ALFA-hphNT1*	This study
PL34	*ESM356; VPS10-mNG::KanMX6; VPH1-mScarlet::natNT2; vps1Δ::6xHis-TEV-Vps1-Δ3K(591-593)-StrepII-ALFA-hphNT1*	This study
PL35	*ESM356; VPS10-mNG::KanMX6; VPH1-mScarlet::natNT2; vps1Δ::6xHis-TEV-Vps1(ΔInsertB(579-587)-StrepII-ALFA-hphNT1*	This study
PL44	*ESM356; VPS10-mNG::KanMX6; VPH1-mScarlet::natNT2; vps1Δ::6xHis-TEV-Vps1-InsB Δ(536-579)-StrepII-ALFA-hphNT1*	This study
PL45	*ESM356; VPS10-mNG::KanMX6; VPH1-mScarlet::natNT2; vps1Δ::6xHis-TEV-Vps1-InsB Δ(536-612)-StrepII-ALFA-hphNT1*	This study
PL54	*ESM356; VPH1-mScarlet::natNT2; ALFA-NB-mNG::LEU2; vps1Δ::6xHis-TEV-Vps1-StrepII-ALFA-hphNT1*	This study
PL55	*ESM356; VPH1-mScarlet::natNT2; ALFA-NB-mNG::LEU2; vps1Δ::6xHis-TEV-Vps1(K42A)-StrepII-ALFA-hphNT1*	This study
PL56	*ESM356; VPH1-mScarlet::natNT2; ALFA-NB-mNG::LEU2; vps1Δ::6xHis-TEV-Vps1(G436D)-StrepII-ALFA-hphNT1*	This study
PL57	*ESM356; VPH1-mScarlet::natNT2; ALFA-NB-mNG::LEU2; vps1Δ::6xHis-TEV-Vps1-Δ3K(591-593)-StrepII-ALFA-hphNT1*	This study
PL58	*ESM356; VPH1-mScarlet::natNT2; ALFA-NB-mNG::LEU2; vps1Δ::6xHis-TEV-Vps1-InsB Δ(579-587)-StrepII-ALFA-hphNT1*	This study
PL59	*ESM356; VPH1-mScarlet::natNT2; ALFA-NB-mNG::LEU2; vps1Δ::6xHis-TEV-Vps1-InsB Δ(536-579)-StrepII-ALFA-hphNT1*	This study
PL60	*ESM356; VPH1-mScarlet::natNT2; ALFA-NB-mNG::LEU2; vps1Δ::6xHis-TEV-Vps1-InsB Δ(536-612)-StrepII-ALFA-hphNT1*	This study
PL68	*ESM356; VPH1-mScarlet::natNT2; YBT1-mNG::KanMX6*	This study
PL69	*ESM356; vps1Δ::His3MX6, VPH1-mScarlet::natNT2; YBT1-mNG::KanMX6*	This study
PL70	*ESM356; VPH1-mScarlet::natNT2; Zrc1-mNG::KanMX6*	This study
PL71	*ESM356; vps1Δ::His3MX6, VPH1-mScarlet::natNT2; Zrc1-mNG::KanMX6*	This study

Strain	Genotype in detail	Source
PL72	*ESM356; VPH1-mScarlet::natNT2; Neo1-mNG::KanMX6*	This study
PL73	*ESM356; vps1Δ::His3MX6, VPH1-mScarlet::natNT2; Neo1-mNG::KanMX6*	This study
PL74	*ESM356; VPH1-mScarlet::natNT2; Lem3-mNG::KanMX6*	This study
PL75	*ESM356; vps1Δ::His3MX6, VPH1-mScarlet::natNT2; Lem3-mNG::KanMX6*	This study
BJ3505	*MATa pep4::HIS3 prb1-Δ1.6R lys2- 208 trp1-Δ101 ura3-52 gal2 can*	Gift from Dr. Andreas Mayer, UNIL
lsp1Δ	*his3D1 leu2D0 ura3D0 MET15 lys2d0 lsp1Δ::KanMx*	Gift from Dr. Mara Duncan, UMICH
pil1Δ	*his3D1 leu2D0 ura3D0 MET15 lys2d0 pil1Δ::KanMx*	Gift from Dr. Mara Duncan, UMICH
ent3Δ	*Mat alpha his3D1 leu2D0 ura3D0 lys2d0 ent3Δ::KanMx*	Gift from Dr. Mara Duncan, UMICH
num1Δ	*his3D1 leu2D0 ura3D0 MET15 lys2d0 num1Δ::KanMx*	Gift from Dr. Mara Duncan, UMICH
sch9Δ	*his3D1 leu2D0 ura3D0 MET15 lys2d0 sch9Δ::KanMx*	Gift from Dr. Mara Duncan, UMICH

Table 2.2 Plasmids used for yeast manipulation

Construct	Vector	Source
6xHis (TEV) Vps1-StrepII	pET15B	This study
His(TEV) Vps1(K42A)-Strep	pET15B	This study
His(TEV) Vps1(G436D)-Strep	pET15B	This study
His(TEV) Vps1(ΔInsertB)-Strep	pET15b	This study
His(TEV) Vps1(Δ3K)Strep	pET15b	This study
His(TEV) Vps1(Δ4F)-Strep	pET15b	This study
6xHis (TEV) Vps1-StrepII-ALFA	pYM16	This study
His(TEV) Vps1(K42A)-StrepII-ALFA	pYM16	This study
His(TEV) Vps1(G436D)-StrepII-ALFA	pYM16	This study
His(TEV) Vps1(Δ3K)-StrepII-ALFA	pYM16	This study
His(TEV) Vps1(Δ4F)-StrepII-ALFA	pYM16	This study
His(TEV) Vps1(ΔN-InsertB)-StrepII-ALFA	pYM16	This study
His(TEV) Vps1(ΔInsertB)-StrepII-ALFA	pYM16	This study
pRS305-pTEF1-NbALFA- 40aaL-CmNG-tCYC1	pRS305	Gift from Dr. Saravanan Palani, IISc
mNeongreen-KanMX6	pDK88	Gift from Dr. Saravanan Palani, IISc
ymScarleti	pYM17	Gift from Dr. Saravanan Palani, IISc

Chapter 3

Reconstituting Vps1 functions on membrane

3.1 Prelude

Vps1 was initially identified as a key player in vacuolar protein sorting, where mutations in Vps1 reroute the trafficking of the vacuolar protease CPY to the secretory pathway[33,34]. Around the same time, Dynamin1, the founding member of the dynamin superfamily, was independently discovered as a microtubule-binding protein[81]. Homology studies revealed that Vps1 possesses a GTPase domain similar to that of Dynamin[37,57]. Interestingly, temperature-sensitive mutations in dynamin cause paralysis in *shibire* mutants[82,83], while analogous mutations in Vps1 mis-localize CPY at non-permissive temperatures drawing functional homologies between both proteins[57].

Extensive characterization of classical dynamins and dynamin-related proteins (DRPs) has shown in the past that these proteins are GTP-binding and membrane-binding proteins. GTP binding and hydrolysis drive conformational changes that allow these proteins to remodel membrane (refer introduction section 1.4). An interesting difference between classical Dynamins versus other DRPs is that classical dynamins possess a pleckstrin homology (PH) domain that specifically binds to $PI(4,5)P_2$, whereas dynamin-like proteins lack a PH domain[59].

While Vps1 was attributed to various cellular processes; including vacuolar protein transport[30,31,39,40], endocytosis[51–54], autophagy[55] and peroxisome division[46–48]; there is no direct evidence on Vps1-mediated membrane remodelling. The closest functional insight comes from vacuolar protein sorting, where the deletion of Vps1 results in the mislocalization of the receptors Vps10 and Vps55 to the vacuole[30,31], suggesting involvement of Vps1 in retrieving these receptors back to the Golgi. This chapter consists our efforts to understand what Vps1 can accomplish when provided with a membrane substrate.

3.2 Probing Vps1 functions on membrane

3.2.1 Membrane binding

To evaluate the membrane-binding potential of Vps1, we utilized an assay developed in our lab called Proximity Labelling of Membrane-associated Proteins (PLiMAP)[72,73]. This method involves the preparation of liposomes containing the lipid of choice, along with a photoactivable probe lipid with a diazirine at the head group and Tetramethylrhodamine fluorophore at the tail region. After incubating the liposomes with Vps1, the photoactivatable head group is exposed to UV light, triggering the activation of the diazirine moiety and generation of a reactive carbene intermediate. Carbene species readily cross-link with C–H

bonds present in all biomolecules, with a high reaction rate constant ($k = 3.1 \times 10^9\ s^{-1}$), and are rapidly quenched in water with a half-life ($T_{1/2}$) of less than 2 ns [84]. Hence, only proteins in immediate contact with the photo-crosslinker are labelled. As a result, this highly reactive species covalently attaches to Vps1 if in close proximity to the membrane. The resulting interaction can then be processed using SDS-PAGE electrophoresis, followed by fluorescence imaging of the protein-lipid complexes. As the readout is proximity labelled, fluorescence signal will be detected on SDS-PAGE gels only if there is Vps1 binding to membrane.

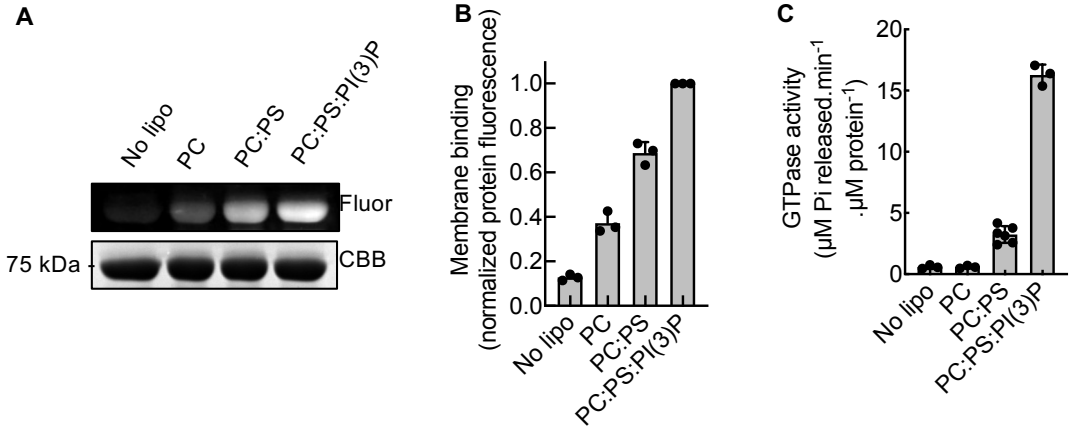

Figure 3.1 Vps1 membrane binding (A) Representative PLiMAP experiment showing fluorescence (Flour) and coomassie brilliant blue (CBB) images of Vps1 without liposomes or mixed with liposomes containing 100% PC, 15%PS or 15%PS/ 5% PI(3)P (B) Quantitation of PLiMAP of Vps1 with liposomes. Data represent the mean ± SD of 3 independent experiments (C) GTPase activity of Vps1 in solution or with liposomes of indicated composition. Data represents the mean ± SD of at least 3 experiments.

Recent reports suggest the involvement of Vps1 in retrograde trafficking of receptors for vacuolar proteins from vacuole to Golgi or endosome, in coordination with retromer complex, Snx4 and SNX-BAR domain containing protein Mvp1[30,39,40]. Phosphatidylinositol 3-phosphate (PI(3)P) is a lipid enriched in the late endosome and the vacuole[85]. Considering the available literature, in order to check membrane affinity of Vps1, we incubated recombinant Vps1 with liposomes containing negatively charged endosome-specific lipid PI(3)P on the background of DOPS and DOPC or negatively charged lipid DOPS zwitterionic lipid DOPC. Intensities from protein exposed to UV in the absence of liposome served as control. Our results demonstrate that Vps1 binds to all three lipids, with an enhanced binding to negatively charged lipids- DOPS and PI(3)P (Figure 3.1.A,B**)**. This is consistent with previous findings reported for other members of the dynamin super family of proteins. Notably, classical dynamins, despite possessing a $PI(4,5)P_2$-specific PH domain, exhibit a preference for membrane with a

high negative charge. Thus, our results highlight the importance of electrostatic interactions in the membrane-binding of Vps1 and other dynamin-like proteins.

3.2.2 GTPase

Dynamin family proteins are known to show stimulated GTPase activity in the presence of membrane[66]. Hence, we tested for stimulation of GTPase activity of Vps1 in the presence of liposomes containing the lipids used to test membrane binding. Vps1 shows a GTP hydrolysis rate of 16.3 min^{-1} with PI(3)P containing membrane compared to DOPS membrane (3.2 min^{-1}) although there was significant binding to DOPS suggesting that Vps1 can specifically form oligomers in the presence of PI(3)P-containing membrane (Figure 3.1.C**)**.

3.2.3 Reconstituting Vps1 functions on tubular membrane topologies

Recent reports show that Vps1 deletion causes longer SNX-BAR tubules that are long lived at the endosomes, suggesting a potential role for Vps1 in regulating tubule dynamics at endosomes[39,40]. Hence, we decided to look at effect of Vps1 on membrane with curved topologies. For this, we prepared membrane nanotubes with the method established in the lab called Supported Membrane Templates (SMrT) technique[75,76]. In this method, a lipid mix of our choice is spotted onto a PEGylated glass coverslip and allowed to dry. The coverslip is then assembled onto a flow cell. When buffer is flowed over the coverslip, the lipids hydrate and form vesicles. Upon attaching the flow cell to a pump, the shear flow of buffer extrudes tubes from the vesicles. This generates a planar bilayer at the source with an array of tubes emerging from it which can be observed under a microscope.

For our experiments, we made membrane nanotubes containing DOPC,DOPS, endosomal lipid PI(3)P, and a small amount of fluorescent lipid Texas-Red rhodamine PE (TxRd-DHPE) for visualization in the ratio 79:15:5:1. TxRd-DHPE equally partitions to the membrane irrespective of membrane curvature and its fluorescence properties remains unchanged after protein binding, making TxRd-DHPE and ideal fluorescent marker for SMrT assays[76,86,87]. When Vps1, along with GTP, was introduced, rapid fission of the membrane nanotubes was observed. Fission was quantified using a parameter called ‘fission index’, defined as the total number of tube fragments in a field divided by the initial total number of tubes. A higher fission index indicates more fission events and a greater number of tube fragments. Vps1 failed to cause fission of templates made of DOPC or DOPS (Figure 3.2.A**)**.

Additionally, to look at the effect of different nucleotide states on Vps1-mediated fission, we prepared membrane nanotubes with the same lipid concentration and flown in Vps1 without any nucleotides or mixed with non-hydrolysable form of GTP- GppNHp and GDP. We observed fission only in the presence of GTP. Our findings show that Vps1-mediated fission is specific to PI(3)P-containing membrane and is dependent on the nucleotide state, occurring only in the presence of GTP (Figure 3.2.A**)**. This suggests that Vps1 plays a PI(3)P-specific and GTP-dependent role in membrane tubule fission, aiding our understanding of its function in endosomal dynamics.

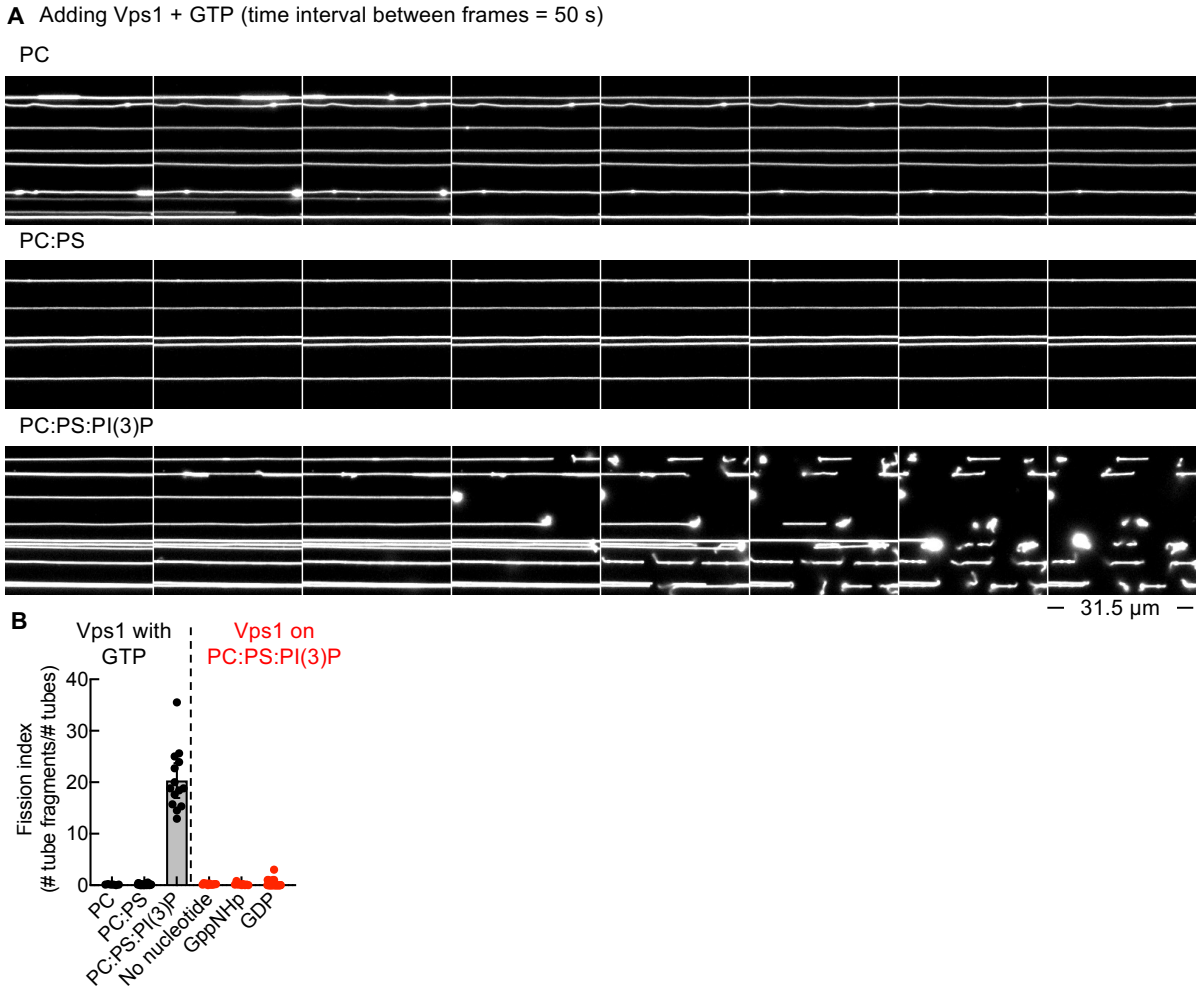

Figure 3.2 Vps1 causes membrane fission (A) Time-lapse images of Vps1 flown to 100% PC 15%PS or 15%PS/ 5% PI(3)P-containing membrane nanotubes (grey) in presence of GTP. (B) Fission index based quantitation of Vps1-mediated fission on membrane nanotubes with lipids indicated in B (grey bars) and on PC:PS:PI(3)P-containing templates in the presence of different nucleotides (red bars). Data represents mean ± SD of at least 10 microscope fields across 2 experiments.

3.3 Discussion

Vps1 is long speculated to be involved in the transport of tubular-vesicular carriers from endosomes to Golgi. But its role in the particular process is unknown. Here we show that in the presence of excess membrane containing PI(3)P lipid, Vps1 can bind to the liposomes with much greater affinity than that of the negatively charged DOPS- or with the zwitterionic DOPC-containing membrane. Previous studies that monitored on Vps1 membrane binding used techniques like liposome sedimentation assay, which rely on the principle that proteins bound to liposomes co-sediment with them during high-speed centrifugation. However, this method presents inherent limitations when applied to Dynamin family proteins, as these proteins tend to oligomerize in solution and may pellet independently of membrane binding, introducing potential bias. Hence, Vps1 binding to PI(3)P was not much evident from such assays[71]. In contrast, the more sensitive PLiMAP assay, that monitor binding under steady-state conditions, has allowed us to more accurately assess the membrane-binding preferences of Vps1. Although, Vps1 binding to membrane is charge dependent, the stimulated GTP hydrolysis specifically with PI(3)P indicates the importance of the lipid of choice in Vps1 assembly on the membrane and its catalytic activity. Previous structural and biochemical studies using lipid nanotubes demonstrated that Vps1 has a strong propensity to self-assemble into scaffolds; however, these studies reported no significant stimulation of GTPase activity on membranes[70]. In contrast, our findings reveal approximately 30-fold stimulation in GTPase activity. The reason for this discrepancy remains unclear, but it may be attributed to intrinsic differences between the Vps1 ortholog from *C. thermophilum* used in earlier studies and the *S. cerevisiae* Vps1 analyzed in our work.

With supported membrane templates, we see that Vps1 causes fission of PI(3)P-containing membrane in the presence of GTP and co-factors, which is not seen in the case of DOPS-containing or with DOPC-containing membrane tubes. The fission also depends on the nucleotide state of Vps1, where it's specific to GTP bound state and not to any other form of GTP hydrolysis state. These findings show that Vps1 is sufficient to cause fission of PI(3)P containing membrane in vitro in the presence of GTP. Although Vps1 causes fission of PI(3)P-containing membrane nanotubes, we see that not all tubes undergo fission. The fission index parameter shows a range of tube fragments from 15 to 25 with the mean of fission index 20, indicating that there are additional factors that dictate Vps1 mediated fission, that needs to be studied closely.

Chapter 4

Factors regulating Vps1-mediated membrane fission

As we discussed in previous chapter, Vps1-mediated fission is lipid and nucleotide dependent. In order to fine tune our understanding on the mechanism, we dwelled into looking at the effect of Vps1-mediated fission upon changing different parameters.

4.1 Curvature dependence

Dynamin family members like Drp1 is known to severe tubes upto 200 nm radius and show complete shut-down of fission above 250 nm comparable to the mitochondria sizes. Whereas classical dynamins Dnm2 shows fission of only tubes below 25 nm radius[88,89]. In order to look at the influence of curvature on Vps1-mediated membrane remodelling, first we looked at the localization of Vps1 onto SMrT templates. As discussed earlier, source region of SMrT templates contain planar bilayer and curved tubes arising from the source making it easier to look at planar and curved membrane topologies at the same time. Vps1 was labelled with Alexa fluor-488 maleimide dye, mixed along with the non-hydrolysable form of GTP; GppNHp, and flown onto 5% PI(3)P containing membrane templates. Remarkably, Vps1 bound exclusively to membrane tubes compared to planar bilayer indicating Vps1 membrane binding is curvature sensitive (Figure 4.2.A**)**.

SMrT templates are visualized using wide-field imaging and as the fluorescence intensities of diffraction-limited, membrane-bound objects are proportional to the net membrane surface area (Area ∝ Intensity)[90]. Hence, intensities from membrane tubes can be correlated to its tube sizes. To check for any tube radius dependence on Vps1's ability to cause membrane fission, we employed a tube size estimation as mentioned previously[76]. The images of unilamellar planar bilayer patches were used to determine the calibration constant K1, where K1= Area/(Integrated fluorescence intensity). Assuming the tube to be an open cylinder with Area= 2.Π.r.l (where 'r' is the radius of the tube and 'l' is the length of the ROI on the tube) , and for constant K1, starting tube radius can be estimated. Furthermore, calculating maximum tube intensity as a function of starting tube radius provides the calibration constant K2 and dividing pixel intensities in fluorescent micrographs by K2 directly provides tube radius. Thus, starting tube radii estimates can be used to arrive at a direct relationship between tube intensity and radius. With this method, we looked further on the dependence of membrane curvature on Vps1 mediated fission.

Indeed, Vps1-mediated fission is tube-radius dependent. Not all tubes undergo fission; only those with a radius of up to 30 nm is severed efficiently by Vps1. The probability of fission

decreases as the tube radius increases, and tubes with a radius greater than 50 nm do not undergo fission. This radius dependence explains the variability in the fission index, as different fields contain tubes of varying sizes (Figure 4.1.A,B**)**. This data aligns well with the indications of Vps1 being the fission catalyst of tubules formed by SNX-BAR proteins at the endosome. Tubules formed by SNX-BAR proteins have a mean diameter of approximately 31 nm (equivalent to a radius of 15 nm)[91]. The tube radius dependence shown by Vps1 falls well within the range of the reported sizes of tubes formed by SNX-BAR proteins on membrane, pointing at Vps1-mediated fission of SNX-BAR tubules.

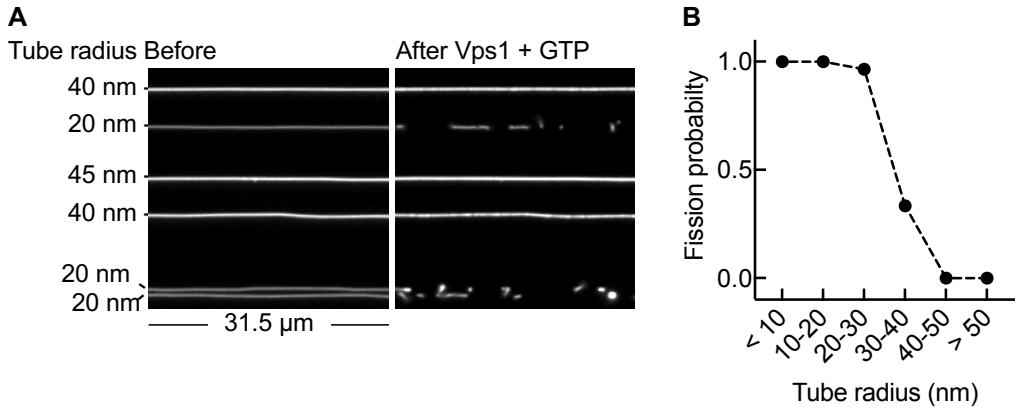

Figure 4.1 Vps1-mediated membrane fission is curvature dependent A) Fission after addition of Vps1 mixed with GTP on tubes of varying sizes B) Fission probability of Vps1 as a function of staring tube radius. Data represent probabilities estimated for 5 tubes of <10 nm, 70 tubes of 10-20 nm, 28 tubes of 20-30 nm, 3 tubes of 30-40 nm, 2 tubes of 40-50 nm and 3 of > 50 nm radius.

4.2 Nucleotide dependence

4.2.1 Vps1 shows nucleotide-dependent oligomerization on curved membrane

We observed that fission occurs only in the presence of GTP. To investigate the fission mechanism further, we introduced labelled Vps1 along with different nucleotide analogues. Vps1 formed clusters or bound uniformly to nanotubes in APO, in the presence of GDP or GppNHp (Figure 4.2**)**. This clustering appeared to be independent of tube size, as both thin and thick tubes within the same microscope field displayed uniform distribution, whereas tubes of intermediate sizes showed clustering. We are unsure of the underlying cause for this variability in distribution at this point. Fluorescence intensity profiles of protein and membrane reveal that with GppNHp, Vps1 and membrane intensities are anti-correlated; regions of Vps1 binding exhibit reduced membrane intensity (Figure 4.2.A**)**. Since nanotubes are diffraction-limited entities, intensity changes can be correlated to molecular size. Therefore, a decrease in membrane intensity suggests a decrease in tube radius, indicating that the tube is undergoing

constriction. However, this phenomenon is absent in the APO or GDP-bound states. While membrane binding and scaffold formation occur in these states, constriction is exclusive to the GTP-bound state.

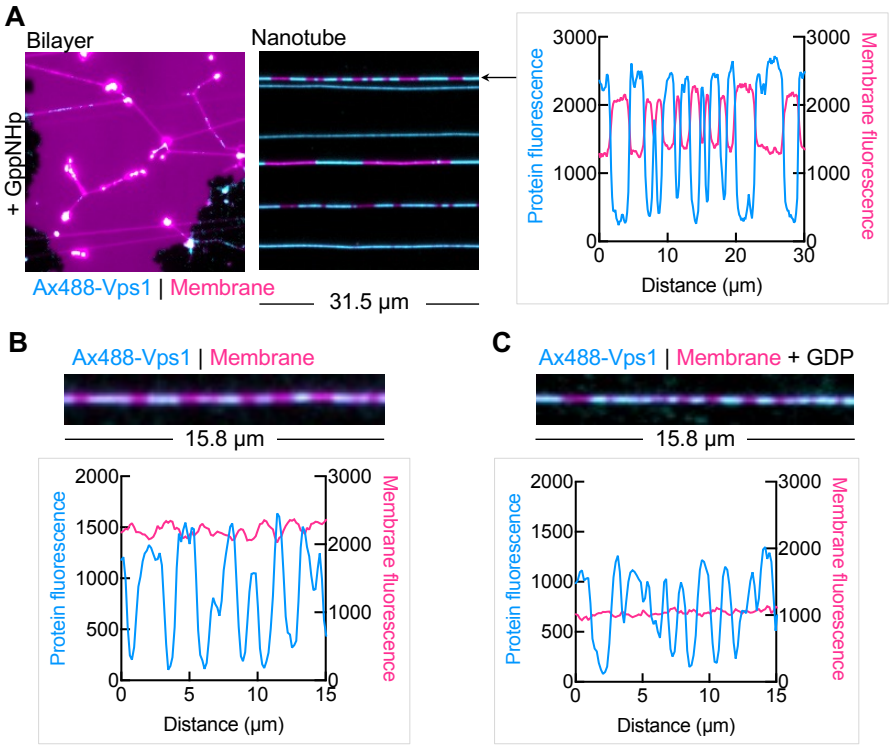

Figure 4.2 Vps1 shows nucleotide dependent oligomerization on curved membranes (A) Representative image and associated line profiles showing distribution of labelled Vps1 with GppNHp (cyan) on planar bilayer and membrane nanotubes (magenta). (B) Representative image and associated line profiles showing distribution of labelled Vps1 in Apo (cyan) on membrane nanotubes (magenta). (C) Representative image and associated line profiles showing distribution of labelled Vps1 with GDP (cyan) on membrane nanotubes (magenta).

4.2.2 Nucleotide hydrolysis-mediated membrane fission

To understand the effect of GTP hydrolysis, we first used the hydrolysis-defective mutant K42A, located in the G-domain [30,70]. K42A mutation is analogous to the well-studied K44A mutation in Dynamin, and the lysine is conserved across Dynamin superfamily [59]. Vps1(K42A) bound PI(3)P-containing membranes as well as Vps1 full-length protein, as observed on PLiMAP (Figure 4.3.A). However, as expected, Vps1(K42A) showed no stimulation of GTPase activity in the presence of membrane (Figure 4.3.B). Negative EM studies show that Dyn1(K44A) tubulates liposomes and constricts the underlying membrane. The addition of Alexa fluor-488 tagged Vps1(K42A) along with GppNHp onto SMrT templates led to the formation of long protein scaffolds on the membrane, which was stable like Vps1-full length, suggesting that oligomerization of Vps1 is not GTPase dependent (Figure 4.3.C,D). Whereas

Vps1(K42A) failed to cause fission of PI(3)P-containing membrane templates (Figure 4.3.E), indicating that GTP hydrolysis is important for Vps1-mediated fission.

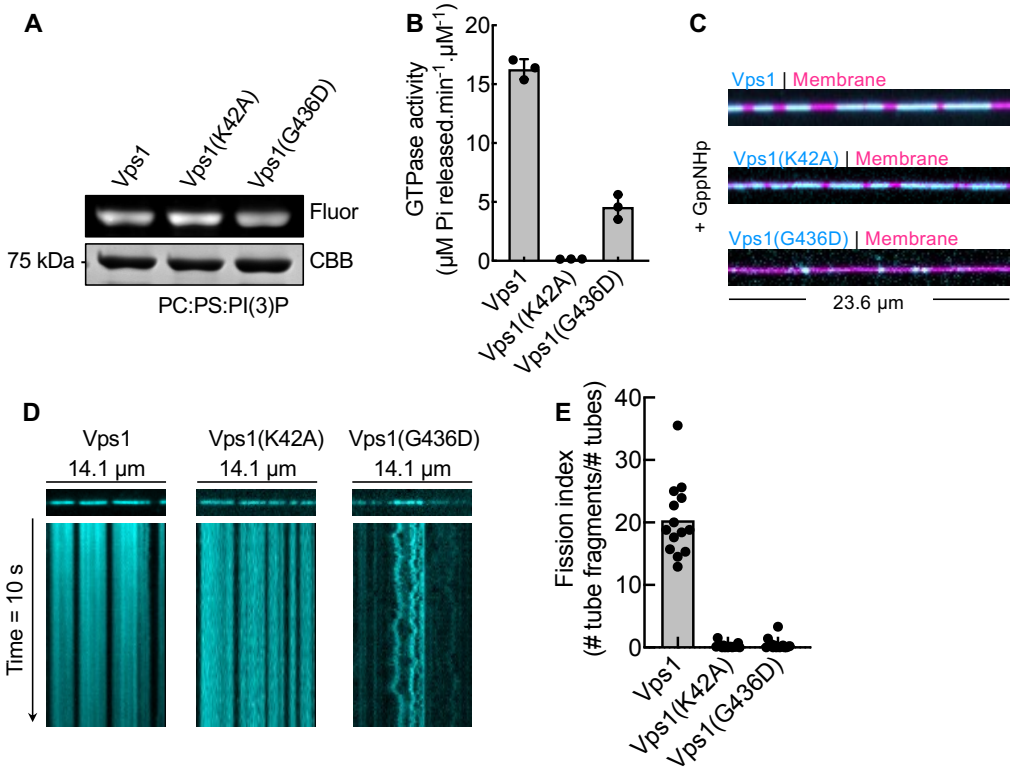

Figure 4.3 Vps1-mediated membrane fission is GTP-hydrolysis and self-assembly dependent A) Representative PLiMAP experiment showing fluorescence (Flour) and coomassie brilliant blue (CBB) images of Vps1, Vps1(K42A) and Vps1(G436D) with PC:PS:PI(3)P-containing liposomes (B) GTPase activity of Vps1(K42A) and Vps1(G436D) with PC:PS:PI(3)P-containing liposomes. Data represents the mean ± SD of 3 experiments. (C) Representative images of labelled Vps1, Vps1(K42A) and Vps1(G436D) (cyan) with GppNHp on PI(3)P-containing membrane nanotubes (magenta).(D) Representative image and kymograph of protein scaffolds (cyan) from time-lapse imaging of Vps1, Vps1(K42A) and Vps1(G436D) on PC:PS:PI(3)P-containing membrane nanotubes (E) Fission index after addition of unlabelled Vps1, Vps1(K42A) and Vps1(G436D) with GTP on PI(3)P-containing membrane nanotubes. Data represents mean ± SD of at least 20 microscope fields across 2 experiments.

4.3 Effect of Vps1 self-assembly on membrane remodelling

To examine self-assembly, we studied the assembly-defective mutant G436D. Dynamin1 G397 involves in self-assembly and the residue is conserved across Dynamin related proteins including Vps1[70,92,93]. Mutation in the analogous residue G436D renders Vps1 dimer in solution[70]. Vps1(G436D) found to bind to PI(3)P-containing membrane but did not exhibit a stimulated GTPase activity (Figure 4.3.A,B). Fluorescently labelled proteins on membrane revealed that, Vps1(G436D) formed smaller, clusters on tubes which tends to move along the

nanotubes with time, as opposed to Vps1 and Vps1(K42A) which formed long stable clusters (Figure 4.3.C,D). Additionally, Vps1(G436D) failed to cause fission on SMrT (Figure 4.3.E).

As observed previously, GTP hydrolysis is not required for membrane binding or scaffold formation but is essential for membrane fission. Similarly, defects in self-assembly do not affect membrane binding but are critical for stimulated GTP hydrolysis and membrane fission.

4.4 Stage-specific analysis of Vps1-mediated fission

To further understand the effect of GTP hydrolysis, we arrested Vps1 on nanotubes in a GTP-bound state, by flowing GppNHp and focusing on the membrane channel with unlabelled Vps1. Under VPs1 with GppNHp, tubes showed clusters of dimmer fluorescence as in the case with labelled protein. When GTP was introduced, further tube constriction occurred, with tubes remaining in this constricted state for an extended period before undergoing fission. Kymograph analysis from a part of the time-lapse image, with the horizontal axis representing tube length and the vertical axis representing time, showed progressive constriction as darker grey regions compared to the surroundings. Additional darkening upon GTP addition marked further constriction, culminating in fission (Figure 4.4.A). These intensity changes were converted to tube radius measurements, revealing that the constricted tube radius was approximately 16 nm, while the pre-fission radius was about 6 nm (Figure 4.4.B). Repeating this analysis across multiple tubes provided consistent estimates of tube radii in constricted and pre-fission states.

Our findings show that Vps1 can constrict the underlying membrane to a radius of approximately 17 nm in the GTP-bound state. GTP hydrolysis further reduces the tube radius to around 6 nm, facilitating fission (Figure 4.4.C). Previous solution structure studies of Vps1 from the related yeast species *C. thermophilum* revealed the Cryo-EM reconstruction of Vps1 in solution[70]. These studies estimated a scaffold lumen diameter of 19 nm (10 nm radius) in GTP bound state. In SMrT templates, the presence of the membrane appears to hinder Vps1 from achieving this scaffolded state. Membrane stimulated GTP hydrolysis of Vps1 likely aids in attaining this state, enabling efficient membrane constriction and subsequent fission.

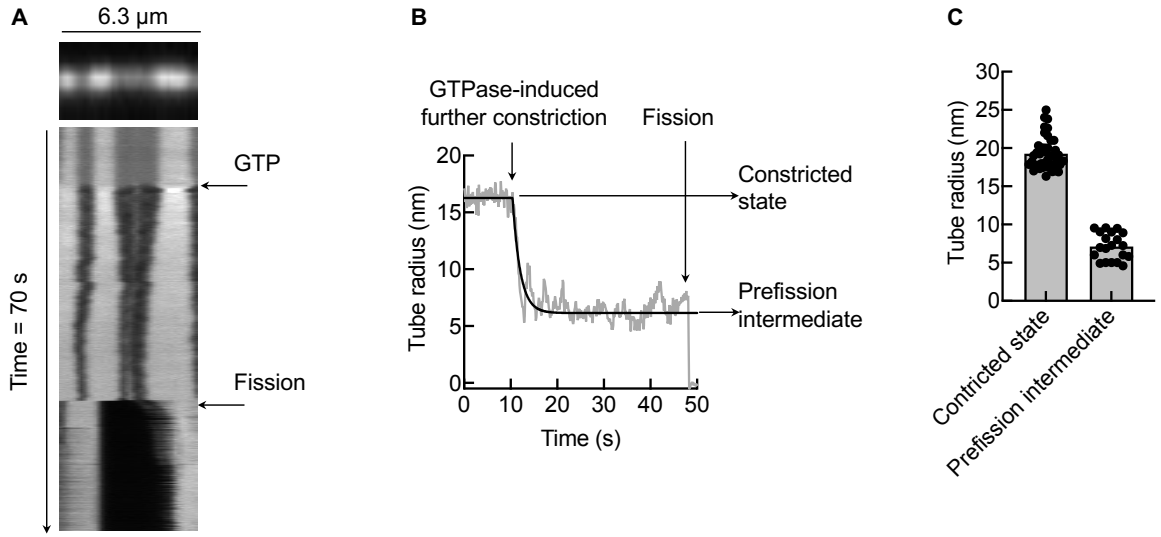

Figure 4.4 Stage-specific analysis of Vps1-mediated fission (A) Kymograph of tube intensities scaled to tube radius from Movie monitoring the effect of GTP hydrolysis on Vps1-preassembled membrane nanotubes (B) Tube radius from (I) plotted as a function of time and fitted to one-phase exponential decay function. (C) Mean tube radius at constricted state and prefission state.

4.5 Discussion

Our results provide the first evidence that Vps1 can constrict and sever membrane tubes. By systematically varying experimental parameters, we identified several factors that regulate Vps1-mediated membrane fission. Our data show that Vps1 binding is highly curvature-dependent, with a preference for curved membrane tubes over planar bilayers. Moreover, the efficiency of Vps1-mediated fission is strongly dependent on tube radius, with tubes less than 30 nm in diameter undergoing efficient fission, a size closely matching the tubules formed at the endosomes, where Vps1 is thought to act. Although Vps1 can bind to membrane in various nucleotide states, membrane constriction occurs exclusively in the GTP-bound state. Analysis of the mutant that impairs GTP hydrolysis indicates that both Vps1 binding and oligomerization occur independently of hydrolysis. Additionally, the oligomerization-defective mutation G436D reveals that Vps1 self-assembly is crucial for effective membrane binding, with binding and oligomerization tightly coupled for scaffold formation and constriction of the underlying tube.

The stage-specific analysis of Vps1 binding and hydrolysis on PI(3)P-containing membrane reveals that initial GTP binding promotes Vps1 scaffold formation and tube constriction, and subsequent GTP hydrolysis induces a conformational change that further constricts the tube. Structural and biochemical studies with dynamin show that GTP hydrolysis changes the

interfaces in the helices to form a two-start helix in the super-constricted state of dynamin. Our assays where the change in the tube dimension is used as a readout for the Vps1 helical structure indicate that Vps1 adopts a helical structure with an approximate lumen diameter of 17 nm in the GTP-bound state, which constricts to around 6 nm upon hydrolysis. This additional constriction likely perturbs the underlying bilayer and facilitates the formation of a hemifission intermediate that ultimately drives fission. Studies on bilayer dynamics have shown that constriction of bilayer to a minimum thickness of bilayer cause the formation of hemifission intermediate that spontaneously changes the lipid arrangement in the bilayer to cause fission[94–97]. Detailed structural analyses of Vps1 in GTP-bound and hydrolysis states will be critical to fully understand the molecular packing and conformational changes underlying its function.

Although our in vitro results delineate the intrinsic capabilities of Vps1 in membrane constriction and fission, further cellular studies are necessary to reflect these findings within the complex environment of the cell.

Chapter 5

Monitoring Vps1 functions in vacuolar protein sorting

In order to understand Vps1 functions, we first sought to look at Vps1 localization in cells. All in vitro assays were performed using Vps1-full length or mutants with a 6xHis tag followed by TEV cleavage site at the N-terminus and a Strep-II tag at the C terminus. In order to expand in vitro findings to cellular functions, we replaced the endogenous Vps1 with the tagged Vps1 constructs used for in vitro studies.

An inherent limitation in the translation of in vitro analysis of proteins to their physiological functions is that the visualization of proteins inside the cell with an attached fluorophore may not be efficient in some cases. This is because the bulk tag itself will interfere with the overall structure of the protein and impact block in its functionality. Multiple reports in the past have shown that Vps1 tagging with tags like GFP affects its physiological function[31,39]. Previously, people circumvent this by expressing a tagged and untagged version of Vps1 in a diploid strain or by having a large linker in between Vps1 and fluorophore so that the fluorophore will not affect Vps1 structure[30,39,55,70].

Hence we resort to ALFA-tag, which is a 13 amino acid long tag used to mark proteins without losing the functionality[98]. The protein of interest can be tagged with an ALFA tag in the background of an ALFA nanobody linked to mNeonGreen (ALFA-nb-mNG). ALFA-ALFA nanobody interaction externally tags the protein of interest without losing the protein functionality[98,99]. Hence, to look at Vps1 localization, we added the ALFA tag at the C-terminus after the Strep-II tag and the construct was replaced at the Vps1 endogenous locus.

5.1 Validation of Vps1 constructs used in cellular studies

For validation of the constructs, we first checked the growth of Vps1 full-length with the above mentioned tags on a non-permissive temperature of 37 °C where Vps1 deletion strain shows growth defect[57]. Tagged Vps1 constructs replaced at the endogenous locus rescued the growth defect 37 °C (Figure 5.1.A). Further, the expression pattern of full-length and mutant replacements at endogenous locus were validated by probing lysate from an equal OD cells with anti-ALFA antibody where all the constructs showed equal expression. Anti-ALFA antibody tends to bind non-specifically to an unknown protein of ~75 kDa in yeast lysaste[99]. The intensities of this non-specific band was considered as the loading control (Figure 5.1.B,C).

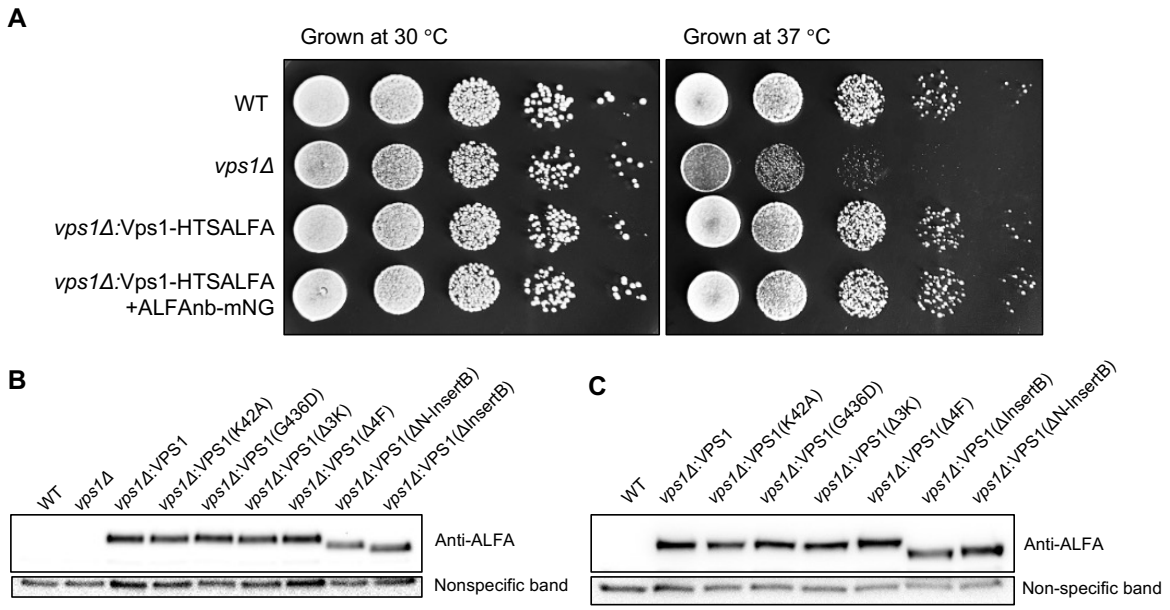

Figure 5.1 Validation of Vps1 endogenous replacement strains (A) Spot assay comparing the growth of WT, *vps1Δ, or* Vps1-HTSALFA added at endogenous locus in *vps1Δ* strain with or without ALFAnb-mNG at 30 °C and 37 °C. (B) Comparison of expression among Vps1 full length and mutants with 6xHis-Tev tags at the N-terminus and Strep-II-ALFA tags at the C-terminus added at the endogenous locus of *vps1Δ* strain in the background of Vps10-mNG. Equal volume of lysates processed from equal OD starting cells were processed and blotted against anti-ALFA antibody. Non-specific band picked up by ant-ALFA antibody at ~75 kDa serve as loading control. (C) Comparison of expression among Vps1 full length and mutants with 6xHis-Tev tags at the N-terminus and Strep-II-ALFA tags at the C-terminus added at the endogenous locus of *vps1Δ* strain in the background of ALFA-nb-mNG. Equal volume of lysates processed from equal OD starting cells were processed and blotted against anti-ALFA antibody. Non-specific band picked up by ant-ALFA antibody at ~75 kDa serve as loading control.

5.2 Effect of Vps1 on vacuolar protein sorting

Full-length Vps1 construct tagged to ALFA-tag on the background of ALFA-nb-mNG was used to probe for Vps1 localization in cells. Vps1 displayed dynamic puncta within cells, whereas the hydrolysis-defective mutant Vps1(K42A) formed larger, immobile puncta, and the self-assembly-defective mutant Vps1(G436D) exhibited cytosolic localization (Figure 5.2.A). Addtionally, the vacuole looked fragmented in the Vps1(K42A) and Vps1(G436D) like in the case of *vps1Δ* (Figure 5.2.A,B).

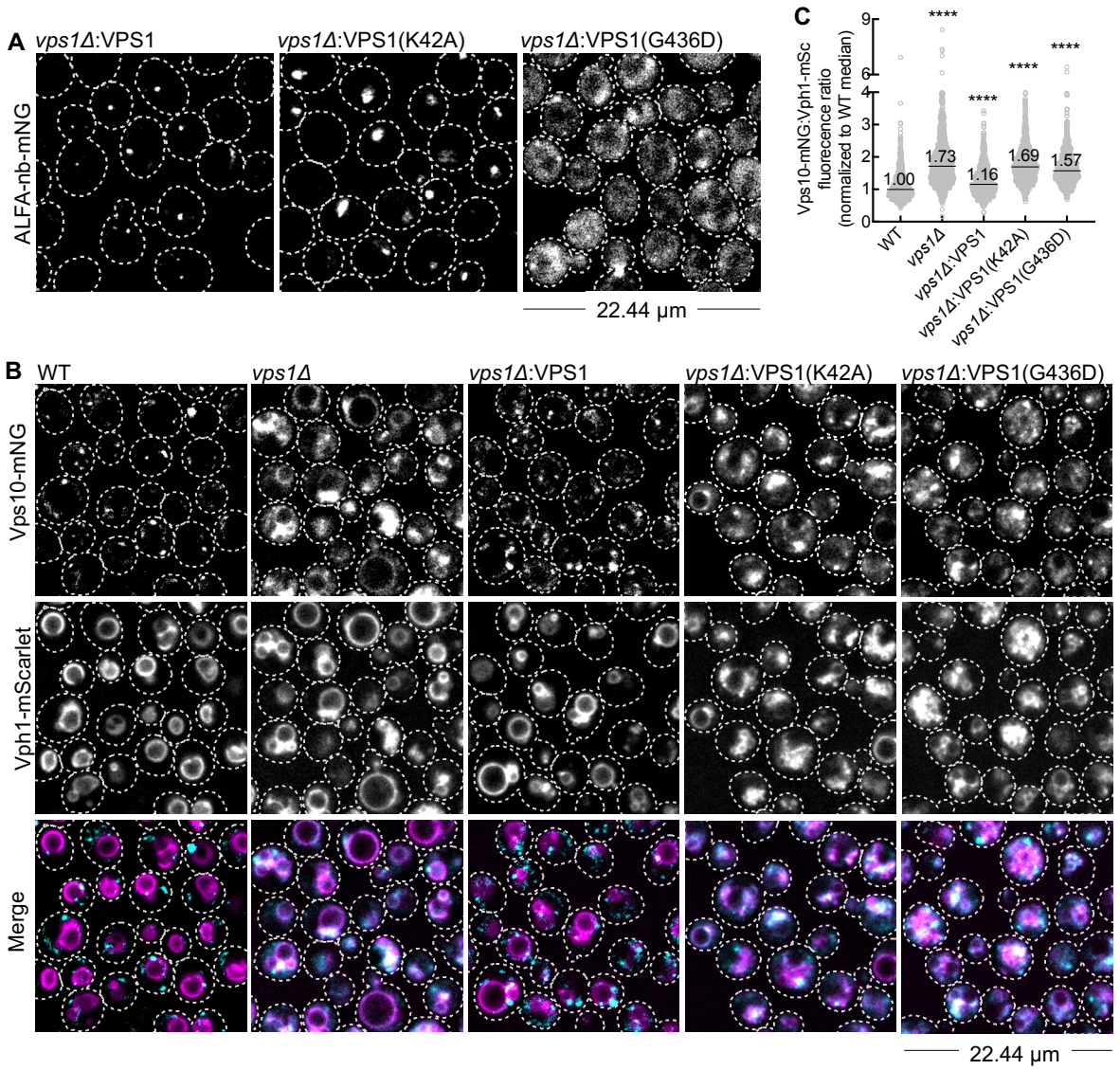

Figure 5.2 Vps1 in cellular trafficking (A) Representative images showing the localization of Vps1, Vps1(K42A) and Vps1(G436D) with ALFA tag rescue on cells expressing ALFA-nb-mNG. (B) Vps10 -mNG localization on WT, *vps1Δ* strain and *vps1Δ* strain rescue by addition of VPS1, VPS1(K42A) or VPS1(G436D) at the endogenous locus. Vph1-mScarlet marks the vacuole. (C) Quantitation of Vps10 localization to vacuole plotted as Vps10:Vph1 ratio normalized to median ratio of WT. Data represent 809 vacuole-like particles for WT, 1212 for *vps1Δ*, 1013 for *vps1Δ*:VPS1, 1095 for *vps1Δ*:Vps1(K42A) and 813 for *vps1Δ*:Vps1((G436D) from 2 experiments. Numbers in the plot show the median ratios. Statistical significance of *vps1Δ* against WT and *vps1Δ*:VPS1 against *vps1Δ* was tested and statistical significance of *vps1Δ*:Vps1(K42A) and *vps1Δ*:Vps1((G436D) against *vps1Δ*:VPS1 was tested using an unpaired Mann-Whitney test with **** depicting $p<0.0001$.

Vps1 deletion results in the mislocalization of the CPY receptor Vps10 to the vacuole[31,39]. In WT cells, Vps10 displays punctate localization, whereas in the *vps1Δ* strain, Vps10

predominantly localizes to the vacuole, suggesting that the retrieval of Vps10 is impaired in the absence of Vps1, implicating Vps1 in the retrieval of proteins from the vacuole to the Golgi (Figure 5.2.B). To study Vps10 trafficking, we developed an in situ scoring system using a vacuolar resident protein, Vph1, as a marker. The Vph1 signal was used as a mask to measure Vps10 receptor intensities on the vacuole. By calculating the ratio of Vps10 to Vph1 intensities, normalized to WT levels, we quantified the increase in vacuolar localization of Vps10 in *vps1Δ* strains. Reintroduction of the Vps1 gene at its endogenous locus rescued Vps10 punctate localization, supporting the role of Vps1 in Vps10 retrieval (Figure 5.2.C). Importantly, addition of Vps1(K42A) or Vps1(G436D) at the endogenous locus did not rescue Vps10 localization confirming that both GTP hydrolysis and self-assembly are crucial for Vps1's role in vacuolar protein trafficking.

5.3 Discussion

Previous studies on Vps1 put out the limitation of tagging with bulk tags like GFP for understanding dynamics, as addition of bulk tags to Vps1 partially or entirely impaired Vps1 functions. Here, we used an emerging ALFA tag-nanobody interaction principle to pseudo-tag Vps1 with the mNeonGreen marker. Our results show that Vps1 pseudo tagging via an ALFA tag-nanobody interaction helps in the visualization of functional Vps1 in cells confirmed by growth at higher temperatures and Vps10 receptor trafficking which are established assays to check Vps1 functionality. Further, to understand the effect of different mutations in Vps1, such as hydrolysis and oligomerization defect, on cargo trafficking, we introduced a fluorescent-based quantitation to look at the localization of Vps10 under these different conditions. This quantitation method gave us a clear readout on the pool of Vps10 that is vacuole localized. Previous studies usually report these differences by looking at the number of cells that show a Vps10 localization to the vacuole or a punctate localization. However, we noticed that for some mutations, there is a punctate as well as a localization in the same cell. The method of quantitation introduced in this chapter looks at VPS10 trafficking to the vacuole irrespective of its punctate pool. By coupling these cellular techniques with the different mutant forms of Vps1, we hope to better understand Vps1 functions in the cell.

Chapter 6

Characterization of Vps1 InsertB region

Classical dynamins have a pleckstrin homology (PH) domain that binds to the membrane. Various Dynamin family proteins have this PH domain missing and instead have an unstructured Variable Domain (VD)[100] as in the case of Dynamin-related protein 1 (Drp1) and the paddle domain in Bacterial Dynamin[101]. In comparison, MxA binds membrane via a small unstructured L4 loop in the stalk region[102]. (Figure 6.1).

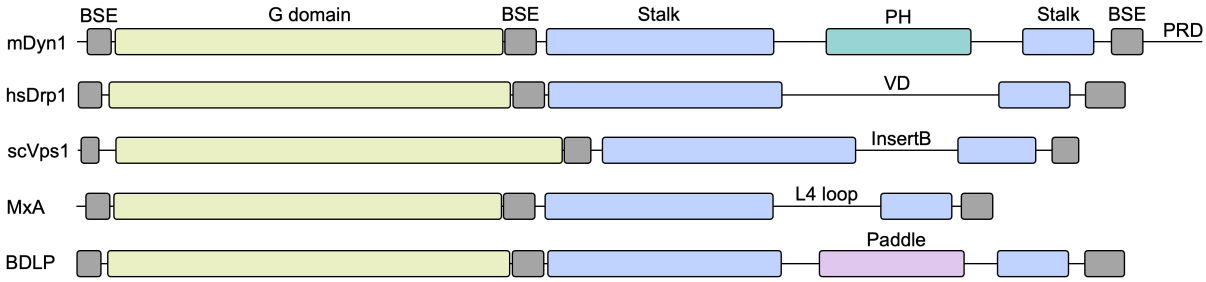

Figure 6.1 Schematic comparing the PH equivalent regions in Dynamin super family proteins.

The InsertB region in Vps1 is a partially structured loop that occupies the same position as the membrane-binding PH domain in Dynamin. Interestingly, this region resembles the unstructured VD of DRP1 in mammals. Cryo-EM reconstruction of DRP1 shows gaps in density at the location where the dynamin PH domain is associated with the membrane. Drp1 binds specifically to cardiolipin-containing membrane[103,104] and causes fission of these membrane[88]. Although the Vps1 InsertB region is equivalent to VD and thought to be involved in membrane binding, there is not much evidence of InsertB involvement in membrane binding. Hence, with the assays established to look at Vps1 functions in vitro and in vivo, we characterized the InsertB region.

6.1 Membrane binding of InsertB mutants

As the boundaries of InsertB were not exactly mentioned anywhere, we used the domain boundaries of Vps1 mentioned in the sole paper that was published on Vps1-InsertB[71]. We marked the aligned sequence as InsertB region, which spans in the range of residues 536-612. Hence, from now on, this stretch will be mentioned as InsertB for all the experiments.

A comparative analysis of the InsertB region across yeast species revealed ~ 47% sequence similarity, with significant conservation, particularly in the C-terminal region. Notably, positively charged hydrophobic residues, known to mediate membrane interactions in other dynamin-like proteins, were conserved across yeast species (Figure 6.2). Hydrophobic

tryptophan and positively charged arginine residues-containing WRG motif in Drp1-VD affects stimulated GTPase activity of Drp1 in the presence of Cardiolipin-containing membrane[105]. Similarly, an adjacent stretch in Drp1 VD with four lysines was shown to be important for Drp1 membrane binding[103]. Whereas a recent study on mutating the conserved lysine K591,K592,K593 to alanine in the Vps1 InsertB region shown not to affect PI(3)P binding but affect PI(4,5)P2 binding in vitro and does not affect Vps10 trafficking in vivo[71] . To explore the functional relevance of these residues, we proceeded to delete specific conserved amino acids within the C-terminal InsertB region and analyzed the effects.

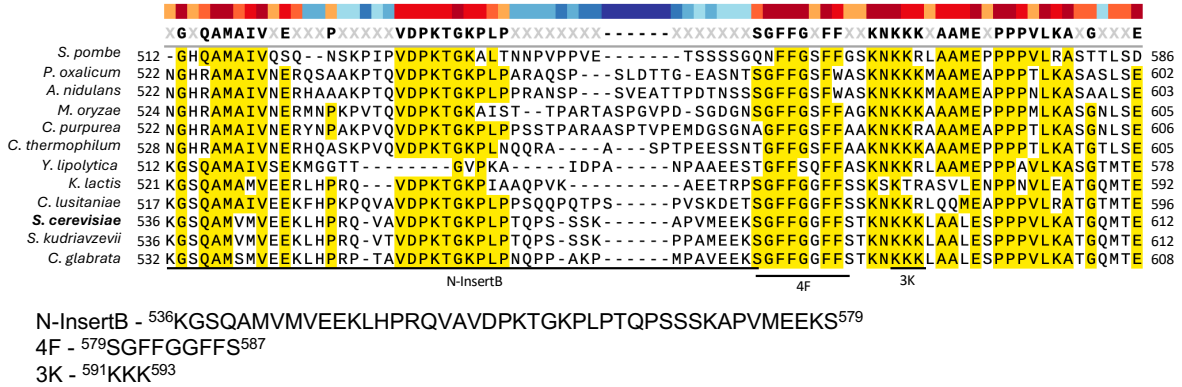

Figure 6.2 Sequence alignment of InsertB region between different yeast species. The N-terminal region of InsertB, Phenylalanine rich region 4F and lysine residues 3K deleted in the study are highlighted.

We deleted the conserved stretch of residues K591, K592, K593 (referred to as Vps1 Δ3K) and a stretch of phenylalanine residues- SGFFGGFFS (referred to as Vps1 Δ4F). We also had the N-terminal portion of InsertB residues 536-579 deleted (Vps1 ΔN-InsertB) and the whole of InsertB region replaced by an unstructured Thrombin stretch (Vps1 ΔInsertB). We could express and purify all the mutant constructs except Vps1 ΔN-InsertB. Hence, Vps1 ΔN-InsertB is not included in the in vitro assays. First, we tested how these mutations affect Vps1 binding to PI(3)P-containing membrane. We see ~ 50% reduction in membrane binding with Vps1 ΔInsertB (Figure 6.3.A,b). Interestingly, Vps1 Δ3K with 3 lysine deletion also reduces membrane binding to similar levels of whole InsertB deletion. Vps1 Δ4F showed similar levels of membrane binding as that of full-length Vps1. However, all these mutants could not stimulate GTPase activity in the presence of PI(3)P-containing membrane (Figure 6.3.C). Additionally, all InsertB mutants were defective in membrane fission (Figure 6.3.F).

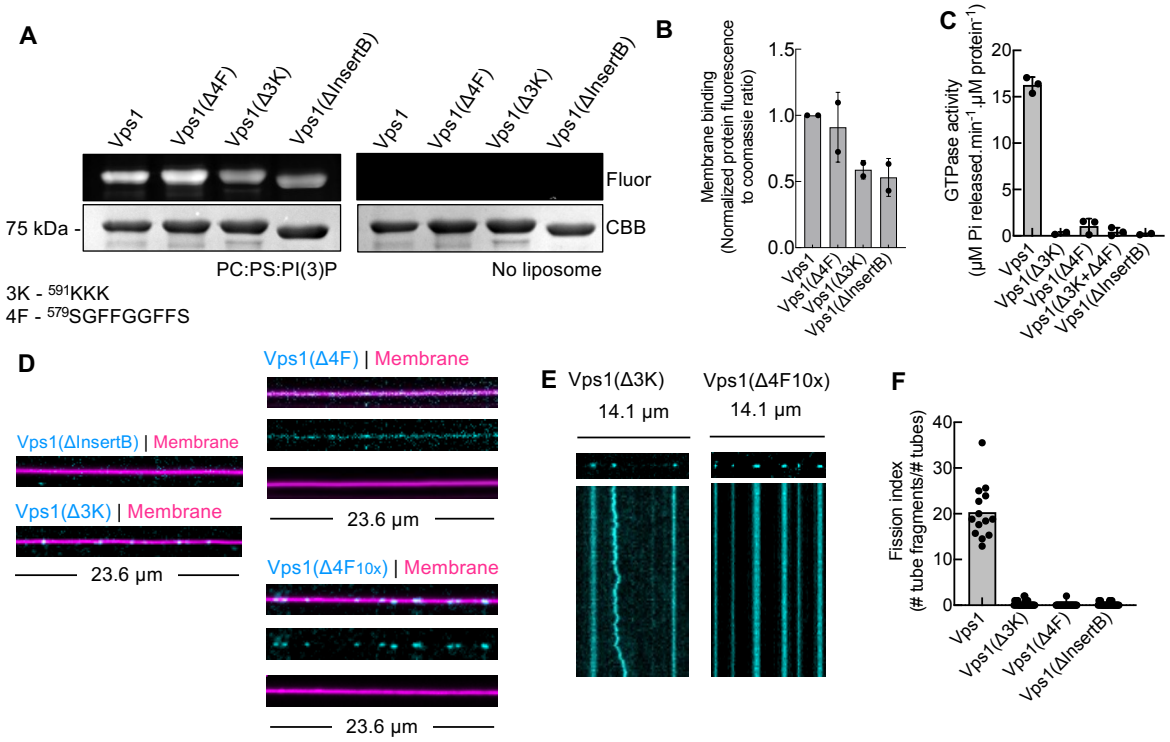

Figure 6.3 Functional analysis of Vps1-InsertB region (A) Representative PLiMAP experiment showing fluorescence (Fluor) and coomassie brilliant blue (CBB) images of Vps1 and InsertB mutants in the presence or absence of PC:PS:PI(3)P-containing liposomes. (B) Quantitation of PLiMAP of Vps1 and InsertB mutants with liposomes. Data represent the mean ± SD of 2 independent experiments. (C) GTPase activity of InsertB mutants with PC:PS:PI(3)P-containing liposomes. Data represents the mean ± SD of at least 2 experiments. (D) Representative images of labelled Vps1(ΔInsertB), Vps1(Δ3K) and 10-times excess Vps1(Δ4F) (cyan) with GppNHp on PI(3)P-containing membrane nanotubes (magenta). (E) Representative image and kymograph of protein scaffolds (cyan) from time-lapse images of D (F) Fission index of InsertB mutants. Data represents mean ± SD of at least 13 microscope fields across 2 experiments.

In order to understand more about the membrane binding, we added labelled mutant proteins to PI(3)P-containing membrane nanotubes in the presence of GppNHp, incubated, washed off unbound proteins and imaged. Vps1(ΔInsertB) does not bind to the tubes, confirming that the InsertB region is involved in Vps1 membrane binding. Vps1(Δ3K) was also rendered defective in membrane binding as the labelled proteins bound very little to the membrane. Of the few regions where bound, Vps1(Δ3K) formed small clusters. However, these clusters were unstable and wiggled around over time. Interestingly, Vps1(Δ4F) showed binding in PLiMAP but did not bind much to PI(3)P-containing membrane nanotubes at equal concentration as of full-length Vps1. Vps1(Δ4F) showed binding only to a few thick tubes and coated uniformly on these tubes. As the protein was binding in PLiMAP, we checked if the binding defect in SMrT

can be rescued by increasing the protein concentration. To our surprise, the addition of 10-times excess of labelled Vps1(Δ4F) bound to membrane tubes and formed clusters as in the case of Vps1 full-length, suggesting that Vps1(Δ4F) is not binding defective. The difference in binding and cluster formation might be attributed to an oligomerization defect (Figure 6.3.D,E).

6.2 Effect of InsertB on Vps1 distribution and cargo trafficking

As the InsertB mutants showed differences in membrane binding, we went ahead to see the mutants' localization inside the cell. For this, all InsertB mutants with the same tags as full-length Vps1 were added at the endogenous locus and expressed under the endogenous promoter. All the mutants showed equal protein levels when measured by western blotting against the ALFA tag. Deleting the whole InsertB rendered Vps1 cytosolic, confirming its requirement for membrane binding. Vps1(Δ3K) showed partial cytosolic localization with small puncta that predominantly localized to the vacuole as marked by Vph1-mScarlet. Meanwhile, Vps1(Δ4F) formed multiple small puncta localized to the vacuole. Interestingly, Vps1(ΔN-InsertB) also showed cytosolic localization as in the case of Vps1(ΔInsertB), suggesting the presence of membrane binding region in the N-terminal portion of InsertB (Figure 6.4.A).

Next, we looked at the effect of InsertB deletion mutations on Vps10 trafficking. By looking at the ratio of Vps10 to Vph1 signals as a measure of Vps10 localization (as discussed in materials and methods and chapter 5.2), Vps1(ΔInsertB) showed complete vacuole localization with a value of 1.93 close to that in *vps1Δ*. In fact, the effect of Vps1(ΔInsertB) was much more adverse than that of the whole Vps1 deletion. Meanwhile, Vps1(Δ4F) showed puncta localization of Vps10 with a ratio of 1.27, close to WT. Introducing Vps1(Δ3K) to cells caused Vps10 to show a mixed distribution of punctate and vacuole localized pools, with a ratio of 1.43, showing a half distribution to vacuole compared to WT or *vps1Δ* (Figure 6.4.B,C). None of the mutants rescued the fragmented vacuole phenotype.

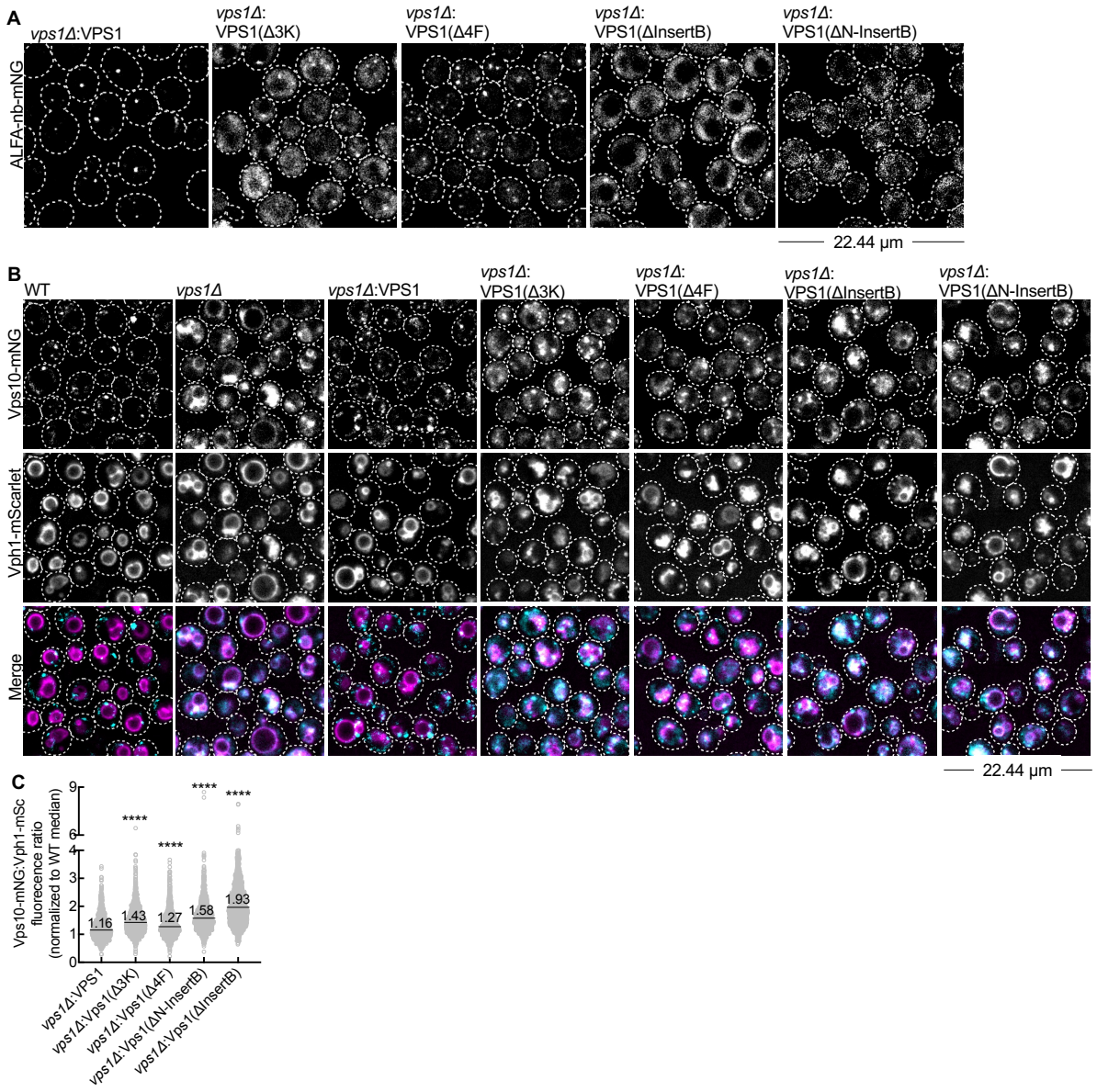

Figure 6.4 Functional analysis of Vps1-InertB region in cells A) Localization of Vps1 or InsertB mutants with ALFA tag on cells expressing ALFA-nb-mNG B) Representative images and C) Quantitation of Vps10 localization on vacuole in the background of Vps1 InsertB mutations plotted as Vps10:Vph1 ratio normalized to median ratio of WT. Vps10-mNG:Vph1-mSc ratios 1099 vacuole-like particles for *vps1Δ:*VPS1(Δ3K), 1006 for *vps1Δ:*VPS1(Δ4F), 1212 for *vps1Δ:*VPS1(ΔN-InsertB)*)* and 1346 for *vps1Δ:*VPS1(ΔInsertB) from 2 experiments. Data is normalized to the median ratio seen in WT. Numbers in the plot show the median ratios. Statistical significance of all mutants against *vps1Δ:*VPS1 was tested using an unpaired Mann-Whitney test with **** depicting p<0.0001.

6.3 Discussion

In this chapter, we looked at the characterization of the less studied InsertB region in Vps1, which was thought to be involved in Vps1 membrane binding. InsertB deletion partially knocked off Vps1 membrane binding under a relatively high lipid-to-protein ratio and showed complete incapability in binding on curved membrane topologies with less lipid-to-protein ratio. This result suggests that InsertB is the prominent binding site in Vps1 and that there is a possibility of alternate weak binding sites in Vps1. Previous studies monitoring membrane binding of the conserved lysines using sedimentation assays shown not to affect PI(3)P binding. However, with our sensitive binding assays we see otherwise. The Vps1(Δ3K) mutant exhibited membrane localization comparable to whole InsertB deletion in vitro, whereas it interestingly showed partial punctate localization in cells and partially rescued Vps10 trafficking. The membrane binding defect in vitro may be partially rescued in vivo by binding to adaptor proteins at the endosomes. Dynamin family proteins use a coincidence detection of simultaneous interaction with the specific lipid on the membrane and partner proteins to recruit on the membrane. Drp1 gets recruited to mitochondria with the help of mitochondrial transmembrane adaptor proteins Mff, Mid49 and Mid51[106]. Dynamins bind to their interactors by PRD-SH3 domain interaction and get recruited to the site of endocytosis[107]. It is possible that apart from membrane binding, regions in InsertB might be responsible for interaction with adaptor proteins.

Furthermore, despite no apparent membrane-binding defect, the Vps1(Δ4F) mutant displayed reduced binding on SMrT templates, which was rescued by excess protein, showed defects in stimulated GTPase activity and failed to cause fission of PI(3)P-containing membrane nanotubes. These differences are similar to those of the oligomerization defective mutant Vps1(G436D). We speculate that the observed differences in binding and cluster formation may not arise from a primary binding defect but could instead result from impaired oligomerization. Surprisingly, the defects reported in vitro are rescued in cells, where Vps1(Δ4F) shows multiple punctate localization and Vps10:Vph1 levels are similar to WT, further pressing on the role of partner proteins in rescuing defects. Interestingly, InsertB N-terminal deletion acted like whole InsertB deletion, considering its possibility of being prominently involved in membrane and adaptor binding. We have little information about the protein partners that recruit Vps1 to its site of action. A careful analysis of the N-terminal region of InsertB might give us hints about this aspect.

Chapter 7

Global analysis of trafficking pathways requiring Vps1

Vacuolar resident proteins are maintained through the intricate process of transport to the vacuole and retrieval of non-resident proteins from the vacuole. Transport to the vacuole is mediated by different arms, such as AP3-mediated sorting[108–110] and Clathrin-coated vesicle-mediated sorting at the Golgi[111,112], which transfers most of the soluble and membrane proteins to the vacuole. The cytosol-to-vacuole (Cvt) pathway also transports a small number of vacuolar hydrolases through selective autophagy[113–115]. While prior studies have focused on the trafficking of individual cargo proteins, we sought to evaluate the global impact of Vps1 deletion on vacuolar protein levels.

7.1 Analysis of global vacuole proteome upon Vps1 deletion

In order to understand the effect of Vps1 deletion on vacuolar proteome, we first isolated vacuoles from WT and *vps1Δ* strain. For this, we first grew both the strains to mid-log phase. Further, using density gradient centrifugation, we isolated vacuoles from these strains and equal quantity of vacuoles from both strains were trypsinized. Then, vacuoles from the *vps1Δ* strain were labelled with heavy formaldehyde, and vacuoles from the WT strain were labelled with light formaldehyde. Equal volume of labelled samples were mixed, and subjected to mass spectrometry analysis (Figure 7.1.A). This approach yielded ratios of heavy- to light-labelled proteins, which will be referred to now on as H:L values.

The data was now plotted as fold change in H:L values (log2 scale) versus significance according to the p-value (log-10 scale), providing us with a distribution of hits, usually referred to as the volcano plot (Figure 7.1.B). Zero fold change is considered as the mid-region of the plot. Then, the values on the left of zero can be considered reduced or depleted in the *vps1Δ* strain, and the ones on the right of zero can be regarded as more enriched in the *vps1Δ* strain. In order to get a stringent measure for protein hits, we employed a cut-off, where ratios greater than 2 were considered enrichment of protein and, ratios less than 0.5 were considered depletion of proteins in the vacuole and between 0.5-2 were considered unchanged. Additionally, the hits were sorted based on a significance of more than 0.1.

Among the 284 proteins identified after implementing the cut-off, 187 were depleted, 11 were enriched, and 86 fell inside the 0.5-2 fold change range, which we considered unchanged (Figure 7.1.C). Most depleted proteins were soluble, while the enriched proteins were predominantly membrane-associated. While Vps10 was among the enriched protein fraction, Vps10 cargo CarboxypeptidaseY (CPY) was depleted in the vacuole as previously reported[31,32,39], giving proof of principle for the mass-spectrometry data (Figure 7.1.B). We

further analyzed the protein pools that are enriched and depleted in the vacuole to understand the processes that Vps1 mediates in Vacuolar protein sorting.

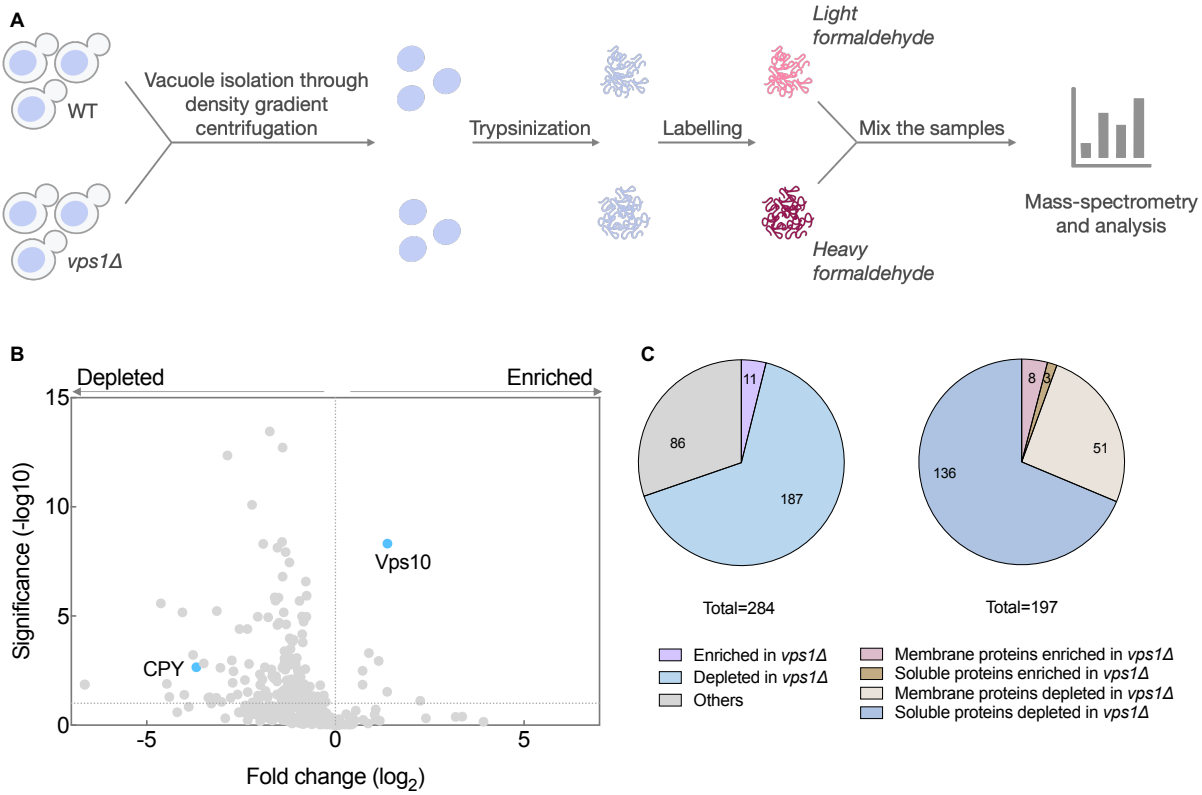

Figure 7.1 Quantitative proteomics of vacuoles from WT and *vps1Δ* strains. (A) Schematic of the experimental workflow. Vacuoles were isolated from mid-log phase WT and *vps1Δ* yeast cells via density gradient centrifugation. Equal amounts of vacuolar protein from each strain were trypsinized, then labeled with heavy (*vps1Δ*) or light (WT) formaldehyde. The labeled samples were mixed in equal volumes and analyzed by mass spectrometry, to get heavy-to-light (H:L) ratios (B) Volcano plot of $\log_2$(H:L) fold changes versus $-\log_{10}$(p-value). Proteins shifted left of the zero fold-change line (negative $\log_2$(H:L)) are depleted in *vps1Δ* vacuoles, whereas those shifted right (positive $\log_2$(H:L)) are enriched. The thresholds used were H:L > 2 (enriched) and H:L < 0.5 (depleted), with a significance cutoff of $p < 0.1$. Vps10 is enriched (blue), while its known cargo Carboxypeptidase Y (CPY) (blue) is depleted in *vps1Δ*, consistent with established observations. (C) Pie charts summarizing the 284 proteins that met the significance and fold-change thresholds. 187 are depleted (blue), 11 are enriched (pink), and 86 remain unchanged (grey). Depleted proteins are predominantly soluble, while enriched proteins are largely membrane-associated.

7.2 Proteins enriched in the vacuole

We first looked at the proteins that are enriched in *vps1Δ* strain. Additional to Vps10, three phospholipid flippases, typically localized to the plasma membrane, ER, or Golgi, were enriched in the vacuole upon Vps1 deletion. Golgi-based P4-ATPse Neo1, a phospholipid flippase, traffics between the Golgi and endosome in a retromer-dependent manner and maintains the phosphatidyl ethanolamine pool in the Golgi and vacuole[116–118]. Vps1 deletion

caused mislocalization of Neo1-mNG to vacuole in a 2-fold pattern similar to Vps10, suggesting Neo1 and Vps10 rely on a shared Vps1-mediated retrieval pathway (Figure 7.2.A). Additionally, proteins involved in the yeast cell wall maintenance were also enriched in the vacuole (Table 7.1). This is in line with the study on the effect of disruption of the plasma membrane recycling pathway on the vacuolar proteome, suggesting other organelle substrates for Vps1.

Table 7.1 Membrane proteins enriched in the vacuole**.**

Standard Name	Name	H:L	PVal H:L	Subcellular location	Human homolog	Function
VPS10	Vacuolar protein sorting/targeting protein VPS10	2.61	4.75E-09	Golgi/Endosome	SORL1	Trafficking of soluble proteins from Golgi to vacuole
DNF2	Phospholipid-transporting ATPase DNF2	2.06	3.33E-01	Plasma membrane	ATP10A	ATP dependent phospholipid flippase
LEM3	Alkyl phosphocholine resistance protein LEM3	9.11	4.17E-01	Plasma membrane/ER	TMEM30A, B	ATP dependent phospholipid flippase
NEO1	Probable phospholipid-transporting ATPase NEO1	2.11	5.43E-01	Golgi/Endosome	ATP9A,B	ATP dependent phospholipid flippase
TOH1	Cell wall protein YJL171C	2.22	1.14E-03	Plasma membrane/ GPI-anchored	None	Cell wall protein of unknown function
CBR1	NADH-cytochrome b5 reductase 1	2.59	2.92E-02	Nuclear/ Mitochondria	CYB5R3	Metabolism > Detoxification > Xenobiotic metabolism
UTR2	Probable glycosidase CRH2	4.75	7.57E-02	Plasma membrane/GPI-anchored	None	Chitin transglycosylase
STV1	V-type proton ATPase subunit a, Golgi isoform	2.26	6.19E-01	Golgi/Endosome	TCIRG1	V-ATPase

7.3 Proteins depleted in the vacuole

Next, we tested some of the mass-spec candidate proteins that showed depletion in the vacuole upon Vps1 deletion. Most of the soluble vacuolar hydrolases were depleted upon Vps1 deletion. Of the membrane proteins that showed depletion, a large pool of amino acid transporters and ion transporters showed depletion (Table 7.2). We tested one of the ion transporter, Zrc1 on our assay system. Zrc1 is a vacuolar resident Zinc transporter[119]. Zrc1-mNG shows a 1.4-fold depletion on *vps1Δ* strains (Figure 7.2.B). Interestingly, another

vacuolar membrane protein, Ybt1, which acts as a bile pigment transporter and a crucial phosphatidylcholine maintaining protein in the vacuole[120], did not show much difference in the localization in our imaging assays (Figure 7.2.C).

Table 7.2 Vacuolar resident membrane proteins depleted in the vacuole upon Vps1 deletion.

Standard Name	Name	H:L	PVal H:L	Human homolog	Function
YPT7	Ypt/Rab-type GTPase YPTx7	0.073	5.97E-04	Rab7A	Small GTPase; effecter protein for fusion machinery
PHO91	Low-affinity phosphate transporter PHO91	0.121	2.31E-03	SLC13A1,2,3,4,5,	Low-affinity vacuolar phosphate transporter
FMP42	Protein FMP42	0.149	1.08E-03	SLC43A1,2,3	Amino acid transporter
ZRC1	Vacuolar zinc transporter ZRC1	0.293	3.26E-01	None	Vacuolar membrane zinc transporter
ZRT3	Zinc-regulated transporter 3	0.218	8.97E-02	None	Vacuolar membrane zinc transporter
DIP5	Dicarboxylic amino acid permease	0.103	1.01E-01	SLC7A1,2,3,14	L-arginine transmembrane transporter activity
VNX1	Low affinity vacuolar monovalent cation/H	0.251	2.90E-01	None	Calcium/H+ antiporter
YBT1	ATP-dependent bile acid permease	0.376	4.03E-09	ABCC8,9,10	Transporter of ATP-binding cassette (ABC) family
NPC1	NPC intracellular sterol transporter 1-related protein 1	0.438	3.45E-01	NPC1	NPC intracellular cholesterol transporter 1

These findings suggest that Vps1 deletion disrupts both the retrieval of proteins from the vacuole and vesicle formation at the Golgi. Enrichment of specific proteins indicates defective retrieval from vacuole, while depletion highlights impaired trafficking pathways to the vacuole. This dual role positions Vps1 as a key regulator of vacuolar protein sorting.

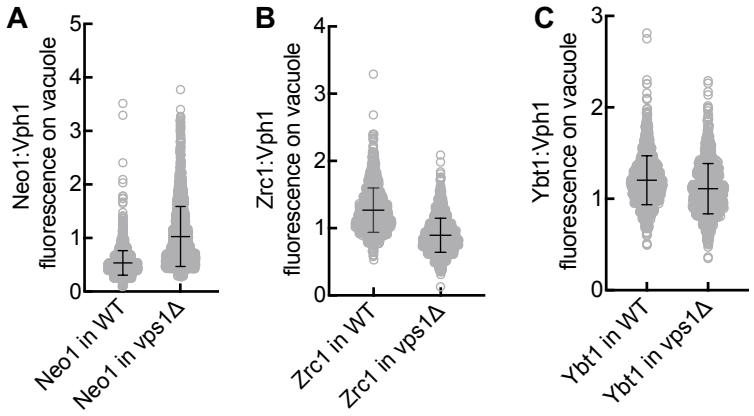

Figure 7.2 Testing protein hits from mass-spectrometry on cells A) Quantitation of proteins enriched in mass-spectrometry; Neo1 localization to the vacuole plotted as Neo1:Vph1 ratios. Data for 2202 particles for WT and 2492 for vps1Δ from 2 experiments. Quantitation of proteins depleted in mass-spectrometry; B) Zrc1 localization to vacuole plotted as Zrc1:Vph1 ratio. Data for 1160 particles for WT and 1505 for vps1Δ from 2 experiments. C) Ybt1 localization to vacuole plotted as Ybt1:Vph1 ratio. Data for 1215 particles for WT and 1181 for vps1Δ from 2 experiments.

7.4 Discussion

This chapter summarizes our efforts to elucidate the role of Vps1 in maintaining the vacuolar proteome. A comparative analysis of the vacuolar proteome in WT versus *vps1Δ* strains revealed a global depletion of vacuolar resident proteins, predominantly soluble proteases. In addition, many ion transport proteins and amino acid transporters were also depleted in the *vps1Δ* strain. Notably, the Rab7 homolog YPT7, which serves as a marker for vacuolar identity and as an initiator for recruiting the fusion machinery[121,122], was severely depleted. This raises questions regarding how the fusion mechanism is maintained in the VPS1 knockout, thereby challenging our understanding of effective material transport to the vacuole necessary for both vacuolar composition and degradation functions. The depletion of these proteins suggests that the trafficking pathway from the Golgi to the vacuole is disrupted. Additionally, mass spectrometry-based analyses in the past have identified Vps1 interaction with AP-3 subunits, suggesting its involvement in the AP-3 trafficking pathway[123]. These results indicate that Vps1's role may not be limited solely to the retrieval of proteins, but might also be essential for vesicle formation at the Golgi. Whereas, our imaging with Zrc1 in WT and *vps1Δ* strains shows clear vacuole localization with no apparent signals from other compartments. This make us wonder about gene transcription and protein degradation-based regulation of protein amounts upon Vps1 deletion.

Only a small subset of proteins were enriched in the vacuole, and most of these are not typical vacuolar resident proteins. Among the enriched proteins are membrane proteins that maintain plasma membrane lipid composition and cell wall integrity. Previous reports suggest that plasma membrane proteins, including Lem3, are recycled back to the plasma membrane via the Golgi Associated Retrieval Pathway (GARP)[124]. Deletion of the GARP complex results in the mislocalization of many of these proteins to the vacuole, as also observed in the case of the Vps1 deletion, indicating that Vps1 may also be involved in vesicle release at the Golgi. Vps1 is also implicated in early endosome-to-late Golgi transport through its association with the GARP complex[125,126].

Additionally, the Neo1 is known to shuttle between Golgi and vacuole, as in the case of Vps10, which utilizes a clathrin-coated vesicle-mediated route for vesicle release from the Golgi. The enrichment of proteins that utilize this route for vacuolar targeting indicates that Vps1 is likely not involved in forming clathrin-coated vesicles at the Golgi, suggesting that Vps1-mediated fission is specific to certain processes. These findings further imply the existence of alternative fission proteins in yeast. Interestingly, there were also non-vacuolar resident proteins that showed less vacuolar localization. Validating these protein depletions might open up insights in protein regulation mechanisms and inter-organelle communication.

The VPS pathway is evolutionarily conserved, and the disruption of analogous mammalian proteins is associated with different diseases in mammals. For instance, the Vps10 homolog Sortilin is linked to Alzheimer's disease[127], deletion of the Neo1 homolog affects neuronal development[128,129], and mutations in genes involved in lysosomal hydrolysis lead to lysosomal storage disorders[130]. Together, these findings emphasize the need for further investigation into the effects of Vps1 deletion on vacuolar homeostasis.

Chapter 8

Screen to identify membrane fission proteins in yeast

8.1 Prelude

Membrane fission is essential for the formation of tubular-vesicular intermediates that help in the transport of various materials between membrane compartments and to outside of the cell. Dynamin is a well-studied fission protein with orthologues across different kingdoms[58,67,131]. Dynamin super family proteins use the GTP binding and hydrolysis-dependent conformational change to drive fission and fusion[59]. There are four recognized Dynamin family proteins in yeast. Two are mitochondrial transmembrane proteins Mgm1 and Fzo1 indicated to be involved in mitochondrial fusion[132,133], and the remaining two, Vps1 and Dnm1, are soluble. While Dnm1 is indispensable for mitochondrial fission[134], its deletion does not markedly affect other membrane trafficking pathways[48]. Despite the central role of Vps1 in vacuole-to-Golgi trafficking[30,31,39,40], endocytosis[51–54], autophagy[55] and peroxisome fission[46–48], Vps1 deletion does not result in widespread disruption of other cellular functions, which strongly suggests the presence of alternative fission mechanisms that safeguard essential trafficking pathways. These observations imply the presence of additional fission factors in yeast that either work in tandem with or independently of the classical dynamin proteins.

The significance of membrane fission extends beyond vesicle formation across organelles; it is fundamental to endocytosis, organelle division, and overall cellular homeostasis. A failure in these processes can lead to imbalances in protein localization, organelle dysfunction, and, ultimately, disease. Notably, many membrane trafficking defects in higher order eukaryotes, including those implicated in neurodegenerative diseases and lysosomal storage disorders, have parallels in yeast.

Extensive screens on vesicular transport using yeast have shed light on processes like secretion, autophagy and degradation pathways[17,18,22,23,33,34]. However, it was hard to directly pin-point players involved in membrane fission from these screens. This might be due to the phenotypic approach used in these screens which primarily looked at vesicle accumulation and without fission, vesicles will not form in the first place. Parallel reports on the involvement of membrane fission catalysts in yeast, are majorly based on the assessment of disruption in transport pathways or organelle morphology in a knock-out/over-expression model or in the presence of different treatment conditions[31,39,48,135].

The combination of our current findings on Vps1 with the inherent strengths of the yeast model system provides a compelling rationale for a large-scale screen to identify additional membrane

fission proteins. In the current study, we perform an unbiased biochemical screen to find membrane fission catalyst using yeast as a model system under different lipid conditions.

8.2 SMrT templates as a system to find novel membrane fission proteins

Although membrane fission is critical for cellular homeostasis, assay systems capable of probing membrane fission reactions have been limited. While in vivo experiments have provided insights into the functional roles of fission catalysts, the resolution of current imaging techniques does not allow us to directly observe the mechanism of fission from protein side. In contrast, reconstitution studies have significantly advanced our understanding of how specific proteins promote membrane remodelling by outlining the minimal machinery required for these processes[136,137]. Although liposome-based approaches, widely used for reconstitution studies, have been highly informative regarding the membrane-binding properties of proteins, they present several limitations as they provide only end-point readouts, lacking the capability for real-time analysis of the sequential events involved in fission. Additionally, membrane templates with an excess reservoir have been employed to investigate fission reactions. Yet, their utility is constrained by the inherent planar nature of the template[138].

In contrast, supported membrane templates (SMrT) have been successfully utilized to monitor membrane fission reactions in real time[75,77,88,89,139]. SMrT offer unique advantages over other model systems such as forming tube-like intermediates for fission assays, enabling real-time tracking of the fission pathway, and exhibiting robustness and ease of use. Moreover, the lipid composition of these nanotubes is tuneable. These advantages motivated us to develop a screening approach for novel membrane fission catalysts in yeast using SMrT as the assay system.

Phosphatidylinositol and its derivatives (PIPs) are one of the less abundant lipids present in the cell yet playing crucial role in important cellular functions[140–143]. They are generated through the phosphorylation of phosphatidylinositol (PI) at different positions on the inositol ring. A plethora of kinases and phosphatases regulate these phosphorylation reactions at different cellular compartments[144,145]. This gives each compartment its own PI-based membrane identity which helps in recruiting specific proteins from the cytosol helping in organellar functions[146]. The specific head groups of PIPs bind to an array of protein domains such as PH, PX, C2, 2xFYVE and BAR domain helps in organelle specific protein recruitment[147]. There are seven

PIPs reported in yeast. Due to the specificity they offer on protein recruitment, here we consider PIPs as variable lipids to screen for fission activity.

8.3 Screen for fission proteins in yeast

Supported membrane nanotubes were prepared as described previously. These templates consisted of a lipid mixture containing 5% of a specific phosphoinositide (PIP) and 15% DOPS, with the remaining lipids composed of DOPC and visualized by the inclusion of 1% TxRd-DHPE. Cytosol prepared from the protease-deficient *S. cerevisiae* strain BJ3505, which had been desalted to remove nucleotides and additional cofactors, was then flowed onto these templates. Fission events were observed in a distinctly PIP-dependent manner; no fission occurred on DOPC control templates or templates lacking the specific PIP (Figure 8.1.A,B).

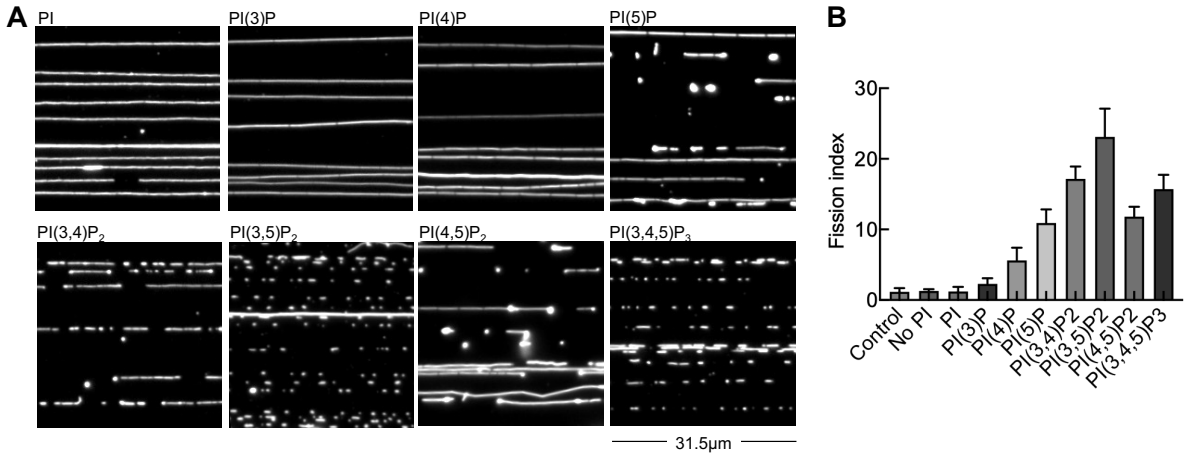

Figure 8.1 PIP-specific membrane fission activity of yeast cytosol A) Representative fluorescence micrographs show supported lipid nanotubes composed of 5% phosphoinositide (PIP), 15% DOPS, and 79% DOPC with 1% TexasRed-DHPE after incubation with nucleotide-depleted yeast cytosol. DOPC-only templates and templates lacking PIPs serve as control. B) Plot showing the fission index under the indicated conditions. Data represents mean ± SD of at least 30 microscope fields across 3 experiments.

In contrast, robust fission activity was detected on templates containing Phosphatidylinositol-3,5-bisphosphate ($PI(3,5)P_2$) followed by Phosphatidylinositol-3,4,5-triphosphate ($PI(3,4,5)P_3$), and Phosphatidylinositol-4,5-bisphosphate ($PI(4,5)P_2$). Surprisingly, the fission observed was nucleotide-independent. Given that Vps1 requires GTP binding and hydrolysis to mediate fission, these results strongly indicate that the protein responsible for the fission activity in our assay is not Vps1.

8.4 Biochemical fractionation of fission activity from yeast lysate

Considering the complexity of the yeast lysate, isolating the specific protein or protein complex responsible for the observed fission activity is challenging. Therefore, the lysate was biochemically fractionated using an anion exchange column to enrich the active component in the lysate (Figure 8.2.A). Equal protein concentrations from the collected fractions were flown onto PI(3,5)P_2-containing membrane nanotubes, and the fission index was calculated for each fraction. Of the seven fractions tested, fraction 2 exhibited the highest fission activity, with a stepwise reduction in activity observed in subsequent fractions (Figure 8.2.B). Since each fraction contained equivalent protein amounts, the high fission index in fraction 2 indicates that the protein(s) responsible for the activity is concentrated in this fraction. Fraction 2 was subjected to size exclusion chromatography (SEC) to refine the protein profile further (Figure 8.2.C). When these SEC fractions were tested on the membrane nanotubes, fraction 6 displayed prominent fission activity, followed by fractions 7 and 5, while the remaining fractions were inactive (Figure 8.2.D). Hence, fraction 6 was processed for protein identification using mass spectrometry.

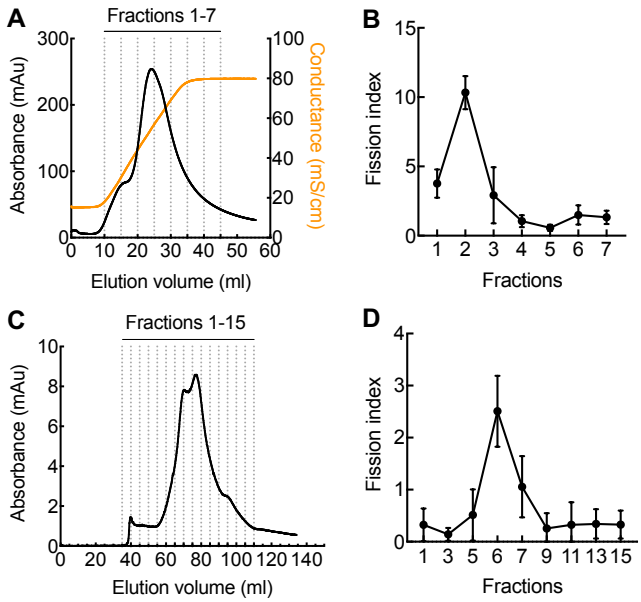

Figure 8.2 Biochemical fractionation of yeast cytosol A) Plot showing the anion exchange chromatogram of yeast cytosol. Fractions that are analyzed further are indicated. B) Fission index quantitation after adding equal protein amounts from each fraction (1–7) on PI(3,5)P_2-containing membrane nanotubes. Data represents the mean ± SD of at leaset 10 fields from 2 experiments. C) Plot showing the size exclusion chromatography (SEC) based separation of Fraction 2 from anion exchange chromatography of yeast cytosol. Fractions that are analyzed further are indicated. D) Fission index quantitation after adding fraction (1–15) on PI(3,5)P_2-containing membrane nanotubes. Data represents the mean ± SD of at leaset 10 fields from 2 experiments.

8.5 Mass spectrometry-based search for putative membrane binding proteins

After performing three independent mass-spectrometry runs with SEC-fraction 6, the hits were identified using protein pilot software with S288C database for identification of the hits. Proteins identified with two or more unique peptides were considered for further analysis. 382 proteins were common to at least two of the three runs, with 236 proteins identified in all three runs. To streamline the candidate pool for subsequent studies, we focused on proteins known to contain membrane-binding domains, based on the rationale that for a protein to cause fission of membrane nanotubes, it must first be capable of membrane binding. This filtering strategy narrowed the list to seven proteins possessing annotated membrane-binding domains, which were subsequently prioritized for further investigation (Table 8.1).

8.6 Testing candidate proteins on SMrT

We first tested the proteins that were common to all three runs. For this, we cloned, expressed, and purified Gvp36 and Lsp1. Gvp36 and Lsp1 both have a BAR domain, a banana-shaped structural motif known for its membrane-binding properties. Previous reports and the YPIB repository for Yeast PI-binding proteins[148] suggest that GVP36 does not exhibit any known PIP specificity, whereas Lsp1 is recognized for its ability to bind other phosphoinositides such as PI, PI4P, PI(4,5)P_2 and PI(3,4,5)P_3. Gvp1 helps in fluid-phase endocytosis and can interact with Other BAR-domain proteins crucial for endocytosis[149,150]. Lsp1 predominantly localizes at the plasma membrane as distinct, punctate structures and along with Pil1 forms eisososmes[151,152]. In addition, structural analysis shows that Lsp1 can self-oligomerize in solution. When Lsp1 was provided with PI(4,5)P_2-containing liposomes, it formed membrane tubes, indicating its membrane remodelling ability as other BAR domain-containing proteins[153].

We checked for the binding ability of Gvp36 and Lsp1 to PI(3,5)P_2-containing membrane using PLiMAP. We find Lsp1, but not Gvp36, to bind PI(3,5)P_2-containing membrane (Figure 8.3.A). Consistent with the binding results, adding Gvp36 showed no apparent effect on PI(3,5)P_2-containing supported membrane nanotubes. However, the addition of Lsp1 showed constriction of the nanotubes but no fission (Figure 8.3.B,D). It is possible that the absence of post-translational modifications in the bacterially expressed Lsp1 renders it incapable of fission. Alternatively, Lsp1 may act to recruit the PI(3,5)P_2-dependent fission protein. In order to confirm these possibilities, we tested lysates prepared from the Lsp1 deletion strain (*lsp1Δ*). If Lsp1 is responsible for the fission of PI(3,5)P_2-containing nanotubes, its removal from the

lysate should abolish fission. We saw robust fission with (lsp1Δ lysate, ruling out Lsp1 as the $PI(3,5)P_2$-dependent fission catalyst (Figure 8.3.C).

Table 8.1 Proteins shortlisted from mass spec analysis of fraction 6 of SEC. Presence of known membrane binding domains was used as the criteria for shortlisting.

Gene	Protein	Frequency in runs	Membrane binding domain	Known functions	Lipid specificity
GVP36	Golgi Vesicle Protein of 36kDa	3	AH/BAR domain	Endocytosis	Unknown
LSP1	Sphingolipid long chain base-responsive protein Lsp1	3	AH/BAR domain	Component of eisosomes	$PI(4,5)P_2$ $PI(3,4,5)P_3$
ENT 3	Epsin-3	2	ENTH domain	Golgi to endosome transport	$PI(3,5)P_2$ PI3P
PiL1	Sphingolipid long chain base-responsive protein Pil1	2	AH/BAR domain	Component of eisosomes	$PI(4,5)P_2$ $PI(3,4,5)P_3$
YPR148C	Uncharacterized protein YPR148C	2	AH/BAR domain	Unknown function	Unknown
SCH9	Serine/threonine-protein kinase Sch9	2	C2 domain	Protein kinase	Unknown
NUM1	Nuclear migration protein Num1	2	PH domain	Controls nuclear migration Helps in dynein-dependent sliding of the microtubules in the bud	Unknown

We extended our search by looking at proteins common in at least 2 of the 3 runs. Purified uncharacterized protein YPR148C did not cause the fission of nanotubes (Figure 8.3.D). The rest of the candidate proteins were tested by the same rationale used for testing lsp1Δ lysate, by flowing lysates made from particular candidate protein deletion strains to see if the lysate shows less fission when compared to WT lysate. After flowing lysates of the deletion strains, we did not see a significant decrease in the fission index compared to WT lysate (Figure 8.3.E). So far, the proteins with annotated membrane binding sites do not show any $PI(3,5)P_2$-dependent fission activity on supported membrane nanotubes.

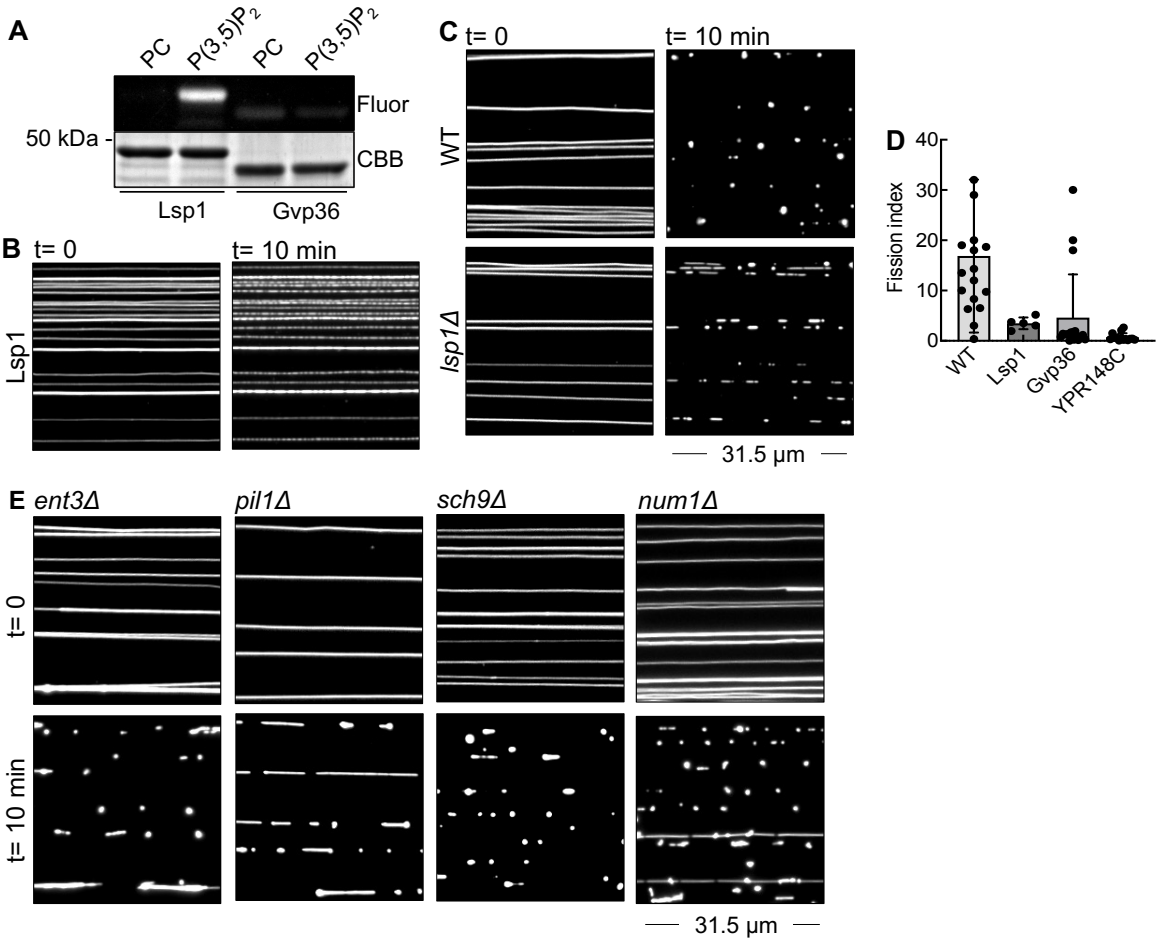

Figure 8.3 Testing candidate proteins for PI(3,5)P₂-dependent membrane fission. A) PLiMAP analysis showing purified Lsp1, but not Gvp36, binds to PI(3,5)P_2-containing membrane. (B) Fluorescence micrographs of supported PI(3,5)P_2-containing nanotubes after the addition of purified Lsp1. (C) Micrograph showing nanotubes 10 min after flowing lysates from Lsp1 deletion strain (*lsp1Δ*) (D) Quantitation of fission index with purified Lsp1, Gvp36 and YPR148C added to PI(3,5)P_2-containing nanotubes. (E) Micrograph showing nanotubes 10 min after flowing lysates from deletion strains of candidate proteins in at least two runs.

8.6 Discussion

Membrane fission is central to cellular physiology, yet identifying the specific proteins involved in membrane fission has been challenging, partly due to the limited availability of assays that directly monitor fission events. In this study, we employed PEG-cushioned SMrT to assay yeast cytosol for proteins mediating the fission of membrane nanotubes enriched with distinct phosphatidylinositols (PIPs). Our results reveal that yeast lysate exhibit PIP-specific fission activity, with particularly robust fission observed on membrane containing PI(3,5)P_2. Notably, this fission activity is nucleotide-independent, which excludes the involvement of dynamin superfamily proteins, known to require nucleotide hydrolysis for their function.

Subsequent biochemical analyses combined with proteomics identified 382 proteins across at least two independent runs.

To further investigate, we tested purified proteins and lysates from deletion strains on $PI(3,5)P_2$-containing membrane nanotubes. None of the proteins with annotated membrane-binding domains demonstrated $PI(3,5)P_2$-dependent fission activity on these supported membrane nanotubes. Proteins with unannotated membrane-binding regions might be involved in the observed fission activity. However, these proteins would not be identified using our current approach. Recent studies have highlighted the nucleotide-independent fission catalyst HPO-27 in *C. elegans* and its mammalian homologue MROH1, illustrating a unique mechanism for lysosomal membrane fission[154]. $PI(3,5)P_2$ is enriched in lysosomes in higher order eukaryotes and vacuoles in yeast, and its increased levels during stress lead to vacuolar fragmentation[155,156]. Unfortunately, yeast does not possess a clear orthologue of HPO-27 or MROH1, though several uncharacterized proteins in our mass spectrometry dataset might serve similar roles.

The biochemical screen discussed in this chapter holds promise for uncovering novel proteins that act as fission catalysts or regulators. Finally, this work aims to deepen our understanding of the fundamental principles governing membrane dynamics and to provide translational insights into the pathological consequences of trafficking defects in higher order eukaryotes.

Chapter 9

Summary, discussion and perspectives

Summary and Discussion

Remodelling of biological membrane is central to different cellular processes and maintains the cellular homeostasis. Membrane fission is the ultimate step for the release of tubular-vesicular intermediates containing different cargoes. Despite this importance, there is less understanding on the proteins that catalyze membrane fission during various cellular processes.

In this study, we show that yeast Dynamin family protein- Vps1 is capable and sufficient to bind, constrict and cause fission of membrane with endosomal lipid composition in vitro. While Vps1 exhibits binding to negatively charged membrane, GTP hydrolysis and fission were seen only in the presence of PI(3)P-containing membrane, highlighting the effect of specific headgroup binding in enhancing catalytic functions of Vps1. PI(3)P is known to be enriched at endosomal membranes[85]. Furthermore, localization studies using the Vps1(K42A) mutant have shown its colocalization with Mvp1 at endosomes, supporting Vps1's role in endosomal membrane remodelling[30]. Vps1-mediated fission shows a tube radius dependency, with maximum fission below 30 nm radius. Vps1 is shown to interact with the tabulator SNX-BAR proteins at endosomes. Cryo-EM analysis of tubules formed by SNX-BAR proteins on PI(3)P-containing liposomes shows a mean radius of 15 nm[91]. These dimensions fall within the range acted upon by Vps1, making the tube radius dependency correlated to the tubes formed by SNX-BAR proteins on membrane. Similarly, mitochondrial fission catalase Drp1 is known to severe membrane nanotubes up to a 200 nm radius and show complete shut-down of fission above 250 nm radius[88], aligning with the mitochondrial sizes.

Stage-specific analysis of Vps1-mediated fission shows that Vps1 binds and constricts the underlying membrane to approximately 17 nm radius in the GTP-bound state. GTP hydrolysis further reduces the tube radius to a pre-fission intermediate of ~ 6 nm before fission occurs. Recent cryo-EM reconstructions of Vps1 from a related yeast species *C. thermophilum*, estimated a scaffold lumen diameter of 19 nm (10 nm radius) in the GTP-bound state[70]. In SMrT templates, the presence of the membrane appears to hinder Vps1 from achieving this scaffolded state. Stimulated GTP hydrolysis of Vps1 in the presence of membrane likely aids in attaining this state by enabling efficient membrane constriction and subsequent fission.

Vps1 was initially identified in genetic screens for proteins involved in Golgi-to-vacuole transport. The most well-characterized role of Vps1 in the VPS pathway involves protein retrieval from endosomes to the Golgi in coordination with the retromer complex, with Vps10 as the primary cargo studied. However, previous analyses have broadly classified the effects

of Vps1 deletion on Vps10 localization in a binary manner. Here, we developed a quantitative assay to assess the extent of Vps1 deletion on Vps10 trafficking by measuring the Vps10 localization relative to the stable vacuolar resident protein Vph1. This approach allowed us to systematically evaluate the effects of different Vps1 mutations on cargo trafficking.

We further characterized the less known InsertB region in Vps1 analogous to the PH-domain in dynamins. Our analysis with different mutations on the InsertB region of Vps1 shows that InsertB is important for the membrane binding ability of Vps1. InsertB deletion partially knocked off Vps1 membrane binding under a high lipid-to-protein ratio and showed complete incapability in binding on curved membrane topologies with less lipid-to-protein ratio, suggesting InsertB to be the prominent binding site and indicating the possibility of alternate binding sites in Vps1.

The inability in membrane binding also affects the oligomerization and stimulated GTP hydrolysis of Vps1 on PI(3)P-containing membrane. Careful analysis of the InsertB region with specific deletions shows that the lysines at the C-terminus of InsertB are critical for membrane binding. It also indicates that the adjacent phenylalanine stretch might help the oligomerization of Vps1 on the membrane. Interestingly, these abnormalities are partially rescued inside the cell, suggesting other interactions with the membrane and maybe adaptor proteins to prevail in the rescue of function. However, the InsertB N-terminal deletion does not rescue cellular functions. It is possible that the N-terminal portion contains alternate membrane binding sites or residues to recognize and recruit Vps1 adaptors. We have little information about the protein partners that recruit Vps1 to its site of action. A careful analysis of the N-terminal region of InsertB might give us hints about this aspect.

Our comparative analysis of the vacuolar proteome in wild-type versus *vps1Δ* strains revealed a global depletion of resident proteins, predominantly soluble proteases, ion transporters, and amino acid transporters with a marked reduction in the Rab7 homolog YPT7, a critical marker for vacuolar identity and fusion machinery recruitment. These findings suggest that the absence of Vps1 disrupts the Golgi-to-vacuole trafficking pathway, indicating that Vps1 may be essential for protein retrieval from the vacuole and vesicle formation at the Golgi.

In contrast, only a limited subset of non-canonical vacuolar proteins were enriched, including non-vacuolar resident membrane proteins involved in plasma membrane lipid composition and cell wall integrity. Some of these proteins, shown to be recycled via the Golgi Associated

Retrieval Pathway (GARP), mislocalize to the vacuole in both GARP and Vps1 deletions, implying a role for Vps1 in vesicle release at the Golgi. Additionally, the enrichment of proteins using clathrin-coated vesicle-mediated routes for vacuolar targeting suggests that Vps1-mediated fission is process-specific and that alternative fission factors may exist

In order to understand alternate fission proteins in yeast, we employed a biochemical screen. Our study utilized PEG-cushioned supported membrane templates (SMrT) to assay yeast lysates for proteins that mediate the fission of membrane nanotubes enriched with specific phosphatidylinositols (PIPs). We observed an apparent PIP-specific fission activity, with particularly robust fission events on membrane containing PI(3,5)P2. Notably, this fission was nucleotide-independent, effectively excluding the involvement of dynamin superfamily proteins that require nucleotide hydrolysis. Biochemical fractionation coupled with proteomics subsequently identified 382 proteins common to at least two of the three independent runs, providing a comprehensive dataset of potential fission regulators.

In further investigations using purified proteins and lysates from deletion strains on PI(3,5)P2-containing nanotubes, none of the proteins with annotated membrane-binding domains exhibited the expected fission activity. This observation suggests that either proteins with unannotated membrane-binding regions or entirely novel factors may be responsible for the observed activity. Recent report on nucleotide-independent fission in *C. elegans* by HPO-27, points towards novel mechanisms of lysosomal fission. While yeast lacks clear orthologues of the nucleotide-independent fission catalysts HPO-27 in *C. elegans* and its mammalian homologue MROH1[154], our dataset includes several uncharacterized proteins that could fulfil a similar role. The results from the screen hint at the complexity of membrane fission mechanisms and highlight the need for continued exploration.

Future perspectives

The Dynamin family of proteins uses co-incidence detection of specific lipids and adaptors to tune its binding to membrane compartments. While our study confirms Vps1's ability to bind and mediate membrane fission in a minimal lipid environment, the identity of its recruiting partner proteins remains unknown. Immunoprecipitation and pull-down assays indicate that Vps1 interacts directly with the BAR-domain protein Mvp1 and the Q-SNARE protein Vam3[30,41,44]. The interaction with Mvp1 suggests a broader network of BAR-domain proteins in yeast that may facilitate Vps1 recruitment. Unlike classical Dynamins, which utilize a C-

terminal PRD domain to bind SH3-domain-containing partners, Vps1 lacks PRD, keeping us wondering about the regions in Vps1 responsible for partner protein interaction. Additionally, Vps1 is thought to interact with the yeast Amphiphysin protein Rvs167 and to help in endocytosis[52]. A detailed study on Vps1 interaction with its partner proteins might shed light on the intricacies of this interaction.

Beyond protein interactions, it is crucial to understand the impact of Vps1 deletion on intracellular trafficking pathways. One fascinating aspect in this regard is the potential for alternative transport routes or compensatory mechanisms for vacuolar protein transport in the absence of Vps1. Studies show that vacuolar proteins take a plasma membrane route to get to the vacuole upon Vps1 deletion[157]. Given the evolutionary conservation of the VPS pathway and its link to human diseases, a systematic investigation of vacuolar protein sorting pathways could reveal critical regulatory mechanisms and functional redundancies.

Lysosomes function analogously to yeast vacuoles in higher order eukaryotes with conserved protein transport pathways across species. However, the mammalian counterpart of Vps1 involved in lysosomal fission remains unidentified. Existing literature suggests that classical Dynamins and Drp1 may play a role in this process, but their precise functions require further investigation. Analyzing mammalian homologs of Vps1 could provide valuable insights into additional players in lysosomal homeostasis and potentially uncover components involved in lysosomal disorders.

Publications

1. **Gopan, S.**[#], Singh, G.[#], Swaminathan, U. Pucadyil, T.J.* 2025. Vacuolar protein sorting-associated protein 1 (Vps1) has membrane constricting and severing abilities required for endosomal protein trafficking. *bioRxiv* 2025.05. 25.656005. ([#]equal contribution)

2. **Gopan, S.**, Pucadyil, T.J.* 2024. The race to uncover fission factors for lysosomal organelles heats up. *Nature* 628, 509-510.

3. Jose, G.P., **Gopan, S.**, Bhattacharyya, S., Pucadyil, T.J.* 2020. A facile, sensitive and quantitative membrane binding assay for proteins. *Traffic* 21:297-305. *(selected for cover).*

References

(1) Bonifacino, J. S.; Glick, B. S. The Mechanisms of Vesicle Budding and Fusion. *Cell* **2004**, *116* (2), 153–166. https://doi.org/10.1016/S0092-8674(03)01079-1.

(2) Cui, L.; Li, H.; Xi, Y.; Hu, Q.; Liu, H.; Fan, J.; Xiang, Y.; Zhang, X.; Shui, W.; Lai, Y. Vesicle Trafficking and Vesicle Fusion: Mechanisms, Biological Functions, and Their Implications for Potential Disease Therapy. *Mol Biomed* **2022**, *3* (1), 29. https://doi.org/10.1186/s43556-022-00090-3.

(3) Zhao, Y. G.; Zhang, H. Phase Separation in Membrane Biology: The Interplay between Membrane-Bound Organelles and Membraneless Condensates. *Developmental Cell* **2020**, *55* (1), 30–44. https://doi.org/10.1016/j.devcel.2020.06.033.

(4) Barlowe, C. K.; Miller, E. A. Secretory Protein Biogenesis and Traffic in the Early Secretory Pathway. *Genetics* **2013**, *193* (2), 383–410. https://doi.org/10.1534/genetics.112.142810.

(5) Barlowe, C.; Helenius, A. Cargo Capture and Bulk Flow in the Early Secretory Pathway. *Annual Review of Cell and Developmental Biology* **2016**, *32* (Volume 32, 2016), 197–222. https://doi.org/10.1146/annurev-cellbio-111315-125016.

(6) Glick, B. S.; Luini, A. Models for Golgi Traffic: A Critical Assessment. *Cold Spring Harb Perspect Biol* **2011**, *3* (11), a005215. https://doi.org/10.1101/cshperspect.a005215.

(7) Huang, S.; Wang, Y. Golgi Structure Formation, Function, and Post-Translational Modifications in Mammalian Cells. *F1000Res* **2017**, *6*, 2050. https://doi.org/10.12688/f1000research.11900.1.

(8) Mayor, S.; Pagano, R. E. Pathways of Clathrin-Independent Endocytosis. *Nat Rev Mol Cell Biol* **2007**, *8* (8), 603–612. https://doi.org/10.1038/nrm2216.

(9) Levine, B.; Kroemer, G. Biological Functions of Autophagy Genes: A Disease Perspective. *Cell* **2019**, *176* (1–2), 11–42. https://doi.org/10.1016/j.cell.2018.09.048.

(10) Antonny, B. Mechanisms of Membrane Curvature Sensing. *Annual Review of Biochemistry* **2011**, *80* (Volume 80, 2011), 101–123. https://doi.org/10.1146/annurev-biochem-052809-155121.

(11) Simunovic, M.; Voth, G. A.; Callan-Jones, A.; Bassereau, P. When Physics Takes Over: BAR Proteins and Membrane Curvature. *Trends in Cell Biology* **2015**, *25* (12), 780–792. https://doi.org/10.1016/j.tcb.2015.09.005.

(12) Morlot, S.; Roux, A. Mechanics of Dynamin-Mediated Membrane Fission. *Annu. Rev. Biophys.* **2013**, *42* (1), 629–649. https://doi.org/10.1146/annurev-biophys-050511-102247.

(13) Sarkar, M.; Pucadyil, T. J. Division of Labor among Fission Dynamins Based on Substrate Size. *Biochemistry* **2025**, *64* (10), 2117–2122. https://doi.org/10.1021/acs.biochem.4c00862.

(14) Jahn, R.; Scheller, R. H. SNAREs — Engines for Membrane Fusion. *Nat Rev Mol Cell Biol* **2006**, *7* (9), 631–643. https://doi.org/10.1038/nrm2002.

(15) Hecht, K. A.; O'Donnell, A. F.; Brodsky, J. L. The Proteolytic Landscape of the Yeast Vacuole. *Cellular Logistics* **2014**, *4* (1), e28023. https://doi.org/10.4161/cl.28023.

(16) Palade, G. Intracellular Aspects of the Process of Protein Synthesis. *Science* **1975**, *189* (4200), 347–358. https://doi.org/10.1126/science.1096303.

(17) Novick, P.; Schekman, R. Secretion and Cell-Surface Growth Are Blocked in a Temperature-Sensitive Mutant of Saccharomyces Cerevisiae. *Proc Natl Acad Sci U S A* **1979**, *76* (4), 1858–1862.

(18) Novick, P.; Field, C.; Schekman, R. Identification of 23 Complementation Groups Required for Post-Translational Events in the Yeast Secretory Pathway. *Cell* **1980**, *21* (1), 205–215. https://doi.org/10.1016/0092-8674(80)90128-2.

(19) Schekman, R.; Novick, P. 23 Genes, 23 Years Later. *Cell* **2004**, *116*, S13–S15. https://doi.org/10.1016/S0092-8674(03)00972-3.

(20) Morishita, H.; Mizushima, N. Diverse Cellular Roles of Autophagy. *Annual Review of Cell and Developmental Biology* **2019**, *35* (Volume 35, 2019), 453–475. https://doi.org/10.1146/annurev-cellbio-100818-125300.

(21) Ohsumi, Y. Historical Landmarks of Autophagy Research. *Cell Res* **2014**, *24* (1), 9–23. https://doi.org/10.1038/cr.2013.169.

(22) Takeshige, K.; Baba, M.; Tsuboi, S.; Noda, T.; Ohsumi, Y. Autophagy in Yeast Demonstrated with Proteinase-Deficient Mutants and Conditions for Its Induction. *The Journal of cell biology* **1992**, *119* (2), 301–311. https://doi.org/10.1083/jcb.119.2.301.

(23) Tsukada, M.; Ohsumi, Y. Isolation and Characterization of Autophagy-Defective Mutants of *Saccharomyces Cerevisiae*. *FEBS Letters* **1993**, *333* (1), 169–174. https://doi.org/10.1016/0014-5793(93)80398-E.

(24) Nakatogawa, H. Mechanisms Governing Autophagosome Biogenesis. *Nat Rev Mol Cell Biol* **2020**, *21* (8), 439–458. https://doi.org/10.1038/s41580-020-0241-0.

(25) Reggiori, F.; Ungermann, C. Autophagosome Maturation and Fusion. *Journal of Molecular Biology* **2017**, *429* (4), 486–496. https://doi.org/10.1016/j.jmb.2017.01.002.

(26) Yim, W. W.-Y.; Mizushima, N. Lysosome Biology in Autophagy. *Cell Discov* **2020**, *6* (1), 1–12. https://doi.org/10.1038/s41421-020-0141-7.

(27) Jiang, P.; Mizushima, N. Autophagy and Human Diseases. *Cell Res* **2014**, *24* (1), 69–79. https://doi.org/10.1038/cr.2013.161.

(28) Cullen, P. J. Endosomal Sorting and Signalling: An Emerging Role for Sorting Nexins. *Nat Rev Mol Cell Biol* **2008**, *9* (7), 574–582. https://doi.org/10.1038/nrm2427.

(29) Suzuki, S. W.; Chuang, Y.-S.; Li, M.; Seaman, M. N. J.; Emr, S. D. A Bipartite Sorting Signal Ensures Specificity of Retromer Complex in Membrane Protein Recycling. *Journal of Cell Biology* **2019**, *218* (9), 2876–2886. https://doi.org/10.1083/jcb.201901019.

(30) Suzuki, S. W.; Oishi, A.; Nikulin, N.; Jorgensen, J. R.; Baile, M. G.; Emr, S. D. A PX-BAR Protein Mvp1/SNX8 and a Dynamin-like GTPase Vps1 Drive Endosomal Recycling. *eLife* **2021**, *10*, e69883. https://doi.org/10.7554/eLife.69883.

(31) Arlt, H.; Reggiori, F.; Ungermann, C. Retromer and the Dynamin Vps1 Cooperate in the Retrieval of Transmembrane Proteins from Vacuoles. *Journal of Cell Science* **2014**, jcs.132720. https://doi.org/10.1242/jcs.132720.

(32) Robinson, J. S.; Klionsky, D. J.; Banta, L. M.; Emr, S. D. Protein Sorting in *Saccharomyces Cerevisiae* : Isolation of Mutants Defective in the Delivery and Processing of Multiple Vacuolar Hydrolases. *Molecular and Cellular Biology* **1988**, *8* (11), 4936–4948. https://doi.org/10.1128/mcb.8.11.4936-4948.1988.

(33) Rothman, J. H.; Stevens, T. H. Protein Sorting in Yeast: Mutants Defective in Vacuole Biogenesis Mislocalize Vacuolar Proteins into the Late Secretory Pathway. *Cell* **1986**, *47* (6), 1041–1051. https://doi.org/10.1016/0092-8674(86)90819-6.

(34) Bankaitis, V. A.; Johnson, L. M.; Emr, S. D. Isolation of Yeast Mutants Defective in Protein Targeting to the Vacuole. *Proc. Natl. Acad. Sci. U.S.A.* **1986**, *83* (23), 9075–9079. https://doi.org/10.1073/pnas.83.23.9075.

(35) Rothman, J. H.; Howald, I.; Stevens, T. H. Characterization of Genes Required for Protein Sorting and Vacuolar Function in the Yeast Saccharomyces Cerevisiae. *The EMBO Journal* **1989**, *8* (7), 2057–2065. https://doi.org/10.1002/j.1460-2075.1989.tb03614.x.

(36) Bonangelino, C. J.; Chavez, E. M.; Bonifacino, J. S. Genomic Screen for Vacuolar Protein Sorting Genes in Saccharomyces Cerevisiae. *Mol Biol Cell* **2002**, *13* (7), 2486–2501. https://doi.org/10.1091/mbc.02-01-0005.

(37) Rothman, J. H.; Raymond, C. K.; Gilbert, T.; O'Hara, P. J.; Stevens, T. H. A Putative GTP Binding Protein Homologous to Interferon-Inducible Mx Proteins Performs an Essential Function in Yeast Protein Sorting. *Cell* **1990**, *61* (6), 1063–1074. https://doi.org/10.1016/0092-8674(90)90070-U.

(38) Marcusson, E. G.; Horazdovsky, B. F.; Cereghino, J. L.; Gharakhanian, E.; Emr, S. D. The Sorting Receptor for Yeast Vacuolar Carboxypeptidase Y Is Encoded by the *VPS10* Gene. *Cell* **1994**, *77* (4), 579–586. https://doi.org/10.1016/0092-8674(94)90219-4.

(39) Chi, R. J.; Liu, J.; West, M.; Wang, J.; Odorizzi, G.; Burd, C. G. Fission of SNX-BAR–Coated Endosomal Retrograde Transport Carriers Is Promoted by the Dynamin-Related Protein Vps1. *Journal of Cell Biology* **2014**, *204* (5), 793–806. https://doi.org/10.1083/jcb.201309084.

(40) Ma, M.; Burd, C. G.; Chi, R. J. Distinct Complexes of Yeast Snx4 Family SNX-BARs Mediate Retrograde Trafficking of Snc1 and Atg27. *Traffic* **2017**, *18* (2), 134–144. https://doi.org/10.1111/tra.12462.

(41) Peters, C.; Baars, T. L.; Bühler, S.; Mayer, A. Mutual Control of Membrane Fission and Fusion Proteins. *Cell* **2004**, *119* (5), 667–678. https://doi.org/10.1016/j.cell.2004.11.023.

(42) Röthlisberger, S.; Jourdain, I.; Johnson, C.; Takegawa, K.; Hyams, J. S. The Dynamin-Related Protein Vps1 Regulates Vacuole Fission, Fusion and Tubulation in the Fission Yeast, Schizosaccharomyces Pombe. *Fungal Genetics and Biology* **2009**, *46* (12), 927–935. https://doi.org/10.1016/j.fgb.2009.07.008.

(43) Alpadi, K.; Kulkarni, A.; Namjoshi, S.; Srinivasan, S.; Sippel, K. H.; Ayscough, K.; Zieger, M.; Schmidt, A.; Mayer, A.; Evangelista, M.; Quiocho, F. A.; Peters, C. Dynamin−SNARE Interactions Control Trans-SNARE Formation in Intracellular Membrane Fusion. *Nat Commun* **2013**, *4* (1), 1704. https://doi.org/10.1038/ncomms2724.

(44) Kulkarni, A.; Alpadi, K.; Sirupangi, T.; Peters, C. A Dynamin Homolog Promotes the Transition from Hemifusion to Content Mixing in Intracellular Membrane Fusion. *Traffic* **2014**, *15* (5), 558–571. https://doi.org/10.1111/tra.12156.

(45) Hoepfner, D.; Van Den Berg, M.; Philippsen, P.; Tabak, H. F.; Hettema, E. H. A Role for Vps1p, Actin, and the Myo2p Motor in Peroxisome Abundance and Inheritance in *Saccharomyces Cerevisiae*. *The Journal of Cell Biology* **2001**, *155* (6), 979–990. https://doi.org/10.1083/jcb.200107028.

(46) Vizeacoumar, F. J.; Vreden, W. N.; Fagarasanu, M.; Eitzen, G. A.; Aitchison, J. D.; Rachubinski, R. A. The Dynamin-like Protein Vps1p of the Yeast Saccharomyces Cerevisiae Associates with Peroxisomes in a Pex19p-Dependent Manner. *Journal of Biological Chemistry* **2006**, *281* (18), 12817–12823. https://doi.org/10.1074/jbc.M600365200.

(47) Ekal, L.; Alqahtani, A. M. S.; Hettema, E. H. The Dynamin-Related Protein Vps1 and the Peroxisomal Membrane Protein Pex27 Function Together during Peroxisome Fission. *Journal of Cell Science* **2023**, *136* (6), jcs246348. https://doi.org/10.1242/jcs.246348.

(48) Kuravi, K.; Nagotu, S.; Krikken, A. M.; Sjollema, K.; Deckers, M.; Erdmann, R.; Veenhuis, M.; Van Der Klei, I. J. Dynamin-Related Proteins Vps1p and Dnm1p Control Peroxisome Abundance in *Saccharomyces Cerevisiae*. *Journal of Cell Science* **2006**, *119* (19), 3994–4001. https://doi.org/10.1242/jcs.03166.

(49) Gurunathan, S. Dynamin and Clathrin Are Required for the Biogenesis of a Distinct Class of Secretory Vesicles in Yeast. *The EMBO Journal* **2002**, *21* (4), 602–614. https://doi.org/10.1093/emboj/21.4.602.

(50) Harsay, E.; Schekman, R. A Subset of Yeast Vacuolar Protein Sorting Mutants Is Blocked in One Branch of the Exocytic Pathway. *The Journal of Cell Biology* **2002**, *156* (2), 271–286. https://doi.org/10.1083/jcb.200109077.

(51) Nannapaneni, S.; Wang, D.; Jain, S.; Schroeder, B.; Highfill, C.; Reustle, L.; Pittsley, D.; Maysent, A.; Moulder, S.; McDowell, R.; Kim, K. The Yeast Dynamin-like Protein Vps1:Vps1 Mutations Perturb the Internalization and the Motility of Endocytic Vesicles and Endosomes via Disorganization of the Actin Cytoskeleton. *European Journal of Cell Biology* **2010**, *89* (7), 499–508. https://doi.org/10.1016/j.ejcb.2010.02.002.

(52) Smaczynska-de Rooij, I. I.; Allwood, E. G.; Mishra, R.; Booth, W. I.; Aghamohammadzadeh, S.; Goldberg, M. W.; Ayscough, K. R. Yeast Dynamin VPS 1 and Amphiphysin RVS 167 Function Together During Endocytosis. *Traffic* **2012**, *13* (2), 317–328. https://doi.org/10.1111/j.1600-0854.2011.01311.x.

(53) Hayden, J.; Williams, M.; Granich, A.; Ahn, H.; Tenay, B.; Lukehart, J.; Highfill, C.; Dobard, S.; Kim, K. Vps1 in the Late Endosome-to-Vacuole Traffic. *J Biosci* **2013**, *38* (1), 73–83. https://doi.org/10.1007/s12038-012-9295-2.

(54) Smaczynska-de Rooij, I. I.; Allwood, E. G.; Aghamohammadzadeh, S.; Hettema, E. H.; Goldberg, M. W.; Ayscough, K. R. A Role for the Dynamin-like Protein Vps1 during Endocytosis in Yeast. *Journal of Cell Science* **2010**, *123* (20), 3496–3506. https://doi.org/10.1242/jcs.070508.

(55) Arlt, H.; Raman, B.; Filali-Mouncef, Y.; Hu, Y.; Leytens, A.; Hardenberg, R.; Guimarães, R.; Kriegenburg, F.; Mari, M.; Smaczynska-de Rooij, I. I.; Ayscough, K. R.; Dengjel, J.; Ungermann, C.; Reggiori, F. The Dynamin Vps1 Mediates Atg9 Transport to the Sites of Autophagosome Formation. *Journal of Biological Chemistry* **2023**, *299* (5), 104712. https://doi.org/10.1016/j.jbc.2023.104712.

(56) Matoba, K.; Kotani, T.; Tsutsumi, A.; Tsuji, T.; Mori, T.; Noshiro, D.; Sugita, Y.; Nomura, N.; Iwata, S.; Ohsumi, Y.; Fujimoto, T.; Nakatogawa, H.; Kikkawa, M.; Noda, N. N. Atg9 Is a Lipid Scramblase That Mediates Autophagosomal Membrane Expansion. *Nat Struct Mol Biol* **2020**, *27* (12), 1185–1193. https://doi.org/10.1038/s41594-020-00518-w.

(57) Vater, C. A.; Raymond, C. K.; Ekena, K.; Howald-Stevenson, I.; Stevens, T. H. The VPSI Protein, a Homolog of Dynamin Required for Vacuolar Protein Sorting in Saccharomycescerevisiae,Is a GTPase with Two Functionally Separable Domains. *The Journal of Cell Biology* **1992**, *119*.

(58) Antonny, B.; Burd, C.; De Camilli, P.; Chen, E.; Daumke, O.; Faelber, K.; Ford, M.; Frolov, V. A.; Frost, A.; Hinshaw, J. E.; Kirchhausen, T.; Kozlov, M. M.; Lenz, M.; Low, H. H.; McMahon, H.; Merrifield, C.; Pollard, T. D.; Robinson, P. J.; Roux, A.; Schmid, S. Membrane Fission by Dynamin: What We Know and What We Need to Know. *The EMBO Journal* **2016**, *35* (21), 2270–2284. https://doi.org/10.15252/embj.201694613.

(59) Jimah, J. R.; Hinshaw, J. E. Structural Insights into the Mechanism of Dynamin Superfamily Proteins. *Trends Cell Biol* **2019**, *29* (3), 257–273. https://doi.org/10.1016/j.tcb.2018.11.003.

(60) Ferguson, S. M.; De Camilli, P. Dynamin, a Membrane-Remodelling GTPase. *Nat Rev Mol Cell Biol* **2012**, *13* (2), 75–88. https://doi.org/10.1038/nrm3266.

(61) Jimah, J. R.; Kundu, N.; Stanton, A. E.; Sochacki, K. A.; Canagarajah, B.; Chan, L.; Strub, M.-P.; Wang, H.; Taraska, J. W.; Hinshaw, J. E. Cryo-EM Structures of

Membrane-Bound Dynamin in a Post-Hydrolysis State Primed for Membrane Fission. *Developmental Cell* **2024**, *59* (14), 1783-1793.e5. https://doi.org/10.1016/j.devcel.2024.04.008.

(62) Danino, D.; Moon, K.-H.; Hinshaw, J. E. Rapid Constriction of Lipid Bilayers by the Mechanochemical Enzyme Dynamin. *Journal of Structural Biology* **2004**, *147* (3), 259–267. https://doi.org/10.1016/j.jsb.2004.04.005.

(63) Hinshaw, J. E.; Schmid, S. L. Dynamin Self-Assembles into Rings Suggesting a Mechanism for Coated Vesicle Budding. *Nature* **1995**, *374* (6518), 190–192. https://doi.org/10.1038/374190a0.

(64) Sweitzer, S. M.; Hinshaw, J. E. Dynamin Undergoes a GTP-Dependent Conformational Change Causing Vesiculation. *Cell* **1998**, *93* (6), 1021–1029. https://doi.org/10.1016/S0092-8674(00)81207-6.

(65) Chappie, J. S.; Acharya, S.; Leonard, M.; Schmid, S. L.; Dyda, F. G Domain Dimerization Controls Dynamin's Assembly-Stimulated GTPase Activity. *Nature* **2010**, *465* (7297), 435–440. https://doi.org/10.1038/nature09032.

(66) Warnock, D. E.; Hinshaw, J. E.; Schmid, S. L. Dynamin Self-Assembly Stimulates Its GTPase Activity*. *Journal of Biological Chemistry* **1996**, *271* (37), 22310–22314. https://doi.org/10.1074/jbc.271.37.22310.

(67) Daumke, O.; Praefcke, G. J. K. Invited Review: Mechanisms of GTP Hydrolysis and Conformational Transitions in the Dynamin Superfamily. *Biopolymers* **2016**, *105* (8), 580–593. https://doi.org/10.1002/bip.22855.

(68) Liu, J.; Alvarez, F. J. D.; Clare, D. K.; Noel, J. K.; Zhang, P. CryoEM Structure of the Super-Constricted Two-Start Dynamin 1 Filament. *Nat Commun* **2021**, *12* (1), 5393. https://doi.org/10.1038/s41467-021-25741-x.

(69) Kong, L.; Sochacki, K. A.; Wang, H.; Fang, S.; Canagarajah, B.; Kehr, A. D.; Rice, W. J.; Strub, M.-P.; Taraska, J. W.; Hinshaw, J. E. Cryo-EM of the Dynamin Polymer Assembled on Lipid Membrane. *Nature* **2018**, *560* (7717), 258–262. https://doi.org/10.1038/s41586-018-0378-6.

(70) Varlakhanova, N. V.; Alvarez, F. J. D.; Brady, T. M.; Tornabene, B. A.; Hosford, C. J.; Chappie, J. S.; Zhang, P.; Ford, M. G. J. Structures of the Fungal Dynamin-Related Protein Vps1 Reveal a Unique, Open Helical Architecture. *Journal of Cell Biology* **2018**, *217* (10), 3608–3624. https://doi.org/10.1083/jcb.201712021.

(71) Smaczynska-de Rooij, I. I.; Marklew, C. J.; Palmer, S. E.; Allwood, E. G.; Ayscough, K. R. Mutation of Key Lysine Residues in the Insert B Region of the Yeast Dynamin

Vps1 Disrupts Lipid Binding and Causes Defects in Endocytosis. *PLoS ONE* **2019**, *14* (4), e0215102. https://doi.org/10.1371/journal.pone.0215102.

(72) Jose, G. P.; Gopan, S.; Bhattacharyya, S.; Pucadyil, T. J. A Facile, Sensitive and Quantitative Membrane-binding Assay for Proteins. *Traffic* **2020**, *21* (3), 297–305. https://doi.org/10.1111/tra.12719.

(73) Jose, G. P.; Pucadyil, T. J. PLiMAP: Proximity-Based Labeling of Membrane-Associated Proteins. *CP Protein Science* **2020**, *101* (1), e110. https://doi.org/10.1002/cpps.110.

(74) Leonard, M.; Song, B. D.; Ramachandran, R.; Schmid, S. L. Robust Colorimetric Assays for Dynamin's Basal and Stimulated GTPase Activities. *Methods Enzymol* **2005**, *404*, 490–503. https://doi.org/10.1016/S0076-6879(05)04043-7.

(75) Dar, S.; Kamerkar, S. C.; Pucadyil, T. J. A High-Throughput Platform for Real-Time Analysis of Membrane Fission Reactions Reveals Dynamin Function. *Nat Cell Biol* **2015**, *17* (12), 1588–1596. https://doi.org/10.1038/ncb3254.

(76) Dar, S.; Kamerkar, S. C.; Pucadyil, T. J. Use of the Supported Membrane Tube Assay System for Real-Time Analysis of Membrane Fission Reactions. *Nat Protoc* **2017**, *12* (2), 390–400. https://doi.org/10.1038/nprot.2016.173.

(77) Swaminathan, U.; Pucadyil, T. J. Reconstituting Membrane Fission Using a High Content and Throughput Assay. *Biochemical Society Transactions* **2024**, *52* (3), 1449–1457. https://doi.org/10.1042/BST20231325.

(78) Gietz, R. D.; Schiestl, R. H.; Willems, A. R.; Woods, R. A. Studies on the Transformation of Intact Yeast Cells by the LiAc/SS-DNA/PEG Procedure. *Yeast* **1995**, *11* (4), 355–360. https://doi.org/10.1002/yea.320110408.

(79) Janke, C.; Magiera, M. M.; Rathfelder, N.; Taxis, C.; Reber, S.; Maekawa, H.; Moreno-Borchart, A.; Doenges, G.; Schwob, E.; Schiebel, E.; Knop, M. A Versatile Toolbox for PCR-based Tagging of Yeast Genes: New Fluorescent Proteins, More Markers and Promoter Substitution Cassettes. *Yeast* **2004**, *21* (11), 947–962. https://doi.org/10.1002/yea.1142.

(80) Xu, X.; Lambrecht, A. D.; Xiao, W. Yeast Survival and Growth Assays. In *Yeast Protocols*; Xiao, W., Ed.; Methods in Molecular Biology; Springer New York: New York, NY, 2014; Vol. 1163, pp 183–191. https://doi.org/10.1007/978-1-4939-0799-1_13.

(81) Shpetner, H. S.; Vallee, R. B. Identification of Dynamin, a Novel Mechanochemical Enzyme That Mediates Interactions between Microtubules. *Cell* **1989**, *59* (3), 421–432. https://doi.org/10.1016/0092-8674(89)90027-5.

(82) van der Bliek, A. M.; Meyerowitz, E. M. Dynamin-like Protein Encoded by the Drosophila Shibire Gene Associated with Vesicular Traffic. *Nature* **1991**, *351* (6325), 411–414. https://doi.org/10.1038/351411a0.

(83) Chen, M. S.; Obar, R. A.; Schroeder, C. C.; Austin, T. W.; Poodry, C. A.; Wadsworth, S. C.; Vallee, R. B. Multiple Forms of Dynamin Are Encoded by Shibire, a Drosophila Gene Involved in Endocytosis. *Nature* **1991**, *351* (6327), 583–586. https://doi.org/10.1038/351583a0.

(84) Admasu, A.; Gudmundsdóttir, A. D.; Platz, M. S.; Watt, D. S.; Kwiatkowski, S.; Crocker, P. J. A Laser Flash Photolysis Study of P-Tolyl(Trifluoromethyl)Carbene. *J. Chem. Soc., Perkin Trans. 2* **1998**, No. 5, 1093–1100. https://doi.org/10.1039/a707586c.

(85) Marat, A. L.; Haucke, V. Phosphatidylinositol 3-phosphates—at the Interface between Cell Signalling and Membrane Traffic. *The EMBO Journal* **2016**, *35* (6), 561–579. https://doi.org/10.15252/embj.201593564.

(86) Hsieh, W.-T.; Hsu, C.-J.; Capraro, B. R.; Wu, T.; Chen, C.-M.; Yang, S.; Baumgart, T. Curvature Sorting of Peripheral Proteins on Solid-Supported Wavy Membranes. *Langmuir* **2012**, *28* (35), 12838–12843. https://doi.org/10.1021/la302205b.

(87) Jung, H.; Robison, A. D.; Cremer, P. S. Detecting Protein-Ligand Binding on Supported Bilayers by Local pH Modulation. *J Am Chem Soc* **2009**, *131* (3), 1006–1014. https://doi.org/10.1021/ja804542p.

(88) Kamerkar, S. C.; Kraus, F.; Sharpe, A. J.; Pucadyil, T. J.; Ryan, M. T. Dynamin-Related Protein 1 Has Membrane Constricting and Severing Abilities Sufficient for Mitochondrial and Peroxisomal Fission. *Nat Commun* **2018**, *9* (1), 5239. https://doi.org/10.1038/s41467-018-07543-w.

(89) Khurana, H.; Baratam, K.; Bhattacharyya, S.; Srivastava, A.; Pucadyil, T. J. Mechanistic Analysis of a Novel Membrane-Interacting Variable Loop in the Pleckstrin-Homology Domain Critical for Dynamin Function. *Proc. Natl. Acad. Sci. U.S.A.* **2023**, *120* (11), e2215250120. https://doi.org/10.1073/pnas.2215250120.

(90) Kunding, A. H.; Mortensen, M. W.; Christensen, S. M.; Stamou, D. A Fluorescence-Based Technique to Construct Size Distributions from Single-Object Measurements:

Application to the Extrusion of Lipid Vesicles. *Biophysical Journal* **2008**, *95* (3), 1176–1188. https://doi.org/10.1529/biophysj.108.128819.

(91) Kovtun, O.; Leneva, N.; Bykov, Y. S.; Ariotti, N.; Teasdale, R. D.; Schaffer, M.; Engel, B. D.; Owen, David. J.; Briggs, J. A. G.; Collins, B. M. Structure of the Membrane-Assembled Retromer Coat Determined by Cryo-Electron Tomography. *Nature* **2018**, *561* (7724), 561–564. https://doi.org/10.1038/s41586-018-0526-z.

(92) Ingerman, E.; Perkins, E. M.; Marino, M.; Mears, J. A.; McCaffery, J. M.; Hinshaw, J. E.; Nunnari, J. Dnm1 Forms Spirals That Are Structurally Tailored to Fit Mitochondria. *The Journal of Cell Biology* **2005**, *170* (7), 1021–1027. https://doi.org/10.1083/jcb.200506078.

(93) Ford, M. G. J.; Jenni, S.; Nunnari, J. The Crystal Structure of Dynamin. *Nature* **2011**, *477* (7366), 561–566. https://doi.org/10.1038/nature10441.

(94) Kozlovsky, Y.; Kozlov, M. M. Membrane Fission: Model for Intermediate Structures. *Biophys J* **2003**, *85* (1), 85–96. https://doi.org/10.1016/S0006-3495(03)74457-9.

(95) Frolov, V. A.; Escalada, A.; Akimov, S. A.; Shnyrova, A. V. Geometry of Membrane Fission. *Chemistry and Physics of Lipids* **2015**, *185*, 129–140. https://doi.org/10.1016/j.chemphyslip.2014.07.006.

(96) Bashkirov, P. V.; Akimov, S. A.; Evseev, A. I.; Schmid, S. L.; Zimmerberg, J.; Frolov, V. A. GTPase Cycle of Dynamin Is Coupled to Membrane Squeeze and Release, Leading to Spontaneous Fission. *Cell* **2008**, *135* (7), 1276–1286. https://doi.org/10.1016/j.cell.2008.11.028.

(97) Shnyrova, A. V.; Bashkirov, P. V.; Akimov, S. A.; Pucadyil, T. J.; Zimmerberg, J.; Schmid, S. L.; Frolov, V. A. Geometric Catalysis of Membrane Fission Driven by Flexible Dynamin Rings. *Science* **2013**, *339* (6126), 1433–1436. https://doi.org/10.1126/science.1233920.

(98) Götzke, H.; Kilisch, M.; Martínez-Carranza, M.; Sograte-Idrissi, S.; Rajavel, A.; Schlichthaerle, T.; Engels, N.; Jungmann, R.; Stenmark, P.; Opazo, F.; Frey, S. The ALFA-Tag Is a Highly Versatile Tool for Nanobody-Based Bioscience Applications. *Nat Commun* **2019**, *10* (1), 4403. https://doi.org/10.1038/s41467-019-12301-7.

(99) Akhuli, D.; Dhar, A.; Viji, A. S.; Bhojappa, B.; Palani, S. ALIBY: ALFA Nanobody-Based Toolkit for Imaging and Biochemistry in Yeast. *mSphere* **2022**, *7* (5), e00333-22. https://doi.org/10.1128/msphere.00333-22.

(100) Strack, S.; Cribbs, J. T. Allosteric Modulation of Drp1 Mechanoenzyme Assembly and Mitochondrial Fission by the Variable Domain. *Journal of Biological Chemistry* **2012**, *287* (14), 10990–11001. https://doi.org/10.1074/jbc.M112.342105.

(101) Low, H. H.; Sachse, C.; Amos, L. A.; Löwe, J. Structure of a Bacterial Dynamin-like Protein Lipid Tube Provides a Mechanism For Assembly and Membrane Curving. *Cell* **2009**, *139* (7), 1342–1352. https://doi.org/10.1016/j.cell.2009.11.003.

(102) Von Der Malsburg, A.; Abutbul-Ionita, I.; Haller, O.; Kochs, G.; Danino, D. Stalk Domain of the Dynamin-like MxA GTPase Protein Mediates Membrane Binding and Liposome Tubulation via the Unstructured L4 Loop. *Journal of Biological Chemistry* **2011**, *286* (43), 37858–37865. https://doi.org/10.1074/jbc.M111.249037.

(103) Bustillo-Zabalbeitia, I.; Montessuit, S.; Raemy, E.; Basañez, G.; Terrones, O.; Martinou, J.-C. Specific Interaction with Cardiolipin Triggers Functional Activation of Dynamin-Related Protein 1. *PLoS ONE* **2014**, *9* (7), e102738. https://doi.org/10.1371/journal.pone.0102738.

(104) Francy, C. A.; Clinton, R. W.; Fröhlich, C.; Murphy, C.; Mears, J. A. Cryo-EM Studies of Drp1 Reveal Cardiolipin Interactions That Activate the Helical Oligomer. *Sci Rep* **2017**, *7* (1), 10744. https://doi.org/10.1038/s41598-017-11008-3.

(105) Mahajan, M.; Bharambe, N.; Shang, Y.; Lu, B.; Mandal, A.; Madan Mohan, P.; Wang, R.; Boatz, J. C.; Manuel Martinez Galvez, J.; Shnyrova, A. V.; Qi, X.; Buck, M.; Van Der Wel, P. C. A.; Ramachandran, R. NMR Identification of a Conserved Drp1 Cardiolipin-Binding Motif Essential for Stress-Induced Mitochondrial Fission. *Proc. Natl. Acad. Sci. U.S.A.* **2021**, *118* (29), e2023079118. https://doi.org/10.1073/pnas.2023079118.

(106) Kraus, F.; Roy, K.; Pucadyil, T. J.; Ryan, M. T. Function and Regulation of the Divisome for Mitochondrial Fission. *Nature* **2021**, *590* (7844), 57–66. https://doi.org/10.1038/s41586-021-03214-x.

(107) Rosendale, M.; Van, T. N. N.; Grillo-Bosch, D.; Sposini, S.; Claverie, L.; Gauthereau, I.; Claverol, S.; Choquet, D.; Sainlos, M.; Perrais, D. Functional Recruitment of Dynamin Requires Multimeric Interactions for Efficient Endocytosis. *Nat Commun* **2019**, *10* (1), 4462. https://doi.org/10.1038/s41467-019-12434-9.

(108) Stepp, J. D.; Huang, K.; Lemmon, S. K. The Yeast Adaptor Protein Complex, AP-3, Is Essential for the Efficient Delivery of Alkaline Phosphatase by the Alternate Pathway to the Vacuole. *The Journal of Cell Biology* **1997**, *139* (7), 1761–1774. https://doi.org/10.1083/jcb.139.7.1761.

(109) Cowles, C. R.; Odorizzi, G.; Payne, G. S.; Emr, S. D. The AP-3 Adaptor Complex Is Essential for Cargo-Selective Transport to the Yeast Vacuole. *Cell* **1997**, *91* (1), 109–118. https://doi.org/10.1016/S0092-8674(01)80013-1.

(110) Llinares, E.; Barry, A. O.; André, B. The AP-3 Adaptor Complex Mediates Sorting of Yeast and Mammalian PQ-Loop-Family Basic Amino Acid Transporters to the Vacuolar/Lysosomal Membrane. *Sci Rep* **2015**, *5* (1), 16665. https://doi.org/10.1038/srep16665.

(111) Hirst, J.; Lui, W. W. Y.; Bright, N. A.; Totty, N.; Seaman, M. N. J.; Robinson, M. S. A Family of Proteins with γ-Adaptin and Vhs Domains That Facilitate Trafficking between the Trans-Golgi Network and the Vacuole/Lysosome. *Journal of Cell Biology* **2000**, *149* (1), 67–80. https://doi.org/10.1083/jcb.149.1.67.

(112) Costaguta, G.; Stefan, C. J.; Bensen, E. S.; Emr, S. D.; Payne, G. S. Yeast Gga Coat Proteins Function with Clathrin in Golgi to Endosome Transport. *MBoC* **2001**, *12* (6), 1885–1896. https://doi.org/10.1091/mbc.12.6.1885.

(113) Watanabe, Y.; Noda, N. N.; Kumeta, H.; Suzuki, K.; Ohsumi, Y.; Inagaki, F. Selective Transport of α-Mannosidase by Autophagic Pathways: STRUCTURAL BASIS FOR CARGO RECOGNITION BY Atg19 AND Atg34*. *Journal of Biological Chemistry* **2010**, *285* (39), 30026–30033. https://doi.org/10.1074/jbc.M110.143545.

(114) Lynch-Day, M. A.; Klionsky, D. J. The Cvt Pathway as a Model for Selective Autophagy. *FEBS Lett* **2010**, *584* (7), 1359–1366. https://doi.org/10.1016/j.febslet.2010.02.013.

(115) Yamasaki, A.; Noda, N. N. Structural Biology of the Cvt Pathway. *Journal of Molecular Biology* **2017**, *429* (4), 531–542. https://doi.org/10.1016/j.jmb.2017.01.003.

(116) Wicky, S.; Schwarz, H.; Singer-Krüger, B. Molecular Interactions of Yeast Neo1p, an Essential Member of the Drs2 Family of Aminophospholipid Translocases, and Its Role in Membrane Trafficking within the Endomembrane System. *Molecular and Cellular Biology* **2004**, *24* (17), 7402–7418. https://doi.org/10.1128/MCB.24.17.7402-7418.2004.

(117) Wu, Y.; Takar, M.; Cuentas-Condori, A. A.; Graham, T. R. Neo1 and Phosphatidylethanolamine Contribute to Vacuole Membrane Fusion in *Saccharomyces Cerevisiae*. *Cellular Logistics* **2016**, *6* (3), e1228791. https://doi.org/10.1080/21592799.2016.1228791.

(118) Dalton, L. E.; Bean, B. D. M.; Davey, M.; Conibear, E. Quantitative High-Content Imaging Identifies Novel Regulators of Neo1 Trafficking at Endosomes. *MBoC* **2017**, *28* (11), 1539–1550. https://doi.org/10.1091/mbc.e16-11-0772.

(119) Miyabe, S.; Izawa, S.; Inoue, Y. The Zrc1 Is Involved in Zinc Transport System between Vacuole and Cytosol in Saccharomyces Cerevisiae. *Biochemical and Biophysical Research Communications* **2001**, *282* (1), 79–83. https://doi.org/10.1006/bbrc.2001.4522.

(120) Gulshan, K.; Moye-Rowley, W. S. Vacuolar Import of Phosphatidylcholine Requires the ATP-Binding Cassette Transporter Ybt1. *Traffic* **2011**, *12* (9), 1257–1268. https://doi.org/10.1111/j.1600-0854.2011.01228.x.

(121) Mayer, A.; Wickner, W. Docking of Yeast Vacuoles Is Catalyzed by the Ras-like GTPase Ypt7p after Symmetric Priming by Sec18p (NSF). *Journal of Cell Biology* **1997**, *136* (2), 307–317. https://doi.org/10.1083/jcb.136.2.307.

(122) Balderhaar, H. J. kleine; Arlt, H.; Ostrowicz, C.; Bröcker, C.; Sündermann, F.; Brandt, R.; Babst, M.; Ungermann, C. The Rab GTPase Ypt7 Is Linked to Retromer-Mediated Receptor Recycling and Fusion at the Yeast Late Endosome. *Journal of Cell Science* **2010**, *123* (23), 4085–4094. https://doi.org/10.1242/jcs.071977.

(123) Schoppe, J.; Mari, M.; Yavavli, E.; Auffarth, K.; Cabrera, M.; Walter, S.; Fröhlich, F.; Ungermann, C. AP-3 Vesicle Uncoating Occurs after HOPS-dependent Vacuole Tethering. *The EMBO Journal* **2020**, *39* (20), e105117. https://doi.org/10.15252/embj.2020105117.

(124) Eising, S.; Thiele, L.; Fröhlich, F. A Systematic Approach to Identify Recycling Endocytic Cargo Depending on the GARP Complex. *eLife* **2019**, *8*, e42837. https://doi.org/10.7554/eLife.42837.

(125) Lukehart, J.; Highfill, C.; Kim, K. Vps1, a Recycling Factor for the Traffic from Early Endosome to the Late Golgi. *Biochem. Cell Biol.* **2013**, *91* (6), 455–465. https://doi.org/10.1139/bcb-2013-0044.

(126) Saimani, U.; Smothers, J.; McDermott, H.; Makaraci, P.; Kim, K. Yeast Dynamin Associates with the GARP Tethering Complex for Endosome-to-Golgi Traffic. *European Journal of Cell Biology* **2017**, *96* (6), 612–621. https://doi.org/10.1016/j.ejcb.2017.04.004.

(127) Rogaeva, E.; Meng, Y.; Lee, J. H.; Gu, Y.; Kawarai, T.; Zou, F.; Katayama, T.; Baldwin, C. T.; Cheng, R.; Hasegawa, H.; Chen, F.; Shibata, N.; Lunetta, K. L.; Pardossi-Piquard, R.; Bohm, C.; Wakutani, Y.; Cupples, L. A.; Cuenco, K. T.; Green,

R. C.; Pinessi, L.; Rainero, I.; Sorbi, S.; Bruni, A.; Duara, R.; Friedland, R. P.; Inzelberg, R.; Hampe, W.; Bujo, H.; Song, Y.-Q.; Andersen, O. M.; Willnow, T. E.; Graff-Radford, N.; Petersen, R. C.; Dickson, D.; Der, S. D.; Fraser, P. E.; Schmitt-Ulms, G.; Younkin, S.; Mayeux, R.; Farrer, L. A.; St George-Hyslop, P. The Neuronal Sortilin-Related Receptor SORL1 Is Genetically Associated with Alzheimer Disease. *Nat Genet* **2007**, *39* (2), 168–177. https://doi.org/10.1038/ng1943.

(128) Meng, T.; Chen, X.; He, Z.; Huang, H.; Lin, S.; Liu, K.; Bai, G.; Liu, H.; Xu, M.; Zhuang, H.; Zhang, Y.; Waqas, A.; Liu, Q.; Zhang, C.; Sun, X.-D.; Huang, H.; Umair, M.; Yan, Y.; Feng, D. ATP9A Deficiency Causes ADHD and Aberrant Endosomal Recycling via Modulating RAB5 and RAB11 Activity. *Mol Psychiatry* **2023**, *28* (3), 1219–1231. https://doi.org/10.1038/s41380-022-01940-w.

(129) Vogt, G.; Verheyen, S.; Schwartzmann, S.; Ehmke, N.; Potratz, C.; Schwerin-Nagel, A.; Plecko, B.; Holtgrewe, M.; Seelow, D.; Blatterer, J.; Speicher, M. R.; Kornak, U.; Horn, D.; Mundlos, S.; Fischer-Zirnsak, B.; Boschann, F. Biallelic Truncating Variants in ATP9A Cause a Novel Neurodevelopmental Disorder Involving Postnatal Microcephaly and Failure to Thrive. *J Med Genet* **2022**, *59* (7), 662–668. https://doi.org/10.1136/jmedgenet-2021-107843.

(130) Platt, F. M.; d'Azzo, A.; Davidson, B. L.; Neufeld, E. F.; Tifft, C. J. Lysosomal Storage Diseases. *Nat Rev Dis Primers* **2018**, *4* (1), 1–25. https://doi.org/10.1038/s41572-018-0025-4.

(131) Ford, M. G. J.; Chappie, J. S. The Structural Biology of the Dynamin-related Proteins: New Insights into a Diverse, Multitalented Family. *Traffic* **2019**, *20* (10), 717–740. https://doi.org/10.1111/tra.12676.

(132) Sesaki, H.; Southard, S. M.; Yaffe, M. P.; Jensen, R. E. Mgm1p, a Dynamin-Related GTPase, Is Essential for Fusion of the Mitochondrial Outer Membrane. *Mol Biol Cell* **2003**, *14* (6), 2342–2356. https://doi.org/10.1091/mbc.E02-12-0788.

(133) De Vecchis, D.; Cavellini, L.; Baaden, M.; Hénin, J.; Cohen, M. M.; Taly, A. A Membrane-Inserted Structural Model of the Yeast Mitofusin Fzo1. *Sci Rep* **2017**, *7* (1), 10217. https://doi.org/10.1038/s41598-017-10687-2.

(134) Bleazard, W.; McCaffery, J. M.; King, E. J.; Bale, S.; Mozdy, A.; Tieu, Q.; Nunnari, J.; Shaw, J. M. The Dynamin-Related GTPase Dnm1 Regulates Mitochondrial Fission in Yeast. *Nat Cell Biol* **1999**, *1* (5), 298–304. https://doi.org/10.1038/13014.

(135) Teis, D.; Saksena, S.; Judson, B. L.; Emr, S. D. ESCRT-II Coordinates the Assembly of ESCRT-III Filaments for Cargo Sorting and Multivesicular Body Vesicle Formation. *EMBO J* **2010**, *29* (5), 871–883. https://doi.org/10.1038/emboj.2009.408.

(136) Takei, K.; Haucke, V.; Slepnev, V.; Farsad, K.; Salazar, M.; Chen, H.; De Camilli, P. Generation of Coated Intermediates of Clathrin-Mediated Endocytosis on Protein-Free Liposomes. *Cell* **1998**, *94* (1), 131–141. https://doi.org/10.1016/S0092-8674(00)81228-3.

(137) Matsuoka, K.; Orci, L.; Amherdt, M.; Bednarek, S. Y.; Hamamoto, S.; Schekman, R.; Yeung, T. COPII-Coated Vesicle Formation Reconstituted with Purified Coat Proteins and Chemically Defined Liposomes. *Cell* **1998**, *93* (2), 263–275. https://doi.org/10.1016/s0092-8674(00)81577-9.

(138) Pucadyil, T. J.; Schmid, S. L. Real-Time Visualization of Dynamin-Catalyzed Membrane Fission and Vesicle Release. *Cell* **2008**, *135* (7), 1263–1275. https://doi.org/10.1016/j.cell.2008.11.020.

(139) Kamerkar, S. C.; Roy, K.; Bhattacharyya, S.; Pucadyil, T. J. A Screen for Membrane Fission Catalysts Identifies the ATPase EHD1. *Biochemistry* **2019**, *58* (1), 65–71. https://doi.org/10.1021/acs.biochem.8b00925.

(140) De Craene, J.-O.; Bertazzi, D.; Bär, S.; Friant, S. Phosphoinositides, Major Actors in Membrane Trafficking and Lipid Signaling Pathways. *IJMS* **2017**, *18* (3), 634. https://doi.org/10.3390/ijms18030634.

(141) Jeschke, A.; Haas, A. Sequential Actions of Phosphatidylinositol Phosphates Regulate Phagosome-Lysosome Fusion. *MBoC* **2018**, *29* (4), 452–465. https://doi.org/10.1091/mbc.E17-07-0464.

(142) Feng, Z.; Yu, C. PI(3,4)P_2 -Mediated Membrane Tubulation Promotes Integrin Trafficking and Invasive Cell Migration. *Proc. Natl. Acad. Sci. U.S.A.* **2021**, *118* (19), e2017645118. https://doi.org/10.1073/pnas.2017645118.

(143) Snider, C. E.; Willet, A. H.; Brown, H. T.; Gould, K. L. Analysis of the Contribution of Phosphoinositides to Medial Septation in Fission Yeast Highlights the Importance of PI(4,5)P_2 for Medial Contractile Ring Anchoring. *MBoC* **2018**, *29* (18), 2148–2155. https://doi.org/10.1091/mbc.E18-03-0179.

(144) Ballabio, A.; Bonifacino, J. S. Lysosomes as Dynamic Regulators of Cell and Organismal Homeostasis. *Nat Rev Mol Cell Biol* **2020**, *21* (2), 101–118. https://doi.org/10.1038/s41580-019-0185-4.

(145) Burke, J. E. Structural Basis for Regulation of Phosphoinositide Kinases and Their Involvement in Human Disease. *Molecular Cell* **2018**, *71* (5), 653–673. https://doi.org/10.1016/j.molcel.2018.08.005.

(146) Posor, Y.; Jang, W.; Haucke, V. Phosphoinositides as Membrane Organizers. *Nat Rev Mol Cell Biol* **2022**, *23* (12), 797–816. https://doi.org/10.1038/s41580-022-00490-x.

(147) Hammond, G. R. V.; Balla, T. Polyphosphoinositide Binding Domains: Key to Inositol Lipid Biology. *Biochimica et Biophysica Acta (BBA) - Molecular and Cell Biology of Lipids* **2015**, *1851* (6), 746–758. https://doi.org/10.1016/j.bbalip.2015.02.013.

(148) Rathod, J.; Yen, H.-C.; Liang, B.; Tseng, Y.-Y.; Chen, C.-S.; Wu, W.-S. YPIBP: A Repository for Phosphoinositide-Binding Proteins in Yeast. *Comput Struct Biotechnol J* **2021**, *19*, 3692–3707. https://doi.org/10.1016/j.csbj.2021.06.035.

(149) Querin, L.; Sanvito, R.; Magni, F.; Busti, S.; Van Dorsselaer, A.; Alberghina, L.; Vanoni, M. Proteomic Analysis of a Nutritional Shift-up in Saccharomyces Cerevisiae Identifies Gvp36 as a BAR-Containing Protein Involved in Vesicular Traffic and Nutritional Adaptation. *Journal of Biological Chemistry* **2008**, *283* (8), 4730–4743. https://doi.org/10.1074/jbc.M707787200.

(150) Prigent, M.; Chaillot, J.; Tisserand, H.; Boy-Marcotte, E.; Cuif, M.-H. Three Members of the Yeast N-BAR Proteins Family Form Heterogeneous Lattices in Vivo and Interact Differentially with Two RabGAP Proteins. *Sci Rep* **2020**, *10* (1), 1698. https://doi.org/10.1038/s41598-020-58606-2.

(151) Walther, T. C.; Brickner, J. H.; Aguilar, P. S.; Bernales, S.; Pantoja, C.; Walter, P. Eisosomes Mark Static Sites of Endocytosis. *Nature* **2006**, *439* (7079), 998–1003. https://doi.org/10.1038/nature04472.

(152) Ziółkowska, N. E.; Karotki, L.; Rehman, M.; Huiskonen, J. T.; Walther, T. C. Eisosome-Driven Plasma Membrane Organization Is Mediated by BAR Domains. *Nat Struct Mol Biol* **2011**, *18* (7), 854–856. https://doi.org/10.1038/nsmb.2080.

(153) Karotki, L.; Huiskonen, J. T.; Stefan, C. J.; Ziółkowska, N. E.; Roth, R.; Surma, M. A.; Krogan, N. J.; Emr, S. D.; Heuser, J.; Grünewald, K.; Walther, T. C. Eisosome Proteins Assemble into a Membrane Scaffold. *Journal of Cell Biology* **2011**, *195* (5), 889–902. https://doi.org/10.1083/jcb.201104040.

(154) Li, L.; Liu, X.; Yang, S.; Li, M.; Wu, Y.; Hu, S.; Wang, W.; Jiang, A.; Zhang, Q.; Zhang, J.; Ma, X.; Hu, J.; Zhao, Q.; Liu, Y.; Li, D.; Hu, J.; Yang, C.; Feng, W.; Wang, X. The HEAT Repeat Protein HPO-27 Is a Lysosome Fission Factor. *Nature* **2024**, *628* (8008), 630–638. https://doi.org/10.1038/s41586-024-07249-8.

(155) Bonangelino, C. J.; Nau, J. J.; Duex, J. E.; Brinkman, M.; Wurmser, A. E.; Gary, J. D.; Emr, S. D.; Weisman, L. S. Osmotic Stress–Induced Increase of Phosphatidylinositol 3,5-Bisphosphate Requires Vac14p, an Activator of the Lipid Kinase Fab1p. *J Cell Biol* **2002**, *156* (6), 1015–1028. https://doi.org/10.1083/jcb.200201002.

(156) Michaillat, L.; Mayer, A. Identification of Genes Affecting Vacuole Membrane Fragmentation in Saccharomyces Cerevisiae. *PLoS ONE* **2013**, *8* (2), e54160. https://doi.org/10.1371/journal.pone.0054160.

(157) Nothwehr, S. E. Golgi and Vacuolar Membrane Proteins Reach the Vacuole in Vpsl Mutant Yeast Cells via the Plasma Membrane. *The Journal of Cell Biology* **1995**, *129*.